# INVESTIGATION OF THE PHASE BEHAVIOR OF BICELLAR MIXTURES BY DIFFERENTIAL SCANNING CALORIMETRY AND VARIABLE PRESSURE $^2H$ NMR

MD. NASIR UDDIN

# Investigation of the Phase Behavior of Bicellar Mixtures by Differential Scanning Calorimetry and Variable Pressure $^2$H NMR

by

© Md. Nasir Uddin
M. Sc., Jahangirnagar University

A thesis submitted to the
School of Graduate Studies
in partial fulfillment of the
requirements for the degree of
Master of Science.

Department of Physics & Physical Oceanography
Memorial University of Newfoundland

April 6, 2010

St. John's Newfoundland

# Contents

# Abstract

Depending on temperature, composition and hydration, mixtures of long and short chain lipids, namely, 1,2-dimyristoyl-*sn*-glycero-3-phosphocholine (DMPC) and 1,2-dihexanoyl-*sn*-glycero-3-phosphocholine (DHPC) can assemble into structures in which the DMPC lipids are aggregated in planar bilayer regions while the DHPC lipids are in the edges of planar bilayers. Such mixture is referred as 'bicellar' and can be used as model membrane to study membrane associated proteins and peptides. We have studied the phase behavior of DMPC/DHPC mixtures of molar ratios 3:1 and 4.4:1 with one or the other lipid deuterated, using differential scanning calorimetry (DSC) and variable pressure $^2$H NMR. Application of pressure shifts the isotropic-nematic and the nematic-lamellar transition temperatures for both mixtures, by roughly the same rate as the DMPC gel-liquid crystal transition. DSC measurements show that DMPC-normalized transition enthalpy is similar to that of pure DMPC. In the nematic temperature range, DMPC chain order does not change much and DSC shows samples absorb heat over that temperature range. Taken together, these observations suggest that isotropic-nematic-lamellar transitions are strongly coupled to the melting of ordered DMPC in the bicelles and the chain melting is not only the process absorbing heat at the transition. It thus appears that some of the heat input goes to changing the hydration of the DHPC headgroups. Pressure reduces the magnetic orientability in DMPC-$d_{54}$ of 3:1 mixture compared to 4.4:1 mixture in nematic phase

temperature range. This may be due to particle size effects. In the nematic and lamellar phase, DHPC-$d_{22}$ chains become more ordered with increasing temperature. This reflects fast exchange of DHPC-$d_{22}$ between highly curved edge regions and planar DMPC-rich regions, and the fraction of time spent by a DHPC molecule in the DMPC-rich environment increases with increasing temperature. This work provides insight into how interactions between the long and short chain lipids in the bicellar mixture drive the observed changes in morphology.

# Acknowledgements

I owe my deepest gratitude to my supervisor Professor Dr. M. R. Morrow who made this work possible, for his constant guidance, tremendous help throughout the project and financial support.

I wish to express my warm and sincere thanks to Professor Dr. Valerie Booth (Department of Biochemistry, MUN) for giving permission to use her lab for DSC measurements and special thanks to Donna Jackman for technical assistance with its operation. I would like to thank Drs. John Katsaras and Mu-Ping Nieh for helpful discussions.

I am grateful to the School of Graduate Studies and Department of Physics and Physical Oceanography for financial support. I wish to thank Professors Dr. John Lewis, Dr. John Whitehead, Dr. Erika Merschrod and Dr. Anand Yethiraj for their great teaching.

I would like to thank Doug, Bretta and Mark for their assistance with NMR experiments and relevant discussions. I am grateful to Wayne Holly for keeping our lab going with an excellent cryogenic facility. I am also appreciative of the support I received from Mahbub, Zahangir, Uttam, Oktay and Terry. I wish to thank my wife Sumi for her unwavering faith in me, understanding, encouragement and support.

Lastly, and most importantly, I wish to thank my parents, for their unflagging love, sacrifice and support throughout my life. I dedicate this thesis to them.

# List of Tables

# List of Figures

# Abbreviations

$^2$H NMR: Deuterium Nuclear Magnetic Resonance

MLV: Multi Lamellar Vesicles

PC: Phosphocholine

DSC: Differential Scanning Calorimetry

DMPC: 1,2-dimyristoyl-*sn*-glycero-3-phosphocholine

DHPC: 1,2-dihexanoyl-*sn*-glycero-3-phosphocholine

DMPC-$d_{54}$: 1,2-dimyristoyl-$d_{54}$-*sn*-glycero-3-phosphocholine

DHPC-$d_{22}$: 1,2-dihexanoyl-$d_{22}$-*sn*-glycero-3- phosphocholine

EFG: Electric Field Gradient

$T_2^{QE}$: Quadrupole echo decay time

# Chapter 1

# Introduction

Important biological processes take place in cell membranes which are selectively permeable lipid bilayers composed of different kinds of amphiphilic molecules, primarily lipids and proteins. Lipid molecules constitute about 50% of the mass of most animal cell membranes and there are approximately $10^6$ lipid molecules in a 1 $\mu m^2$ area of lipid bilayer in the plasma membrane of a small animal cell [1]. The membrane lipids are in general amphiphilic in nature, so lipid bilayers consists of a hydrophilic part and a hydrophobic part. Among all the lipids, phospholipids are most abundant. A variety of protein molecules are embedded into the lipid bilayers in the cell membrane. The membrane proteins constitute $\sim$ 30% of all the proteins encoded in the human genome and less than 0.2% of resolved protein structures are membrane proteins [1, 2, 3, 4].

The lipid molecules spontaneously form bilayer vesicles or micelles when hydrated. Upon hydration, phospholipids with longer hydrocarbon chains (more than 10 carbons on each chain), such as 1,2-dimyristoyl-*sn*-glycero-3-phosphocholine (DMPC) can form bilayers for a wide range of temperature whereas lipids with shorter chains (about 6 carbons on each chain), such as 1,2-dihexanoyl-*sn*-glycero-3-phosphocholine

(DHPC) can form micelles [5, 6, 7]. Depending on temperature and pressure, lipid bilayers exist mainly in two phases - the gel phase, in which lipid chains are ordered, at low temperature an the liquid crystalline phase, in which lipid chains are disordered, at high temperature.

Depending on temperature, composition and hydration, mixtures of a short chain phospholipids, such as DHPC with a longer chain lipid, such as DMPC can assemble into structures in which the longer chain lipids are preferentially aggregated in planar bilayer regions while the shorter chain lipids are in highly curved regions that close the edges of such planar bilayers [8, 9, 10, 11, 12]. In this thesis, the term 'bicellar mixture' has been used for DMPC/DHPC mixtures as suggested by Soong *et al.* [13]. Due to their ability to undergo spontaneous alignment in a magnetic field under certain conditions, some aggregates of bicellar lipids are of considerable interest as model membranes in which membrane associated peptides and proteins can be studied by nuclear magnetic resonance (NMR) [14, 15].

Several experimental techniques such as NMR spectroscopy, IR spectroscopy, neutron scattering, light scattering, fluorescence-based techniques etc., have been employed to study lipid assemblies [16, 17, 18, 19, 20, 21, 22, 23, 24, 25]. Deuterium NMR ($^2$H-NMR) spectroscopy is one of the more versatile methods for the study of molecular orientation and membrane dynamics. Previous observations by deuterium NMR on chain-perdeuterated DMPC (DMPC-$d_{54}$) in DMPC-$d_{54}$/DHPC mixtures [8, 11, 12, 26] have shown spectra characteristic of fast isotropic reorientation at lower temperature, axially-symmetric reorientation about an axis oriented perpendicular to the applied magnetic field over a small, intermediate range of temperature and, axially symmetric reorientation about spherically-distributed bilayer normal orientations at high temperature. Observations of chain-perdeuterated DHPC (DHPC-$d_{22}$)in corresponding DMPC/DHPC-$d_{22}$ mixtures [11, 12] suggest that, at intermediate and high

temperatures, one fraction of the short-chain lipid component may undergo isotropic reorientation while other fractions exist in anisotropic environments with small degrees of orientational order.

Using small angle neutron scattering data, Katsaras and coworkers [27, 28, 29] concluded that the morphological phases exhibited on warming DMPC/DHPC mixtures from low to high temperature are an isotropic phase, consisting of bicellar particles undergoing rapid thermal reorientation, a magnetically alignable chiral nematic phase consisting of entangled wormlike micelles, and a multilamellar bilayer vesicle phase. Most researchers now accept the isotropic-nematic-lamellar phase scheme, though various morphologies of bicellar mixtures have been suggested by researchers since the initial investigation of bicellar mixtures [8, 11, 12, 27, 29, 30, 31, 32, 33].

One interesting feature of phospholipid bilayers is their response to increases in hydrostatic pressure. The effects of pressure on lipid bilayers have been investigated using a variety of techniques including neutron scattering, X-ray diffraction, optical transmission microscopy, and $^2$H-NMR spectroscopy [16, 17, 18, 21, 22, 23, 24, 25]. For lipid bilayers the lipid-chain orientational order as well as the main transition temperature increase with increasing pressure. The pressure sensitivity of the main DMPC gel-to-liquid crystalline phase transition has been reported as $\sim 0.23$°C/MPa by neutron diffraction [34] and $\sim 0.19$°C/MPa by deuterium NMR [36]. High pressure can induce lipid chain interdigitation that is not normally observed at ambient pressure [21, 22, 34, 35].

It is noted that susceptibility to pressure-induced ordering of the phospholipid chains in multilamellar vesicles comprising a single lipid species, depends on proximity of the temperature to the main phase transition temperature at ambient pressure for bilayers of that lipid [36]. In multilamellar vesicles comprising binary lipid mixtures, both species exhibit susceptibilities to pressure-induced ordering that fall between

the values of either species individually [37]. This is presumed to reflect the influence of an average ordering potential within the mixed lipid bilayers. Some suggested morphologies of bicellar mixtures differ from multilamellar vesicle geometry in ways that might affect their responses to applied hydrostatic pressure. In particular, some proposed DMPC/DHPC structures contain regions of high local curvature which are enriched in the shorter chain lipid component. In effect, such morphologies contain edges which are not present in multi-lamellar vesicle samples.

The objective of this work is to address the following questions:

- How do pressure and temperature affect the ordering and mixing of long and short chain lipid components in bicellar mixtures?
- How do observed changes in enthalpy relate to the changes in bicellar mixture morphology observed by NMR at ambient pressure?
- What does the comparison of NMR and calorimetry observations suggest regarding the role of headgroups in the behavior of bicellar mixtures?

To gain insight into these questions, variable-pressure $^2$H-NMR and differential scanning calorimetry (DSC) experiments were performed on DMPC/DHPC bicellar mixtures with molar ratios of 3:1 and 4.4:1. The effect of pressure on bicellar lipid mixtures was previously studied using residual dipolar couplings [38] and a tentative pressure-temperature phase diagram for the DMPC/DHPC system, obtained using small-angle X-ray scattering, was recently reported [33]. Some DSC observations have also been reported [39, 40, 41]. Considered together, the DSC and variable-pressure NMR observations described in this thesis suggest a way of understanding how interactions between the long and short chain lipids in the bicellar mixture drive the observed changes in morphology.

The thesis has been organized in the following way, the objectives of the present work and a short review of some earlier work are presented in Chapter 1. Chapter

2 deals with a brief introduction to lipid assemblies and their phases and a review of bicellar mixtures in which we are interested. Chapter 3 includes NMR theory relevant to the experiments. Details of experimental techniques are given in Chapter 4. In Chapter 5 experimental results and discussions are presented. A summary and concluding remarks are presented in Chapter 6.

# Chapter 2

# Lipid Assemblies

Phospholipids and their assembled structures have been an area of intense study for the past several decades. Some reviews on phospholipids and membrane properties can be found in the literature [2, 3, 42].

Lipid molecules consist of a polar head group which can be charged or zwitterionic, thus tending to interact with water, and an apolar hydrocarbon chain region which avoids water due to the hydrophobic effect. Lipid molecules can exist in a variety of organized structures under hydration. The particular polymorphic forms of lipid assemblies depend not only on the structure of the lipid molecules and the degree of hydration but also on variables such as temperature, pressure, ionic strength and pH [2]. When the hydration level is high the multi-bilayers manage to form larger closed structure called liposomes. The multibilayer liposomes are known as multi-lamellar vesicles (MLV) while single bilayer liposomes are called uni-lamellar vesicles (ULV). Examples of lipid assemblies in aqueous environments are shown in Fig. 2.1.

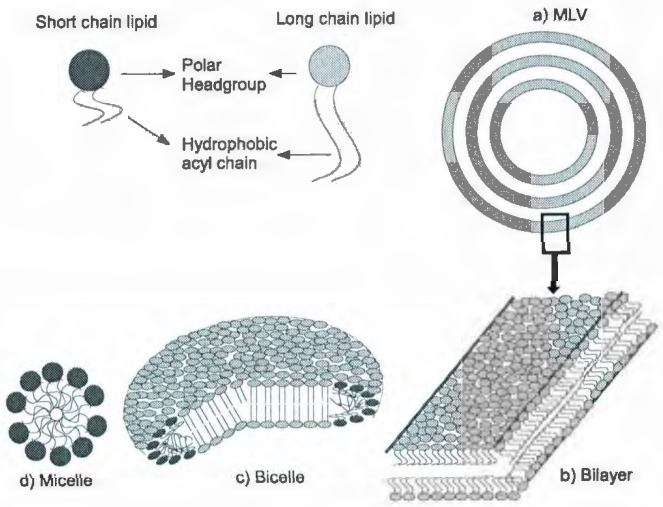


Figure 2.1: Lipid aggregates: a) Multi-lamellar vesicles (MLV), b) Partial lipid bilayer formed by long chain lipids c) Bicelle formed by short and long chain lipids mixtures under certain condition, d) Micelle formed by short chain lipids.

## 2.1 Lipid Phases

Several phases have been reported for lipid assemblies in contact with water [3]. The attractive van der Waals interaction between adjacent lipid molecules and the hydrophobic nature of the lipid chains are important factors for determining the phase behavior of lipid assemblies. Lipids with relatively long chains (typically carbon number above 10) have more area over which interaction takes place. This increases the strength of the Van der Waals interactions and eventually decreases the lipid mobility. Lipids with relatively short chains (carbon number about 6) show more fluidity than long chain lipids at a given temperature, meaning that acyl chains are typically more disordered for short chain lipids for given conditions [43]. At high lipid concentrations short chain lipids form micelles as a consequence of hydrophobic effect [44] while long chain lipids form two dimensional bilayered sheets or lamellae. The

lamellar phase can show different states depending on temperature.

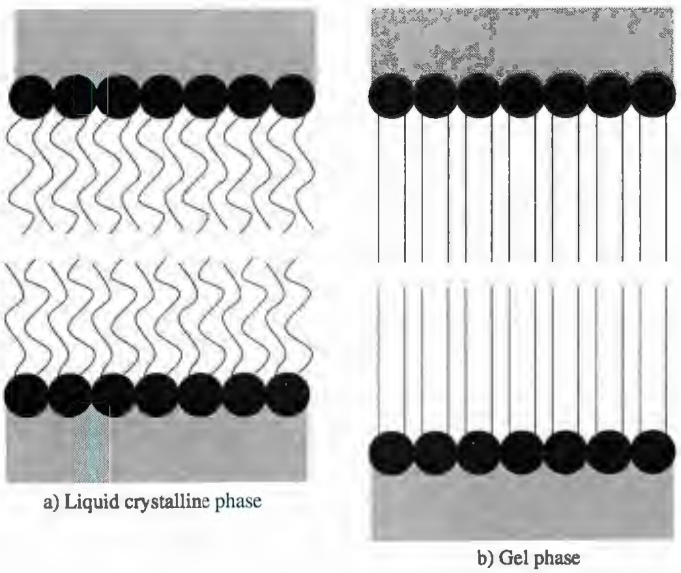


Figure 2.2: Lipid bilayer phases: a) Lamellar liquid crystalline ($L_\alpha$) phase (lipid chains are disordered), b) Lamellar gel ($L_\beta$) phase (lipid chains are ordered).

*Lamellar gel phase:* At low temperature, bilayers of long chain lipids such as DMPC are in the lamellar gel phase ($L_\beta$). In this phase the hydrocarbon chains are mostly ordered into the all-trans configuration. The area per lipid decreases with increasing chain order. Consequently lipids with larger head groups (such as PCs) can be tilted with respect to the membrane normal. This tilted gel phase is denoted by $L'_\beta$ [3, 18]. Moreover, the full extension of the hydrocarbon chains increases the bilayer thickness. Another phase that can be observed at low temperature, due to the mismatch between the headgroup and the acyl chain volume, is known as ripple gel phase.

*Lamellar liquid crystalline phase:* At high temperature the hydrocarbon chains are mostly disordered by trans-gauche isomerisation around carbon-carbon bonds and lipid molecules can diffuse laterally through the bilayer. Generally most lipids in biological membranes are in this fluid or lamellar liquid crystalline phase ($L_\alpha$) [3, 18]. Depictions of liquid crystalline and gel phases are shown in Figs. 2.2(a) and 2.2(b) respectively.

## 2.2 Bicellar Mixtures

As stated earlier, 'bicellar mixtures' consist of long chain (12-18 carbons) plus short chain (6-8 carbons) lipids in a mixture. Assemblies of such mixtures represent a crossover between lipid vesicles and micelles. The binary mixtures of short and long chain lipids have been treated as 'bicelles' in general by many researchers since they first began to attract experimental interest. This approach was based on the assumption that the mixtures can form disks and become oriented in a magnetic field at certain ranges of temperature. The terminology 'bicelles' was first proposed by Charles R. Sanders in 1995 to describe the lipid mixtures as 'bilayered micelles' following the pioneering work of Preetha Ram in James Prestgard's lab at Yale university who first observed magnetic alignment of anionic bile salt-phosphatidylcoline mixtures in 1988 [14, 45]. Several reviews of bicellar mixture properties are available [10, 15, 28, 46, 47].

In order to explore the structure and dynamics of membrane proteins and associated macromolecules in their natural membrane environment, several model membrane-like systems have been explored such as micelles, unilamellar vesicles (ULV), multilamellar vesicles (MLV), and mechanically enhanced oriented bilayers stacked on glass surfaces [46]. Magnetically oriented bilayered model membranes have been of particular interest because of the ease with which they can be attained in an

aqueous environment. We have used DMPC/DHPC mixtures to study bicellar mixture properties, as both the lipid components are easily obtainable in normal and chain deuterated form and such mixtures have been studied extensively by others [8, 9, 10, 11, 12, 13, 26, 27, 28, 29, 32, 33]. Structural properties of DMPC and DHPC lipids are given in the following section.

### 2.2.1 Structural properties of DMPC and DHPC lipids

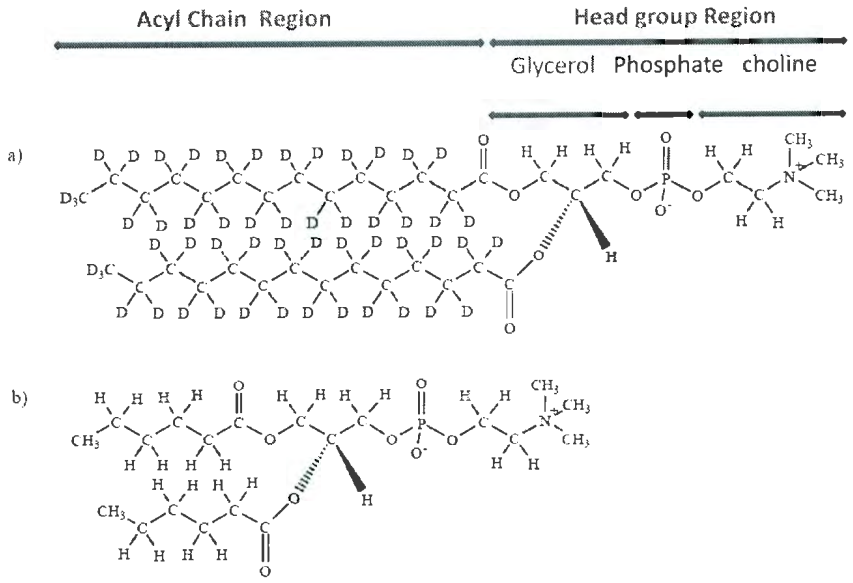


Figure 2.3: Chemical structure of lipids, e.g., a) DMPC-$d_{54}$ with the acyl chains perdeuterated and b) DHPC lipids.

In this work, 1,2-dimyristoyl-*sn*-glycero-3-phosphocholine (DMPC), 1,2-dihexanoyl-

*sn*-glycero-3-phosphocholine (DHPC) and their deuterated analogues, 1,2-dimyristoyl-$d_{54}$-*sn*-glycero-3-phosphocholine (DMPC-$d_{54}$), 1,2-dihexanoyl-$d_{22}$-*sn*-glycero-3- phosphocholine (DHPC-$d_{22}$) have been used to prepare the bicellar mixtures. The molecular structure of deuterated DMPC (14:0/14:0), DMPC-$d_{54}$ and DHPC (6:0/6:0) lipids are shown in Fig. 2.3. Both the lipids are saturated and zwitterionic in nature. When dispersed in water, DMPC forms smectic lamellar phase bilayers whereas DHPC forms micelles [5, 6, 7]. These phospholipids consist of two fatty acids, a glycerol backbone and a phosphocholine headgroup. The headgroup end of the molecule is hydrophilic because of the charge separation. The carbon chain region of the fatty acids are hydrophobic and attached to the headgroup via the glycerol backbone[3, 48].

### 2.2.2 Morphology of bicellar mixtures

In addition to DMPC/DHPC mixtures, bicellar mixtures can also be prepared from combinations of DMPC/DCPC, DPPC/DHPC, DiOMPC/DiOHPC or TBBPC/DCPC [10, 50, 53]. The morphologies of binary mixtures of short and long chain lipids vary widely and depend upon several physical parameters such as the molar ratio ($q$) between long and short chain lipids, temperature and water content. It has variously been suggested that the morphology of the phase that orients in a strong magnetic field might be disk-shaped micelles, cylindrical wormlike micelles, or perforated lamellae [29, 49, 50]. This phase will be referred to as magnetically-orientable here and will be discussed in more detail below. Magnetic alignment, in this context, means that the bilayer normal is perpendicular to the direction of static magnetic field due to the anisotropy of the magnetic susceptibility of the system.

Bicellar disks of 30-100nm diameter and 4-5nm thickness have been observed by electron microscopy [50, 53]. It was initially believed that the disk-shaped bilayered

micelles could reorient isotropically or be oriented magnetically, depending on the lipid molar ratio [11, 49, 51]. Later, the discoid phase of bicelles formed at low molar ratio ($q \leq 1$) below the gel to liquid crystalline phase transition of the long chain lipid component of the mixtures was identified as the isotropic bicelle phase [52].

There have also been suggestions that the oriented phase is a perforated lamellar morphology composed of multilamellar sheets in which short chain lipids play the role of stabilizing the edges of the holes [30, 31, 53, 54, 55, 56, 57].

### 2.2.3 Proposed structure for magnetically alignable bicellar mixtures

Bicellar mixtures with molar ratios of DMPC/DHPC between 2.5 and 6.7, attain spontaneous alignment in magnetic fields greater than 1 Tesla at temperatures between 25°C and 50°C and lipid concentration between 0.05 and 0.35 g/mL [10, 28, 30, 51, 58]. The onset of orientation on warming is just above the DMPC gel-to-fluid transition temperature. As noted above, several structures for magnetically orientable phases have been suggested in the past. These include discoidal micelles, perforated lamellae, and bilayered ribbons or wormlike micelles. It was generally accepted in the 1990s that the magnetically alignable phases observed by NMR were disk shaped [8, 9, 45, 59]. In 1998, Prosser proposed as the name of this phase, nematic discoidal liquid crystal or discoidal micelles [10]. However, the discoidal micelle model for the magnetically alignable phase has been challenged by many researchers as the model is based only on NMR data. The Katsaras group and a few others found by using small-angle neutron scattering (SANS), polarized optical microscopy (POM) and cryo-transmission electron microscopy (cryo-TEM) that the bilayer disk model is not sufficient to describe the behavior of bicellar lipid mixtures and the tempera-

tures at which magnetic alignment takes place [29, 31, 54, 60]. Based on the scheme inferred from recent small-angle neutron scattering studies [27, 28, 29], the magnetic orientation observed by $^2$H NMR on warming DMPC/DHPC mixtures into the intermediate range of temperature likely reflects a magnetically-alignable chiral nematic phase consisting of entangled wormlike micelles or bilayered ribbons. It was also suggested that in the presence of lanthanide ions, the magnetically-alignable phase might be a smectic phase of perforated bilayers [11, 30, 60]. Using Pluronic F68 as a diffusion marker, recent observations of DMPC/DHPC bicellar mixtures, either neutral or negatively charged, confirm that the magnetically alignable phase is bilayered ribbons for zwitterionic bicellar mixtures and perforated lamellae for charged bicellar mixtures [13].

### 2.2.4 'Bicellar Mixture' Phases

Mixtures of short and long chain lipids such as DMPC and DHPC can undergo thermotropic phase transitions above and below the magnetically oriented phase. Depending on the molar ratio and concentration, such mixtures may form isotropic bicellar disks at low temperature. In the bicellar disks, long chain lipids (such as DMPC) are assembled in planar bilayer regions in which the hydrocarbon chains are mostly ordered while the short chain lipids (such as DHPC) are segregated into the edge regions with high curvature in which the hydrocarbon chains are highly disordered. The bicellar particles undergo rapid thermal reorientation [27, 28]. In the resulting isotropic phase, the bicellar disks possess no long range positional or orientational order. Fig. 2.4(a) shows the cross sectional view of a bicellar disk.

Near the main transition of the long chain lipid, bicellar mixtures show a transition from the isotropic to the nematic phase. The nematic phase has long range

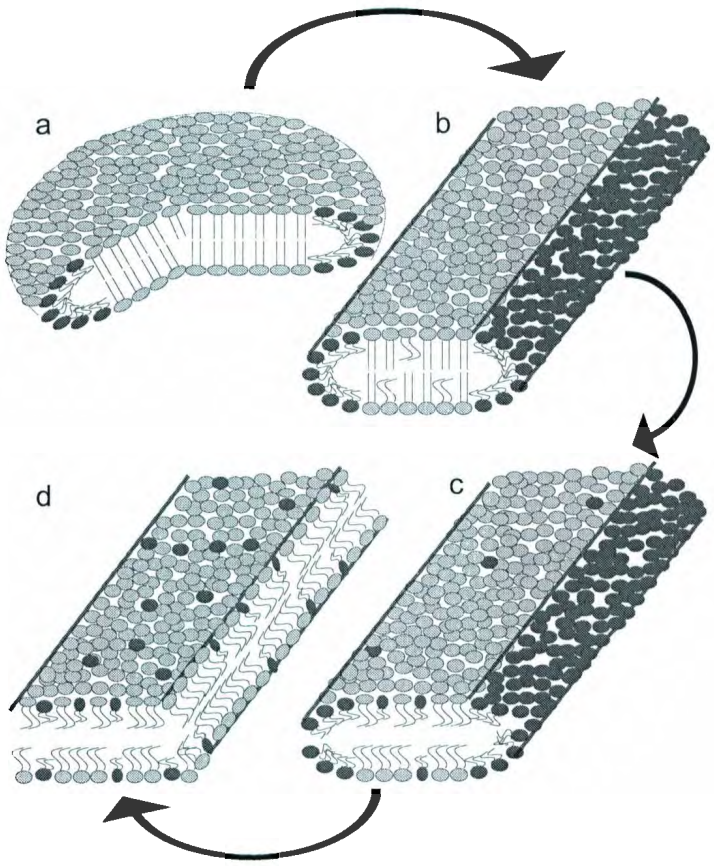


Figure 2.4: Phases for bicellar lipid mixtures: a) Isotropic phase, b) Nematic (partially oriented), c) Chiral Nematic (oriented) and d) Lamellar phase.

orientational order as the bilayer normals tend to align. Fig. 2.4(b) represents the nematic phase of bicellar mixtures where the long chain molecules are presumably in gel-like conformation. Fig. 2.4(c) indicates the chiral nematic phase where the long chain lipid molecules are more fluid and are magnetically aligned. In the chiral nematic phase, long chain lipid chain order is less ordered and characteristic of the liquid crystalline ($L_\alpha$) phase. Some of the short chain lipids from the edge region may diffuse into the bilayer region. At high temperature another phase transition occurs

from chiral nematic to lamellar phase. A typical cross section of a lamellar phase is shown in Fig. 2.4(d). In this phase all the short chain lipids diffuse into the bilayer section and form complete bilayer sheets [13].

# Chapter 3

# $^2$H-NMR Background

Nuclei with angular momentum and magnetic moments precess in a magnetic field with specific frequencies. Application of a current oscillating at the precession frequency to a coil oriented perpendicular to the applied field can tip the magnetic moments away from the applied field. If the duration of this radio frequency pulse is chosen to leave the nuclear magnetic moments precessing in a plane perpendicular to the applied magnetic field, the precessing magnetization can be detected via the oscillating voltage induced into the coil. This effect is generally known as Nuclear Magnetic Resonance.

Precession frequency can be perturbed by electron density at the nucleus (chemical shift), scalar coupling through bonds, quadrupole interaction for spins $\geq 1$, etc. In solution, chemical shift and scalar coupling are important and orientation dependent interactions are averaged to zero. Lipid bilayers fall in the category of partially ordered system and lipids in bilayers reorient anisotropically [61]. As a result, orientation dependent interactions are only partially averaged by molecular motions. Changes in motion at transitions (thermotropic or barotropic) can be detected by probing the relevant interactions by means of NMR.

Deuterium has a nucleus with spin angular momentum $I = 1$ and the precession is perturbed by the orientation-dependent quadrupole interaction. Although deuterium has the drawbacks of low natural abundance, low gyro-magnetic ratio and a spin of 1 rather than $\frac{1}{2}$ compared to the more common nuclei such as $^1$H, $^{13}$C for NMR spectroscopy, deuterium NMR is useful for probing the details of molecular motions in biological membranes. Deuterium NMR can detect changes in molecular anisotropic motions resulting from the changes of temperature or pressure and thus can provide information about amplitude, symmetry of motions and dynamics which can be interpreted in terms of phase behavior, orientational order etc. [61, 62, 63, 64].

## 3.1 The Electric Quadrupole Interaction

In a deuterium NMR experiment, the hydrogen atoms along the hydrocarbon acyl chains of the lipid molecules are replaced by deuterium in order to study lipid motions. That is, for DMPC, which has two saturated chains of length 14, there are 54 carbon-deuterium (C-D) bonds per lipid to give DMPC-$d_{54}$. In the case of DHPC, having only saturated chains of length 6, the number of C-D bonds is 22 to give DHPC-$d_{22}$. The highly anisotropic distribution of electron density in the C-D bond creates an electric field gradient at the positions of the deuteron nuclei. The deuteron quadrupole moment interacts with the electric field gradient of the C-D bond. This interaction perturbs the Zeeman energy levels and splits the resulting transitions. The orientation dependence of the splitting allows the dynamical and re-orientational properties of lipid assemblies to be explored.

As stated at the beginning of this chapter, lipid bilayers can be treated as partially ordered systems with similarities to liquid crystalline systems. The spin Hamiltonian describing the interactions involved in such a liquid crystalline system consists of

the Zeeman Hamiltonian $H_Z$ due to the external fields, the quadrupolar Hamiltonian $H_Q$, the chemical shift Hamiltonian $H_{CS}$, the dipolar Hamiltonian $H_D$ and the scalar spin-spin coupling Hamiltonian $H_J$ due to the local fields [65]. The result is

$$H = H_Z + H_Q + H_{CS} + H_D + H_J. \tag{3.1}$$

For a C-$^2$H bond in a methylene group, the contributions due to the chemical shift, dipolar and spin-spin coupling interactions are much smaller than the quadrupole interaction and they can be neglected. Thus the deuteron can be regarded as an isolated spin-1 nucleus. The quadrupole interaction can be treated as a first order perturbation of the Zeeman interaction (23.2 MHz in a 3.55 T magnetic field) because the quadrupole interaction is small (splitting is less than 252 kHz) [61, 62]. Thus the total Hamiltonian of the system can be written as

$$H = H_Z + H_Q. \tag{3.2}$$

The Hamiltonian for the Zeeman interaction between the magnetic moment and the static magnetic field can be expressed as

$$H_Z = -\gamma\hbar(\vec{I}.\vec{B_0}) = -\gamma\hbar\omega_0 I_z \tag{3.3}$$

where $\vec{I}$ is the spin angular moment, $\gamma$ the gyromagnetic ratio ($2\pi \times 6.536 \times 10^{-6} s^{-1} T^{-1}$ for deuterium), $h$ is Plank's constant divided by $2\pi$, and $\omega_0 = \gamma B_0$ is the nuclear Larmour frequency [64].

The allowed values of $I_z$ are $m$ = -1, 0, +1 and energy levels of the Zeeman interaction are

$$E_m = -\gamma\hbar\omega_0 m. \tag{3.4}$$

For a deuterium atom in a molecule, the Zeeman levels are shifted by the interaction between the electric quadrupole moment of the deuterium nucleus and the

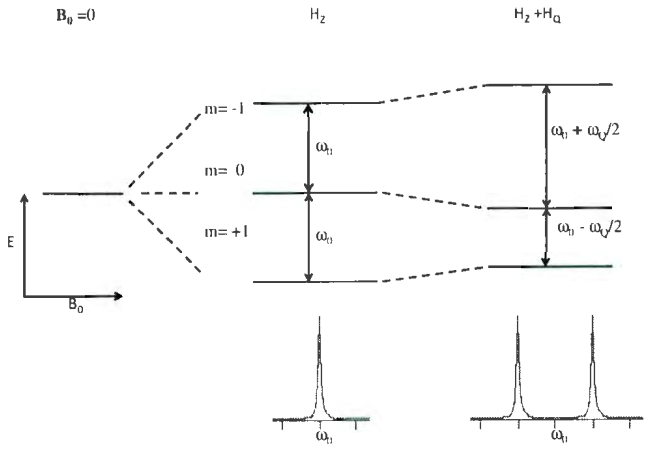


Figure 3.1: Transition between spin states of deuterium under the effect of the Zeeman and quadrupolar interactions. The resulting $^2$H NMR spectrum without (left) and with (right) quadrupole interactions are shown.

electric field gradient in the vicinity of the nucleus. Fig. 3.1 shows the Zeeman levels and $^2$H-NMR spectra for the unperturbed case and in the case of perturbation by the quadrupole interaction. Perturbation of the Zeeman levels separates the resonance into a doublet split by $\omega_Q$.

The energy of interaction of the nucleus with its surrounding charge distribution is given by [61, 66]

$$E = \int \rho(\vec{r})V(\vec{r})d\tau \tag{3.5}$$

where $\rho(\vec{r})$ is the charge density, V($\vec{r}$) is the electric potential and the integral is over the nuclear volume.

Following the treatments of Davis [61] and Slichter [66] the electric potential can be expressed in a Taylor series to give,

$$V(\vec{r}) = V(0) + \sum_{\alpha} \alpha \frac{\partial V}{\partial \alpha}\Big|_{\vec{r}=0} + \frac{1}{2!}\sum_{\alpha}\sum_{\beta} \alpha\beta \frac{\partial^2 V}{\partial\alpha\partial\beta}\Big|_{\vec{r}=0} + \ldots\ldots \tag{3.6}$$

where $\alpha$, $\beta$ = x, y, z.

The interaction energy can be expressed as,

$$E = V(0)\int \rho(\vec{r})d\tau + \sum_{\alpha} V_{\alpha}\int \alpha\rho(\vec{r})d\tau + \frac{1}{2}\sum_{\alpha,\beta} V_{\alpha\beta}\int \alpha\beta\rho(\vec{r})d\tau + \ldots\ldots \tag{3.7}$$

where the first term is the energy of a point charge. The second term involves the electric dipole moment of the nucleus, which is zero as the center of mass and the center of charge coincide. The third term is the energy due to the quadrupole interaction. The quantity

$$V_{\alpha\beta} = \frac{\partial^2 V}{\partial\alpha\partial\beta}\Big|_{\vec{r}=0} \tag{3.8}$$

is the electric field gradient tensor (EFG tensor). The EFG tensor is a symmetric traceless second rank tensor and can be represented by a $3 \times 3$ matrix. The matrix can be diagonalized by a rotation to the principal axis system where $V_{\alpha\beta} = 0$ if $\alpha \neq \beta$. As the electron density at the nucleus is zero, Laplace's equation, $\nabla^2 \mathrm{V} = 0$ must be satisfied. The traceless second rank EFG tensor has five independent components. In the principal axis system, the EFG tensor becomes [61, 64]

$$\mathrm{V}^P = \begin{bmatrix} V_{xx}^P & 0 & 0 \\ 0 & V_{yy}^P & 0 \\ 0 & 0 & V_{zz}^P \end{bmatrix} \tag{3.9}$$

giving two independent diagonal components.

The quadrupolar energy of interaction is given as

$$E_Q = \frac{1}{2}\sum_{\alpha,\beta} V_{\alpha\beta}\int \alpha\beta\rho(\vec{r})d\tau. \tag{3.10}$$

Now the quadrupole moment is defined as

$$Q_{\alpha\beta} = \int (3\alpha\beta - \delta_{\alpha\beta} r^2)\rho(\vec{r})d\tau \tag{3.11}$$

where $\delta_{\alpha\beta} = 1$ if $\alpha = \beta$ or $\delta_{\alpha\beta} = 0$ if $\alpha \neq \beta$ [67]. Therefore,

$$Q_{\alpha\beta} = 3\int \alpha\beta\rho(\vec{r})d\tau - \int \delta_{\alpha\beta} r^2 \rho(\vec{r})d\tau \tag{3.12}$$

so that

$$\int \alpha\beta\rho(\vec{r})d\tau = \frac{1}{3}[Q_\alpha\beta + \int \delta_{\alpha\beta} r^2 \rho(\vec{r})d\tau] \tag{3.13}$$

Substituting Eq. 3.13 to 3.10 gives

$$E_Q = \frac{1}{6}\sum_{\alpha,\beta} V_{\alpha\beta}[Q_{\alpha\beta} + \int \delta_{\alpha\beta} r^2 \rho(\vec{r})d\tau] \tag{3.14}$$

which can be rewritten as

$$E_Q = \frac{1}{6}\sum_{\alpha,\beta}[V_{\alpha\beta}Q_{\alpha\beta} + V_{\alpha\beta}\int \delta_{\alpha\beta} r^2 \rho(\vec{r})d\tau]. \tag{3.15}$$

Because of Laplace's equation, the second term goes to zero [66] and hence

$$E_Q = \frac{1}{6}\sum_{\alpha,\beta} V_{\alpha\beta}Q_{\alpha\beta}. \tag{3.16}$$

The quadrupole Hamiltonian $H_Q$ is expressed as the scalar product of the EFG tensor with the quadrupole moment tensor. Among the different possible formulations of this product, the most convenient one given by Slichter [66], is

$$H_Q = \frac{eQ}{6I(2I-1)}\sum_{\alpha,\beta} V_{\alpha\beta}[\frac{3}{2}(I_\alpha I_\beta + I_\beta I_\alpha) - \delta_{\alpha\beta} I^2] \tag{3.17}$$

where $I$ is the spin angular momentum. In the principal axis system, Eq. 3.17 can be written as

$$H_Q = \frac{eQ}{6I(2I-1)}[V_{xx}(3I_x^2 - I^2) + V_{yy}(3I_y^2 - I^2) + V_{zz}(3I_z^2 - I^2)]. \tag{3.18}$$

Because of Laplace's equation, $V_{xx} + V_{yy} + V_{zz} = 0$, Eq. 3.18 becomes

$$H_Q = \frac{eQ}{6I(2I-1)}[V_{zz}(3I_z^2 - I^2) + (V_{xx} - V_{yy})(I_x^2 - I_y^2]. \tag{3.19}$$

It is convenient to define the (scalar) electric field gradient as [66]

$$eq = V_{zz} \tag{3.20}$$

and the assymmetry parameter as

$$\eta = \left| \frac{V_{xx} - V_{yy}}{V_{zz}} \right| \tag{3.21}$$

with inequality condition $0 \leq \eta \leq 1$.

The nuclear quadrupole Hamiltonian then becomes

$$H_Q = \frac{e^2qQ}{4I(2I-1)}[(3I_z^2 - I^2) + \eta(I_x^2 - I_y^2]. \tag{3.22}$$

where $e$ is charge and $Q$ is the scalar quadrupole moment ($Q_{deuterium} = 2.875 \times 10^{-27} Cm^2$) [64]. Eq. 3.22 is the final expression for the quadrupolar Hamiltonian in the principal axis system of the EFG tensor.

In order to find the effects of the quadupolar Hamiltonian on the Zeeman levels, it is required to transform the EFG tensor from the principal axis system to the laboratory coordinate system [62]. This transformation can be achieved by Wigner rotation matrices $D^{(2)}(\alpha\beta\gamma)$ in a spherical coordinate system. Choosing the Euler angles to be $\alpha = \phi$, $\beta = \theta$, $\gamma = 0$, the quadrupolar Hamiltonian in the laboratory coordinate system becomes

$$H_Q = \frac{e^2qQ}{8}[3I_z^2 - I(I+1)][(3\cos^2\theta - 1) + \eta \sin^2\theta \cos 2\phi] \tag{3.23}$$

In the case of C-$^2$H bonds, the EFG tensor is approximately axially symmetric ($\eta \leq 0.05$), so the term containing $\eta$ can be neglected. Eq. 3.23 becomes

$$H_Q = \frac{e^2qQ}{8}[3I_z^2 - I(I+1)](3\cos^2\theta - 1). \tag{3.24}$$

The total Hamiltonian in this situation can be written as

$$H = -\gamma\hbar B_0 I_z + \frac{e^2qQ}{8}[3I_z^2 - I(I+1)](3\cos^2\theta - 1) \tag{3.25}$$

The energy levels that are shifted by the quadrupolar interaction along with the Zeeman levels are given to first order perturbation where $I = 1$ for deuterium by

$$E_m = -\gamma\hbar B_0 m + \frac{e^2qQ}{8}[(3m^2 - 2)(3\cos^2\theta - 1)] \tag{3.26}$$

where the eigenvalues are $m$ = -1, 0 +1. Thus the three levels for deuterium are

$$E_{+1} = -\gamma\hbar B_0 + \frac{e^2qQ}{8}(3\cos^2\theta - 1), \tag{3.27}$$

$$E_0 = -\frac{e^2qQ}{4}(3\cos^2\theta - 1), \tag{3.28}$$

and

$$E_{-1} = \gamma\hbar B_0 + \frac{e^2qQ}{8}(3\cos^2\theta - 1). \tag{3.29}$$

According to selection rules, $\Delta m = \pm 1$, the resonance energies are

$$E_0 - E_{+1} = \gamma\hbar B_0 - \frac{3e^2qQ}{8}(3\cos^2\theta - 1) \tag{3.30}$$

$$E_{-1} - E_0 = \gamma\hbar B_0 + \frac{3e^2qQ}{8}(3\cos^2\theta - 1) \tag{3.31}$$

The difference between these two resonances gives quadrupole splitting $\Delta\omega_Q$ [68]. Using $E = \hbar\omega$, we get

$$\Delta\omega_Q = \frac{3e^2qQ}{4h}(3\cos^2\theta - 1) \tag{3.32}$$

where $\frac{e^2qQ}{h} \approx 167$ kHz is known as the static quadrupole coupling constant for a deuterium nucleus in a carbon-deuterium bond [64].

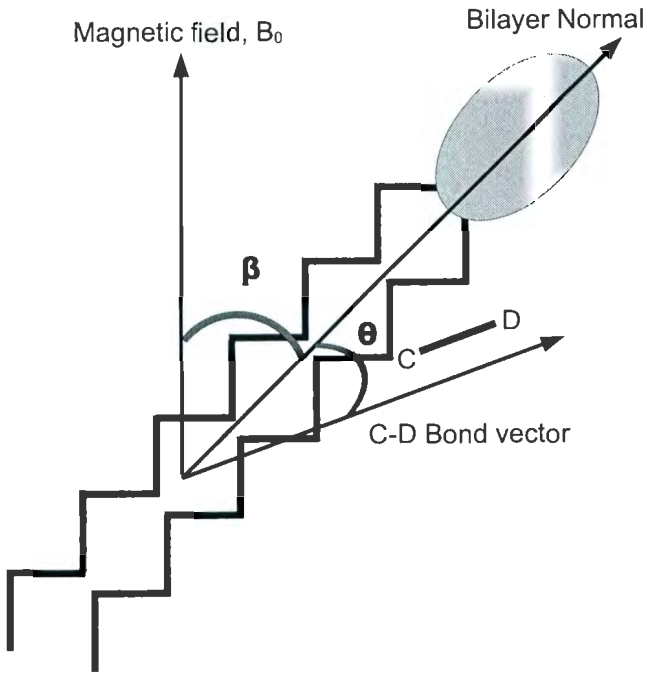


Figure 3.2: Orientation of lipid molecules in bilayer.

## 3.2 Effect of molecular motions and shape of spectrum:

In lipid bilayers, several motions such as reorientation about the bilayer normal and chain fluctuations are present. Eqs. 3.30 and 3.31 in the previous section are based on the assumption of a static C-$^2$H bond, but molecular motions modulate the quadrupolar interaction. Because of the symmetry of motion in a fluid bilayer, it is convenient to transform from the EFG principle axis system to the laboratory frame in two steps.

The first transformation is from the EFG principal axis system to the system attached to the bilayer normal through Euler angles $\alpha$, $\beta$ and $\gamma$. The second transformation is from the system attached to the bilayer normal to the laboratory system through the Euler angles $\alpha'$, $\beta'$ and $\gamma'$. In phospholipid bilayers, the bilayer normal is an axis of symmetry for molecular motions and, in this case, $\alpha'$, $\gamma'$ and $\gamma$ are arbitrary. For simplicity they can be set to zero [61, 62, 63]. However several motions of the C - $^2$H bond relative to the laboratory system modulate the Euler angles ($\alpha$, $\beta$ and $\beta'$). Faster motions (rotations, fluctuation and trans-gauche isomerization in chains) of the C - $^2$H bond about the bilayer normal modulate $\alpha$ and $\beta$ while much slower motions of the bilayer normal relative to the lab system modulate the angle $\beta'$. Choosing the Euler angles $\alpha = \phi$, $\beta = \theta$ and $\beta' = \beta$ for convenience, the quadrupolar Hamiltonian can then be written as

$$\langle H_Q \rangle = \frac{e^2qQ}{16}[3\cos^2\beta - 1]\left\langle (3\cos^2\theta - 1) + \eta\sin^2\theta\cos 2\phi \right\rangle [3I_z^2 - 2] \tag{3.33}$$

where the angular bracket denotes time average over chain motions in the time scale of the experiment. If we assume axially symmetric motions, $\eta$ is zero. Hence

$$\langle H_Q \rangle = \langle \omega_Q \rangle [I_z^2 - \frac{2}{3}] \tag{3.34}$$

where $\langle \omega_Q \rangle$ is quadrupole splitting and is given by the equation

$$\langle \omega_Q \rangle = \frac{3e^2qQ}{8h}(3\cos^2\beta - 1)\left\langle 3\cos^2\theta - 1 \right\rangle . \tag{3.35}$$

This expression is approximately correct for the C - $^2$H bonds in the lipid hydrocarbon chain where $\eta$ is very small [62, 64].

The quadrupole splitting can be expressed in terms of an orientational order parameter, $S_{CD}$, which is defined by

$$S_{CD} = \frac{1}{2}\left\langle 3\cos^2\theta - 1 \right\rangle . \tag{3.36}$$

In terms of the orientational order parameter, the quadrupole splitting can be written as

$$\langle \omega_Q \rangle = \frac{3e^2qQ}{4h}(3\cos^2\beta - 1)S_{CD} \tag{3.37}$$

or

$$\Delta\nu_Q = \frac{3e^2qQ}{4h}(3\cos^2\beta - 1)S_{CD}. \tag{3.38}$$

The average in $S_{CD}$ reflects the motions experienced by the C-$^2$H bond in the hydrocarbon chains of the lipid molecules on the NMR time scale. An average of the order parameter over all deuterated sites, $\langle S_{CD} \rangle$ can be used to characterize the state of an ordered, anisotropic system undergoing molecular motions. The orientational order parameter is zero for fast, isotropic reorientation and is one for extended, rigid acyl chains.

The structure of the $^2$H NMR spectrum is related to the quadrupolar splitting as given in Eq. 3.37. For any particular deuterium on the acyl chain, the spectrum consists of a doublet with intensity at $\omega_0 \pm \Delta\omega_Q$. A spherical distribution of the bilayer normal orientation in a vesicle leads to a superposition of doublets resulting in the powder pattern spectrum shown in Fig. 3.3. This shape is characteristic of fast axially symmetric reorientation in the liquid crystalline phase of spherical vesicles. The prominent edges correspond to the equatorial region having a larger number of population of lipid molecules. In the equatorial region, bilayer normals are perpendicular to the magnetic field direction so that $\beta = 90°$ and the splitting becomes

$$\Delta\nu_Q = \frac{3e^2qQ}{4h}S_{CD}. \tag{3.39}$$

The 0° edges are due to the lipids oriented parallel to the magnetic field direction which gives largest splitting.

Generally, $^2$H NMR spectra provide a way to distinguish different structural phases

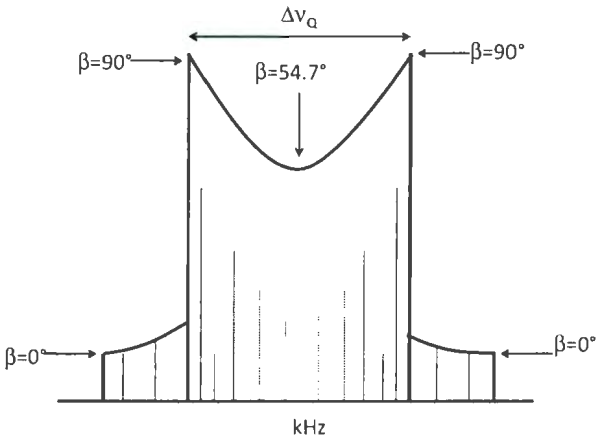


Figure 3.3: $^2$H NMR powder pattern spectrum. The vertical axis indicates intensity.

of a sample. In this work, we are interested in two long and short chain lipid mixtures which form a very complicated system of morphologies with the variation of temperature and pressure. We will use the shape of the $^2$H-NMR spectra to distinguish the states of the mixtures. Fig. 3.4 shows spectra in different phases for DMPC-$d_{54}$/DHPC lipid mixtures at ambient pressure. At low temperature, the spectra are characteristic of isotropic reorientation on the timescale of the quadrupole echo experiment. A typical example of a spectrum in the isotropic phase is shown in Fig. 3.4(a). Fig. 3.4(b) represents the spectrum characteristic of an anisotropic bilayer phase in which chain reorientation is not axially symmetric on the time scale of deuterium NMR experiment. For this spectrum, the sample is presumably in the nematic phase and partially oriented in the magnetic field. With further elevation of temperature, the spectra become characteristic of axially symmetric chain reorientation, about an axis perpendicular to the applied magnetic field. Fig. 3.4(c) shows an example of the oriented phase spectrum in nematic phase. Fig. 3.4(d) represents a spectrum

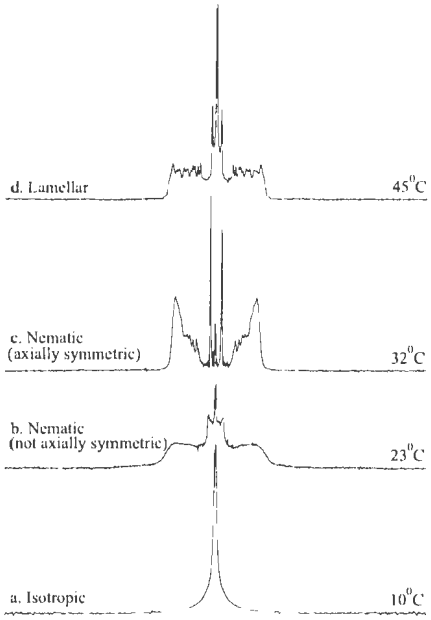


Figure 3.4: $^2$H NMR spectra for DMPC-$d_{54}$/DHPC (3:1) at ambient pressure showing the characteristic of isotropic phase, nematic phase (not axially symmetric and axially symmetric) and lamellar phase.

characteristic of the lamellar phase at high temperature. In the lamellar phase the motions are axially symmetric about a spherical distribution of symmetry axes.

## 3.3 Quadrupole Echo Sequence

$^2$H NMR spectra of partially ordered systems have splittings of tens of kHz. This necessitates the use of short, high power radio frequency (rf) pulses. To avoid distortion due to the resulting receiver dead time, a quadrupole echo pulse sequence [61, 69, 70] is used for $^2$H NMR studies of such systems. This pulse sequence consists of two $\frac{\pi}{2}$

rf pulses separated by a time $\tau$. The pulses are shifted in phase by $\frac{\pi}{2}$. A diagram for the quadrupole echo sequence and echo formation is shown in Fig. 3.5.

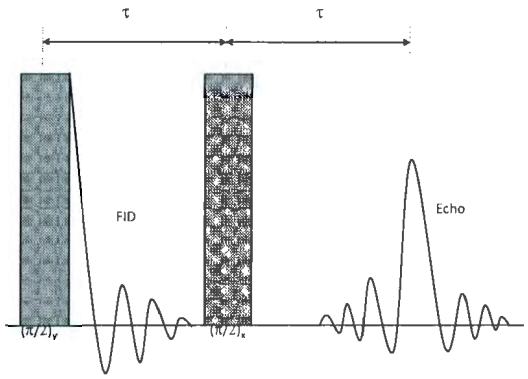


Figure 3.5: Quadrupole echo decay pulse sequence and echo formation.

The first rf pulse excites the spins in the sample, tipping the magnetization 90° away from equilibrium position. The resulting precession of the magnetization about the static field direction is known as the FID (free induction decay). The signal induced in the coil decays at a characteristic time due to the dephasing of the spins in the sample. Following the second $\frac{\pi}{2}$ pulse which inverts the accumulated phase, a refocusing of the nuclear magnetization takes place at a time $2\tau$ after the first pulse. If the delay $2\tau$ is chosen long enough, such that the echo forms after the probe ring down and beyond the dead time of the receiver, an undistorted $^2$H NMR spectrum can be obtained. The echo amplitude observed at time $2\tau$ is sensitive to any molecular motions that modulate the quadrupole interaction during that time. If the pulse separation is increased, the echo occurs at a later time with a decrease in amplitude. The characteristic time for the echo decay is known as transverse relaxation time and is denoted by $T_2^{QE}$. This can be used as a parameter to study the effect of external factors such as temperature and pressure which influence the motions of molecules

on the lipid bilayers system [71].

The quadrupole echo can be understood in terms of the evolution of the density matrix following the two pulses. In order to observe how the two pulses create the quadrupole echo, a density matrix formalism can be used with the assumption that the spin system is in equilibrium at t = 0. The following description is based on treatments by Davis [61, 69] and Bloom [70].

$$Q_1 = \frac{1}{\sqrt{2}} I_x = \frac{1}{2} \begin{pmatrix} 0 & 1 & 0 \\ 1 & 0 & 1 \\ 0 & 1 & 0 \end{pmatrix} \qquad Q_2 = \frac{1}{\sqrt{2}} I_y = \frac{1}{2} \begin{pmatrix} 0 & -i & 0 \\ i & 0 & -i \\ 0 & i & 0 \end{pmatrix}$$

$$Q_3 = \frac{1}{\sqrt{2}} I_z = \frac{1}{\sqrt{2}} \begin{pmatrix} 1 & 0 & 0 \\ 0 & 0 & 0 \\ 0 & 0 & -1 \end{pmatrix} \qquad Q_4 = \frac{1}{\sqrt{6}} (3I_z^2 - 2) = \frac{1}{\sqrt{6}} \begin{pmatrix} 1 & 0 & 0 \\ 0 & -2 & 0 \\ 0 & 0 & 1 \end{pmatrix}$$

$$Q_5 = \frac{1}{\sqrt{2}} (I_x I_z + I_z I_x) = \frac{1}{2} \begin{pmatrix} 0 & 1 & 0 \\ 1 & 0 & -1 \\ 0 & -1 & 0 \end{pmatrix} \qquad Q_6 = \frac{1}{\sqrt{2}} (I_y I_z + I_z I_y) = \frac{1}{2} \begin{pmatrix} 0 & -i & 0 \\ i & 0 & i \\ 0 & -i & 0 \end{pmatrix}$$

$$Q_7 = \frac{1}{\sqrt{2}} (I_x^2 - I_y^2) = \frac{1}{\sqrt{2}} \begin{pmatrix} 0 & 0 & 1 \\ 0 & 0 & 0 \\ 1 & 0 & 0 \end{pmatrix} \qquad Q_8 = \frac{1}{\sqrt{2}} (I_x I_y + I_y I_x) = \frac{1}{\sqrt{2}} \begin{pmatrix} 0 & 0 & -i \\ 0 & 0 & 0 \\ i & 0 & 0 \end{pmatrix}$$

$$Q_9 = \epsilon = \frac{1}{\sqrt{3}} \begin{pmatrix} 1 & 0 & 0 \\ 0 & 1 & 0 \\ 0 & 0 & 1 \end{pmatrix}$$

Table 3.1: Nine dimensional operator space [61].

The time dependent density matrix for a spin-1 system can be written as a superposition of orthogonal operators as

$$\rho(t) = \sum_q C_q(t) Q_q = C_3(t) Q_3 \tag{3.40}$$

where, at $t = 0$,

$$C_3(0) = \frac{\sqrt{2}\hbar\omega_0}{3k_B T}. \tag{3.41}$$

The operator space $Q_q$ has nine dimensions and is expressed in terms of nine $[(2I+1)^2]$ $3 \times 3$ matrices given in table 3.1.

In terms of the basis operator $Q_q$, the Zeeman Hamiltonian for the effect of the applied magnetic field along z-axis can be expressed as

$$H_Z = -\sqrt{2}\omega_0 Q_3. \tag{3.42}$$

In the rotating frame, the Hamiltonian during first rf pulse, of strength $\omega_1$ along x-axis for a time $t_{\omega_1}$, is given by

$$H_1 = -\sqrt{2}\hbar\omega_1 Q_1 \tag{3.43}$$

The evolution of the density matrix is described by the quantum mechanical form of the Liouville theorem [67],

$$i\hbar\frac{d\rho}{dt} = [H, \rho]. \tag{3.44}$$

The resulting equation of motion for the evolution of the state vector under the influence of $H_1$ is

$$i\hbar\frac{d}{dt}[\sum_q C_q(t) Q_q] = -\sqrt{2}\hbar\omega_1 [Q_1, \sum_q C_q(t) Q_q]. \tag{3.45}$$

The necessary commutators for $Q_1$ with other $Q_i$ are,

$$[Q_1, Q_3] = -\frac{i}{\sqrt{2}} Q_2 \tag{3.46}$$

and

$$[Q_1, Q_2] = \frac{i}{\sqrt{2}} Q_3. \tag{3.47}$$

Eq. 3.45 then becomes

$$i\hbar[\frac{dC_2}{dt}Q_2 + \frac{dC_3}{dt}Q_3] = -\sqrt{2}\hbar\omega_1[C_3(\frac{-i}{\sqrt{2}})Q_2 + C_2(\frac{i}{\sqrt{2}})Q_3]. \tag{3.48}$$

Multiplying from left by $Q_2$ or $Q_3$ and taking the trace, we obtain

$$\frac{dC_2}{dt} = \omega_1 C_3 \tag{3.49}$$

and

$$\frac{dC_3}{dt} = -\omega_1 C_2. \tag{3.50}$$

Differentiating Eq. 3.49 with respect to time $t$ and substituting from Eq. 3.50 gives

$$\frac{d^2C_2(t)}{dt^2} = -\omega_1^2 C_2(t). \tag{3.51}$$

The solution of the second order differential equation, Eq. 3.51 is

$$C_2(t) = A\cos(\omega_1 t) + B\sin(\omega_1 t). \tag{3.52}$$

The initial condition $C_2(0) = 0$ gives A = 0, so that

$$C_2(t) = B\sin(\omega_1 t). \tag{3.53}$$

Differentiating Eq. 3.53 and substituting the result into Eq. 3.49 gives an expression for $C_3(t)$. Using the value of $C_3(0)$ from Eq. 3.41 finally gives

$$C_2(t_{\omega_1}) = \frac{\sqrt{2}\hbar\omega_0}{3k_BT}\sin(\omega_1 t_{\omega_1}) \tag{3.54}$$

and

$$C_3(t_{\omega_1}) = \frac{\sqrt{2}\hbar\omega_0}{3k_BT}\cos(\omega_1 t_{\omega_1}). \tag{3.55}$$

The state vector thus precesses in $(Q_2, Q_3)$ plane of the operator space with frequency $\omega_1$. If the pulse duration and amplitude are such that $\omega_1 t_{\omega_1} = \frac{\pi}{2}$, then a state vector initially along the positive z-axis will rotate into the positive y-axis [61].

We will assume that the pulse has the right duration to leave only $C_2$ non-zero. The system now starts from non-zero $C_2$ and evolves for time $\tau$ under the influence of the axially symmetric quadrupole Hamiltonian

$$H_Q = \frac{1}{3}\omega_Q(3I_z^2 - 2) = \sqrt{\frac{2}{3}}\hbar\omega_Q Q_4. \tag{3.56}$$

The equation of motion during this time is,

$$i\hbar\frac{d}{dt}[\sum_q C_q(t)Q_q] = -\sqrt{\frac{2}{3}}\hbar\omega_Q[Q_4, \sum_q C_q(t)Q_q]. \tag{3.57}$$

Now we need the operator which is coupled to $Q_2$ by rotation about $Q_4$. As before, we find that $C_2$ couples to $C_5$. The time derivatives of $C_2$ and $C_5$ can be calculated as before and are given by

$$\frac{dC_2}{dt} = \omega_Q C_5 \tag{3.58}$$

and

$$\frac{dC_5}{dt} = -\omega_Q C_2 \tag{3.59}$$

with solutions,

$$C_2(\tau) = \frac{\sqrt{2}\hbar\omega_0}{3k_BT}\cos(\omega_Q\tau) \tag{3.60}$$

and

$$C_5(\tau) = \frac{\sqrt{2}\hbar\omega_0}{3k_BT}\sin(\omega_Q\tau). \tag{3.61}$$

These solutions indicate that the state vector precesses in the $(Q_2, Q_5)$ plane about $Q_4$ with angular frequency $\omega_Q$.

The second pulse is now applied along the y axis in rotating frame and used to form the quadrupole echo. Both coefficients $C_2$ and $C_5$ are non-zero during this pulse

[61]. The evolution of both coefficients can be calculated by using the Hamiltonian

$$H_2 = -\sqrt{2}h\omega_2 Q_2 \tag{3.62}$$

where $\omega_2$ is the strength of second pulse with duration $t_{\omega_2}$. The resulting equation of motion due to the second pulse is then

$$i\hbar\frac{d}{dt}[\sum_q C_q(t)Q_q] = -\sqrt{2}h\omega_2[Q_2, \sum_q C_q(t)Q_q]. \tag{3.63}$$

Because $[Q_2, Q_2] = 0$,

$$\frac{dC_2}{dt} = 0 \tag{3.64}$$

and $C_2$ is unaffected by the transverse field during the pulse. The evolution resulting from $H_Q$ can be neglected when $\omega_Q \ll \omega_2$. One of the commutators needed is

$$[Q_2, Q_5] = \frac{i}{\sqrt{2}}(Q_7 - \sqrt{3}Q_4). \tag{3.65}$$

In addition

$$[Q_2, Q_4] = \frac{3i}{\sqrt{6}}Q_5 \tag{3.66}$$

and

$$[Q_2, Q_7] = -\frac{i}{\sqrt{2}}Q_5 \tag{3.67}$$

We thus obtain

$$[Q_2, (Q_7 - \sqrt{3}Q_4)] = -\sqrt{2}iQ_5. \tag{3.68}$$

Using the Eqs. 3.63 - 3.68 we finally get

$$\frac{dC_5}{dt} = -2\omega_2[\frac{1}{2}(\sqrt{3}C_4 - C_7)], \tag{3.69}$$

$$\frac{dC_4}{dt} = \omega_2\sqrt{3}C_5, \tag{3.70}$$

and

$$\frac{dC_7}{dt} = -\omega_2 C_5. \tag{3.71}$$

Similarly, we can write

$$\frac{d}{dt}[\frac{1}{2}(\sqrt{3}C_4 - C_7)] = 2\omega_2 C_5. \tag{3.72}$$

Thus $C_5$ is coupled to $\frac{1}{2}(\sqrt{3}C_4 - C_7)$. Combining the Eqs. 3.69, 3.70 and 3.71, we obtain

$$\frac{d^2C_5}{dt^2} = -4\omega_2^2 C_5. \tag{3.73}$$

The solution of this second order differential equation 3.73 for $t_{\omega_2}$ with $\omega_2 t_{\omega_2} = \frac{\pi}{2}$ is written as

$$C_5(t_{\omega_2}) = \frac{\sqrt{2}\hbar\omega_0}{3k_BT}\sin(2\omega_Q\tau) \tag{3.74}$$

Also

$$\frac{1}{2}[\sqrt{3}C_4(t_{\omega_2}) - C_7(t_{\omega_2})] = 0. \tag{3.75}$$

Above equations imply that the state vector rotates about $Q_4$ in the ($Q_5$, $\frac{1}{2}[\sqrt{3}Q_4 - Q_7]$) plane with angular frequency $2\omega_2$.

After the pulse the system evolves under the influence of quadrupole Hamiltonian and $C_2$ and $C_5$ are given by

$$C_2(t) = \frac{\sqrt{2}\hbar\omega_0}{3k_BT}\cos[\omega_Q(t-2\tau)] \tag{3.76}$$

$$C_5(t) = -\frac{\sqrt{2}\hbar\omega_0}{3k_BT}\sin[\omega_Q(t-2\tau)] \tag{3.77}$$

The quadrupole echo signal can be attained from the expression of $C_2(t)$ which is expressed as

$$\langle I_y(t)\rangle = \frac{\sqrt{2}\hbar\omega_0}{3k_BT}\cos[\omega_Q(t-2\tau)] \tag{3.78}$$

The Eq. 3.78 describes a signal which is symmetric about $t = 2\tau$ and has a maximum at this time. If we neglect the relaxation, the amplitude should be equal to the amplitude of initial FID. In this way, the quadrupole echo recovers the $^2H$-NMR signal completely a time $2\tau$ after the first pulse which may be chosen longer than the receiver deadtime.

# Chapter 4

# Experimental Setup

## 4.1 Sample Preparation

All the lipids (DMPC, DHPC and the chain perdeuterated versions of these lipids DMPC-$d_{54}$, DHPC-$d_{22}$) were purchased from Avanti Polar Lipids (Alabaster, AL) in powder form and used without further purification. Dry lipids, with either DMPC or DHPC chain perdeuterated, were combined to give DMPC/DHPC molar ratios of either 3:1 or 4.4:1 and a total lipid mass of 17-40 mg. Dry lipid mixtures were then dissolved in 2:1(v/v) chloroform/methanol. The solvent was removed by rotary evaporation at 45°C and then held under vacuum in a dessication chamber overnight to remove residual solvent. Samples were then hydrated in 300-500 $\mu$L of 100 mM HEPES buffer (pH = 7), vortexed, and sonicated with sonicator bath for 15 minutes with the heater turned off, followed by 4-5 cycles of freezing and thawing to make the dispersion more homogeneous. Excess buffer, if any, was removed by centrifuging the sample for a minute and then drawing off any excess buffer with a polyethylene pipette. In order to maximize the amount of lipid in the NMR sample. Samples were sealed in polyethylene capsules formed by heat-sealing the ends of short segments

of disposable pipettes. These pillow shaped capsules were used because hydrostatic pressure cannot be transmitted to samples through traditional NMR glass tubes. For DSC measurements, the same protocol to prepare the samples was followed except for the addition of more buffer to give a concentration of approximately 2 mg/ml before sonication and freeze/thaw cycling. Samples of DMPC/DHPC for both molar ratios were prepared specifically for DSC, and small samples for DSC were also extracted during preparation of the DMPC-$d_{54}$/DHPC (4.4:1) and DMPC/DHPC-$d_{22}$ (4.4:1) mixtures for NMR. All samples were kept in a freezer at about -18°C when not in use.

## 4.2 $^2$H-NMR

### 4.2.1 $^2$H Spectrometer

Wideline deuterium NMR spectra at selected temperatures and pressure were obtained using a spectrometer [72] based on a 3.5 T superconducting magnet (Nalorac Cryogenics, Martinez, CA) corresponding to a $^2$H resonance frequency of 23.2 MHz and a locally assembled data acquisition system. The NMR probe used was a variable-pressure [73] design with a beryllium copper cell into which the coil and polyethylene sample cell can be inserted and pressurized with hydraulic oil (AW ISO grade 32). Pressures were measured using a Bourdon tube gauge. The temperature of the sample pressure cell was measured using a thermocouple and controlled to ±0.1°C using an Omega (Laval, QC) CYC3200 temperature controller.

The NMR spectrometer consists of a 1kW amplifier (Herley Industries Inc., Lancaster, PA), quadrature detector, a pulse programmer, and a computer to collect the data. Fig. 4.1 shows a block diagram of the spectrometer. A brief description of the

operation of the spectrometer follows. The PTS-160 frequency synthesizer provides a

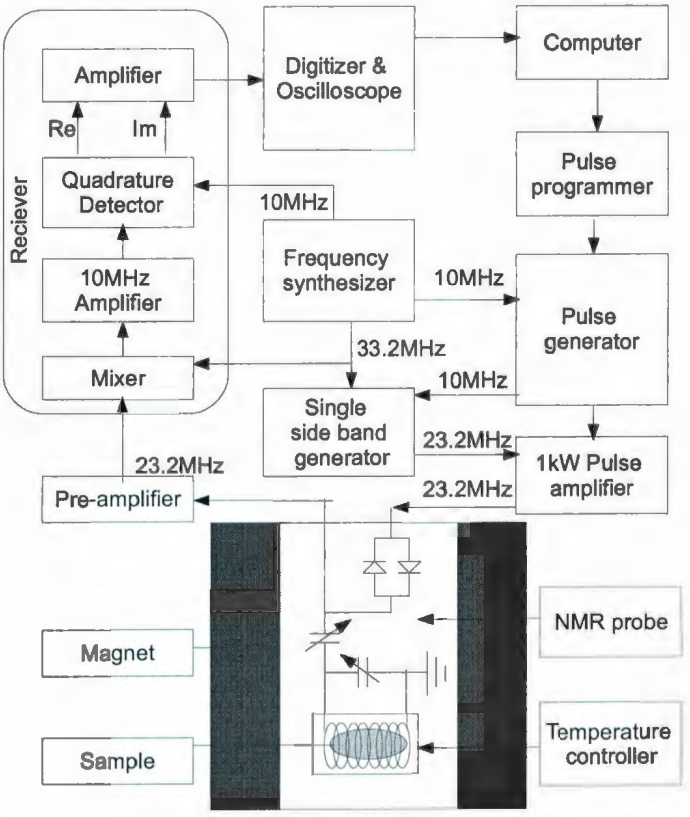


Figure 4.1: Block diagram of $^2$H NMR spectrometer.

33.2 MHz reference to the single sideband generator and a 10 MHz signal to the pulse generator. The 10 MHz signal is converted into pulses with phases of 0, $\frac{\pi}{2}$, $\pi$ and $\frac{3\pi}{2}$ in the pulse generator under the control of the pulse programmer. The 10 MHz pulses are then fed into the single side band generator where the 33.2 MHz and 10 MHz signals are combined to produce radio frequency pulses at the deuterium resonance frequency of 23.2 MHz. The 1 kW amplifier amplifies the pulse and transmits it into the sample through the probe tuning circuit and the rf coil. The sample produces a

weak signal which is amplified by the preamplifier. The signal is then fed into the receiver which combines the 23.2 MHz NMR signal with a 33.2 MHz continuous wave signal from the frequency synthesizer to generate a 10 MHz carrier modulated by the NMR signal. This signal is sent to an amplifier in the receiver section and then to the quadrature detector which separates the real and imaginary parts of the NMR signal by comparing it with the 10 MHz reference signal coming from the frequency synthesizer. The NMR signal is amplified again, digitized, and finally sent to the computer for analysis. It is necessary to shift the points in the collected signals by a fraction of the dwell time in order to start the Fourier transform from the top of the echo [62]. To improve the quality of the signal the method of oversampling [74] was used. Data collection and analysis was done with a visual basic NMR program, MEMNMR written by Jason Emberley.

### 4.2.2 High Pressure Probe

To apply pressure to the samples in this project, a home-built high pressure probe designed by B. Bonev [73] was used. The probe is capable of experiments at pressures up to 270 MPa and temperatures from -30°C to 70°C. Fig. 4.2 shows a schematic diagram of the high pressure probe adapted from [73] and more details about the system can be found there. An aluminum tube (9) inserted into the superconducting magnet (13) separates the interior of the probe from the magnet wall. Adjustable supports (5-12) allow the sample (2) to be set in the region of highest magnetic field homogeneity. The solid brass rods (5) form the main structural elements of the device. The high pressure chamber (1) is suspended on three thin walled stainless steel tubes (3) that provide thermal insulation between the pressure chamber and the support. All the components of the probe except the Styrofoam insulation (21) and

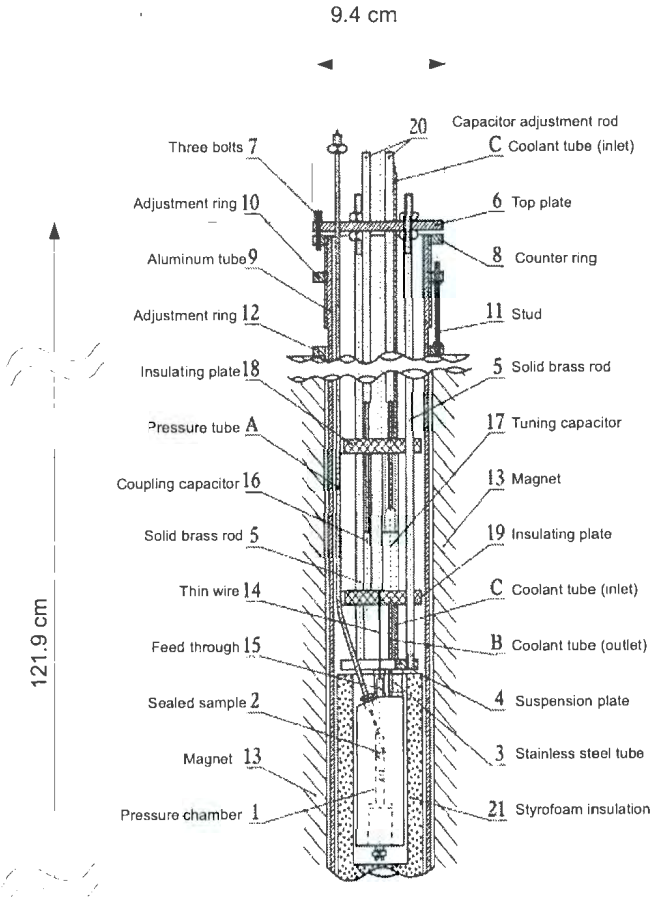


Figure 4.2: High pressure probe (adapted and reprinted, with permission, from [73]).

the external aluminum tube (9) are attached to the top plate (6) through the solid brass rods (5).

### 4.2.3 Experimental Details

To obtain $^2$H-NMR spectra of lipid mixtures, a quadrupole echo sequence $(\frac{\pi}{2})_y$ - $\tau$ - $(\frac{\pi}{2})_x$ -$\tau$- was used [69] with pulses separated by a delay of 35 $\mu$s. The $\frac{\pi}{2}$ pulse length was typically 3 to 4 $\mu$s. The sequence included a 0.1 s pre-pulse interval and a 0.6 s recovery period to allow the sample to completely equilibrate before each pulse pair.

Depending on the signal strength, 8,000 to 20,000 transients were averaged. Free induction decays were digitized with a dwell time of 2 $\mu$s for fluid bilayer phases and 5 $\mu$s for narrow spectra characteristic of micelles or highly disordered phases. Effective digitization dwell times after oversampling [74] were 4 $\mu$s for DMPC-$d_{54}$/DHPC samples and 10 $\mu$s for DMPC/DHPC-$d_{22}$ samples unless otherwise noted. No line broadening was applied except for DMPC/DHPC-$d_{22}$ (3:1) in the nematic temperature range and pressures above ambient where 200 Hz line-broadening was applied to some data sets. The time domain data were then Fourier transformed to obtain frequency domain spectra. Spectra were obtained over a series of temperatures from 10°C to 68°C at ambient pressure, 66 MPa, 102 MPa and 135 MPa. At ambient pressure, data collection started at 10°C and extended to 65°C in 2° steps except for the highest and lowest temperatures where spectral shapes were less sensitive to temperature and 5° steps were used. At higher pressures, the starting temperature was adjusted to accommodate pressure-induced changes in phase boundaries as described below. For each sample composition, at least two independent samples were prepared and studied to test for reproducibility.

Samples were allowed to equilibrate for at least 40 min at each temperature before the start of data collection. In order to attain temperatures below room temperature, air was circulated through a liquid nitrogen heat exchanger and used to cool the copper oven containing the coil and sample in the NMR probe. Over the course of the experiments, some repairs were made to the high pressure probe. Some of the wires connecting the temperature controller to the copper oven of the high pressure probe were broken and repaired. A brass shim in the sample chamber was pulled out as a result of the large size of one sample capsule. The brass shim was subsequently positioned carefully and relatively smaller sample containers used. Prior to acquisition of transients, spectrometer frequency and other parameters were carefully adjusted to

minimize intensity in the imaginary channel. For some DMPC/DHPC-$d_{22}$ samples, the signal-to-noise ratio was limited by the small amounts of deuterated material present. In such cases, the signal-to-noise ratio was increased by zeroing the imaginary channel prior to Fourier transformation.

## 4.3 Differential Scanning Calorimetry (DSC)

Differential Scanning Calorimetry is a useful thermal analysis technique for the study of phase behavior of model or biological membranes. Several reviews of DSC are available [75, 76, 77, 78]. DSC measures excess heat capacity of a vesicle suspension as a function of temperature. The resulting scan can indicate thermotropic phase transitions.

The basic DSC instrument consists of two matched cells for sample and reference solutions mounted in an adiabatic chamber [78]. Both the cells are heated simultaneously at a programmed rate by heaters controlled to maintain zero temperature difference between the cells. In our case the sample is a tiny amount of lipid mixture in a buffer solution while the reference material is the corresponding buffer. When equal amounts of heat are applied to both cells, the temperatures of both the sample and reference increase. A feed-back system adjusts the heat to the sample cell linearly with time in order to maintain zero temperature difference. When the sample undergoes a physical transformation such as a phase transition, a fraction of heat is either absorbed or released by the sample. The instrumental control system then responds to supply more or less heat to the sample cell in order to eliminate any temperature difference between the cells. The data output from the DSC is proportional to the extra power which is required to keep the sample and reference cells at the same temperature.

Multi-lamellar lipid suspensions undergo phase transitions from the gel to fluid phase by absorbing heat. This gives endothermic peaks in the DSC thermogram [77]. The transition is identified as the peak centered at $T_m$. The maximum in excess heat capacity ($C_p$) occurs at $T_m$.

Because $C_p = \frac{dH}{dT}$, the transition enthalpy ($\Delta H_{cal}$, usually expressed in kcal/mol) can be obtained by integration of $C_p$ versus temperature to give

$$\Delta H_{cal} = m \int_{T_1}^{T_2} C_p dT \tag{4.1}$$

where $m$ is the molecular weight, and $T_1$ and $T_2$ are the initial and final temperatures of the transition. In practice, the heat capacity is extracted from the ratio of the excess power supplied to the sample cell ($\frac{dH}{dt}$) and the scan rate ($\frac{dT}{dt}$) [75, 80], so that

$$\Delta H_{cal} = m \int_{T_1}^{T_2} (\frac{dH}{dt})/(\frac{dT}{dt}) dT. \tag{4.2}$$

DSC measurements were performed using a Microcal (Northhampton, MA) MC-2 instrument. The lipid concentration in the sample cell was 2 mg/ml except for DMPC/DHPC (4.4/1) where the concentration was 4 mg/ml. The scan rate for all samples was 30°C/h in the ascending temperature mode up to 55°C after equilibration at 10°C. Data analysis was performed using Origin 6.1 (OriginLab Corp., Northhampton, MA). Prior to integration, the segments of baseline spanning a few degrees above and below the transition on each scan were selected and fit to a quadratic function. The resulting baseline function was subtracted from each scan to give $\Delta C_P$ versus temperature. To check for reproducibility, three consecutive scans of each sample were done. The final two scans of each set were used for analysis.

# Chapter 5

# Results and Discussion

## 5.1 $^2$H-NMR

In order to observe the effects of pressure on lipid chain order and bilayer orientation in bicellar mixtures, $^2$H NMR observations were made on DMPC/DHPC mixtures at molar ratios of 3:1 and 4.4:1 with one or the other lipid chain perdeuterated (DMPC-$d_{54}$/DHPC or DMPC/DHPC-$d_{22}$). These ratios were selected to match previously reported observations [11, 12].

Spectra were collected over a range of temperatures while pressure was held constant as detailed below. Deuterium NMR spectra were collected at ambient pressure and high pressures (66 MPa, 102 MPa and 135 MPa) for each lipid mixture. The temperature range was chosen such that the transitions from isotropic to nematic and nematic to lamellar phase were observed for each pressure. As stated earlier, this identification of phases is based on small-angle neutron scattering observations of bicellar mixtures [27, 28, 29].

Figs. 5.1-5.4 display $^2$H NMR spectra. Vertical bars next to each spectral sequence are used to indicate the approximate temperature range over which each sample is

presumed to be in the nematic phase. It is noted that the vertical bars used here are based solely on DMPC-$d_{54}$/DHPC spectra. Within the range of temperatures identified as corresponding to nematic organization, reorientation of DMPC-$d_{54}$ changes from being not axially symmetric on the characteristic $^2$H NMR time scale to being axially symmetric as temperature is raised.

### 5.1.1 DMPC/DHPC at Ambient Pressure

Fig. 5.1 shows $^2$H NMR spectra at selected temperatures for 3:1 and 4.4:1 molar ratio mixtures of DMPC-$d_{54}$/DHPC and DMPC/DHPC-$d_{22}$ at ambient pressure (the complete set of spectra are given in Appendix A). The sequences of spectra obtained are consistent with those reported previously for DMPC-$d_{54}$/DHPC [8, 11, 12, 26] and DMPC/DHPC-$d_{22}$ [11, 12] mixtures. It should be noted that complete chain-perdeuteration of a lipid bilayer sample typically lowers observed phase transitions by a few degrees. In comparing spectra with one or the other lipid component deuterated, the higher deuteration of the DMPC-$d_{54}$/DHPC samples is therefore expected to lower observed transitions by 2-3° relative to corresponding transitions observed in the DMPC/DHPC-$d_{22}$ mixtures.

At low temperatures for all samples, spectra for both lipid components display narrow peaks that are characteristic of isotropic reorientation on the quadrupole echo experiment timescale. At these temperature, observations by Katsaras and coworkers [13], and Winter and coworkers [33] suggest that the isotropically-reorienting particles are bicelle disks with the edges enriched in the shorter DHPC and the planar regions enriched in DMPC. These bicellar disks are formed below the gel to liquid crystalline phase transition temperature of DMPC.

At 23°C, the ambient pressure DMPC-$d_{54}$/DHPC spectra for both of the lipid ra-

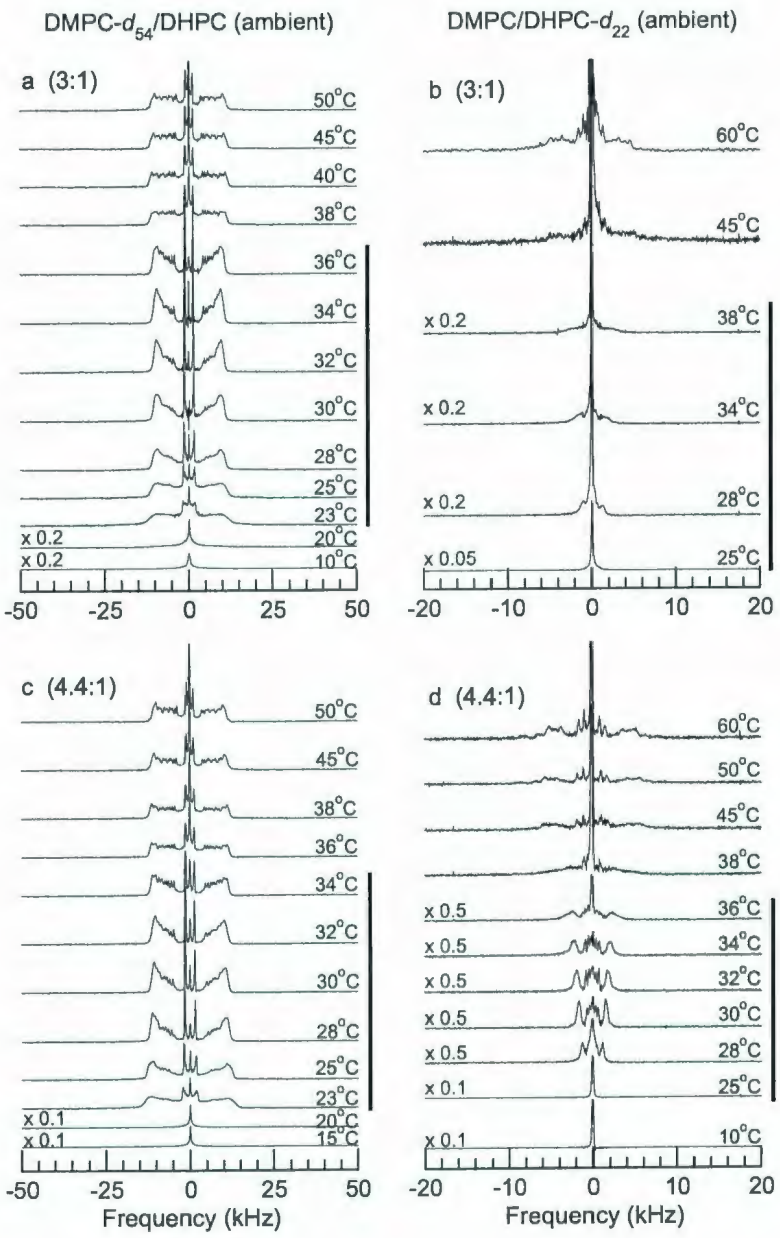


Figure 5.1: $^2$H-NMR spectra at ambient pressure and selected temperatures for dispersions of (a) DMPC-$d_{54}$/DHPC (3:1), (b) DMPC/DHPC-$d_{22}$ (3:1), (c) DMPC-$d_{54}$/DHPC (4.4:1), and (d) DMPC/DHPC-$d_{22}$ (4.4:1) in 100 mM HEPES buffer (pH=7.0). Based on DMPC-$d_{54}$/DHPC spectra, vertical bars next to each spectra indicate the approximate temperature range over which each sample is presumed to be in the nematic phase.

tios become wider and characteristic of an anisotropic bilayer phase in which chain reorientations are more restricted and not axially symmetric on the $^2$H NMR timescale. The corresponding spectra are shown in Figs. 5.1(a) and 5.1(c). The transition at this temperature is presumed to be from isotropically-reorienting bicelles to nematic wormlike micelles and will be referred to as the isotropic to nematic phase transition. The wormlike micelles presumably consist of the short chain lipid, DHPC, at edges and the long chain lipid, DMPC, in the planar region. Just above this transition, the DMPC reorientation is more characteristic of the gel bilayer phase than the liquid crystalline phase. The bilayers normals might be partially oriented with the magnetic field direction but the lack of axially symmetric chain reorientation makes it difficult to judge bilayer orientation.

Between 25°C and 28°C, the DMPC lipid chains become less ordered and both the DMPC-$d_{54}$/DHPC spectra shown in Figs. 5.1(a) and 5.1(c) become increasingly characteristic of axially symmetric chain reorientation, predominantly about an axis perpendicular to the applied magnetic field. Near these temperatures, DHPC molecules begin to interact with DMPC molecules and the DMPC/DHPC-$d_{22}$ spectra becomes less characteristic of isotropic reorientation.

For both DMPC-$d_{54}$/DHPC samples at ambient pressure, the spectra observed in the temperature range 28-36°C and 28-34°C, shown in Figs. 5.1(a) and 5.1(c) respectively, are characteristic of significant, but not complete, bilayer orientation. This may be due to the low magnetic field (3.55 T) available in this variable-pressure spectrometer or it may reflect some orientational metastability in the highly viscous wormlike micelles phase that has previously been identified as the magnetically-orientable morphology of this system [27]. According to Katsaras *et al.*, the sample morphology in the temperature range for which bilayer orientation is seen in a magnetic field is a chiral nematic phase made up of ribbon-like, or worm-like micelles with DHPC

molecules at the edges of the wormlike micelles [13]. It is also mentioned that the temperature range over which partial orientation is observed in our work is lower than that reported by Sternin *et al.* [12] for corresponding samples.

At the lower end of the temperature range in which DMPC-$d_{54}$ begins to display spectra characteristic of anisotropic reorientation, isotropic reorientation of DHPC-$d_{22}$ still persists as mentioned by Sternin *et al.* [12]. This may indicate that DHPC cannot diffuse into the DMPC planar regions until the temperature has risen into the range where DMPC-$d_{54}$ begin to melt and displays axially-symmetric reorientation.

Spectra from the DMPC/DHPC-$d_{22}$ sample with molar ratio 4.4:1 in the temperature range 28-34°C (Fig. 5.1d) contain almost no component characteristic of isotropic reorientation. Orientational order parameters from these spectra are small but non zero. This implies that effectively all of the DHPC is partially oriented. The spectra in this range are qualitatively similar to those reported by Sternin *et al.* [12] except for the lower degree of magnetic orientation and the small discrepancy in temperatures.

In addition to a DHPC-$d_{22}$ population undergoing anisotropic reorientation in the intermediate range of temperature identified as corresponding to the nematic phase, spectra for the 3:1 mixture of DMPC/DHPC-$d_{22}$, shown in Fig. 5.1(b), also indicate a significant DHPC-$d_{22}$ fraction that reorients isotropically. This may be due to the higher fraction of short chain lipid in the DMPC/DHPC-$d_{22}$ (3:1) sample.

The narrow peaks at the spectral midpoints (Fig. 5.1a and 5.1c) suggest that a very small fraction of DMPC-$d_{54}$ reorients isotropically in the nematic phase temperature range. Spectra characteristic of magnetic orientation persist to between 36°C and 38°C for DMPC-$d_{54}$/DHPC (3:1) and to between 34°C and 36°C for DMPC-$d_{54}$/DHPC (4.4:1). Spectra for both DMPC-$d_{54}$/DHPC (3:1) and DMPC-$d_{54}$/DHPC (4.4:1) display sharp transition from the magnetically alignable phase to the lamellar

phase at 38°C and 36°C as shown in Figs. 5.1(a) and 5.1(c) respectively.

Near the upper end of the nematic temperature range shown in Fig. 5.1, more DHPC molecules are lost from the edges of wormlike micelles or bilayered ribbon and incorporated into the DMPC-rich bilayered region and the ordering of DHPC increases with temperature (Fig. 5.1b and 5.1d). Katsaras and coworkers suggest that the bilayered ribbon's edges become unstable causing individual ribbons to partially fuse to form the regions with extended lamellar sheets and then fold into multi-lamellar vesicles as temperature is increased further [13]. Above these temperatures, spectra from the DMPC-$d_{54}$ component are characteristic of axially symmetric reorientation about a spherically-distributed symmetry axis presumably in a lamellar phase.

The corresponding spectra for DMPC/DHPC-$d_{22}$ in the lamellar phase temperature range are superpositions of doublets with distinct splittings suggesting distributions of orientational order parameters along the DHPC-$d_{22}$ chain. The 60°C spectrum for DMPC/DHPC-$d_{22}$ (3:1) was obtained by averaging 20,000 transients with an effective dwell time 4 $\mu$s in order to increase signal-to-noise ratio. The resulting spectrum is similar to the spectrum previously reported by Sternin *et al.* at 60°C for DMPC/DHPC-$d_{22}$ (4.55:1) [12]. While differences in quadrupole echo decay time and optimization of the spectrometer for wideline spectroscopy rule out quantitative analysis of the partitioning of lipid components between isotropic and anisotropic environments, the spectra for DMPC/DHPC-$d_{22}$ (3:1) indicate a significant fraction of isotropically-reorienting DHPC-$d_{22}$ across both the nematic and lamellar phase temperature ranges. As also noted by Sternin and coworkers [12], the observed spectra suggest that DHPC-$d_{22}$ in the lamellar phase is present in two anisotropic environments characterized by different degrees of orientational order. The maximum DHPC-$d_{22}$ splitting in the more ordered environment is about 44% of the maximum DMPC-$d_{54}$ splitting in the corresponding sample.

From the spectra in Fig. 5.1, it is clear that the quadrupole splittings for DMPC-$d_{54}$/DHPC spectra decrease slightly with increasing temperature above the onset of the nematic phase while the quadrupole splittings from DMPC/DHPC-$d_{22}$ spectra increase significantly with increasing temperature. This suggests that the partial ordering of DHPC-$d_{22}$ for temperatures above the onset of the nematic phase reflects exchange of DHPC-$d_{22}$ between highly curved 'edge' regions, characterized by low orientational order, and planar DMPC-rich regions characterized by greater orientational order. The observed temperature dependence suggests that the fraction of time spent by a DHPC molecule in the DMPC-rich environment increases with increasing temperature. This interpretation would also account for the observation that the ambient pressure spectra for DMPC/DHPC-$d_{22}$ ((4.4:1) in the range 30-34°C are characteristic of partial orientation. In contrast to the (4.4:1) mixture, the ambient pressure spectra for DMPC/DHPC-$d_{22}$ (3:1) contain a small component corresponding to isotropic DHPC reorientation at all temperatures. This difference is discussed below.

### 5.1.2 DMPC/DHPC at High Pressure

Figs. 5.2-5.4 show $^2$H-NMR spectra at 66 MPa, 102 MPa, and 135 MPa for DMPC-$d_{54}$/DHPC and DMPC/DHPC-$d_{22}$ at molar ratios of 3:1 and 4.4:1. Before discussing specific observations at each pressure, some general trends are noted. The application of pressure shifts the temperature at which anisotropic reorientation, presumably characteristic of the onset of nematic phase, is first apparent in the DMPC-$d_{54}$/DHPC spectra on warming from the isotropic phase. For example, application of 135 MPa raises the isotropic-nematic transition by 21°C for the 3:1 mixture and by 25°C for the 4.4:1 mixture. From these values the pressure sensitivity of the isotropic-nematic tran-

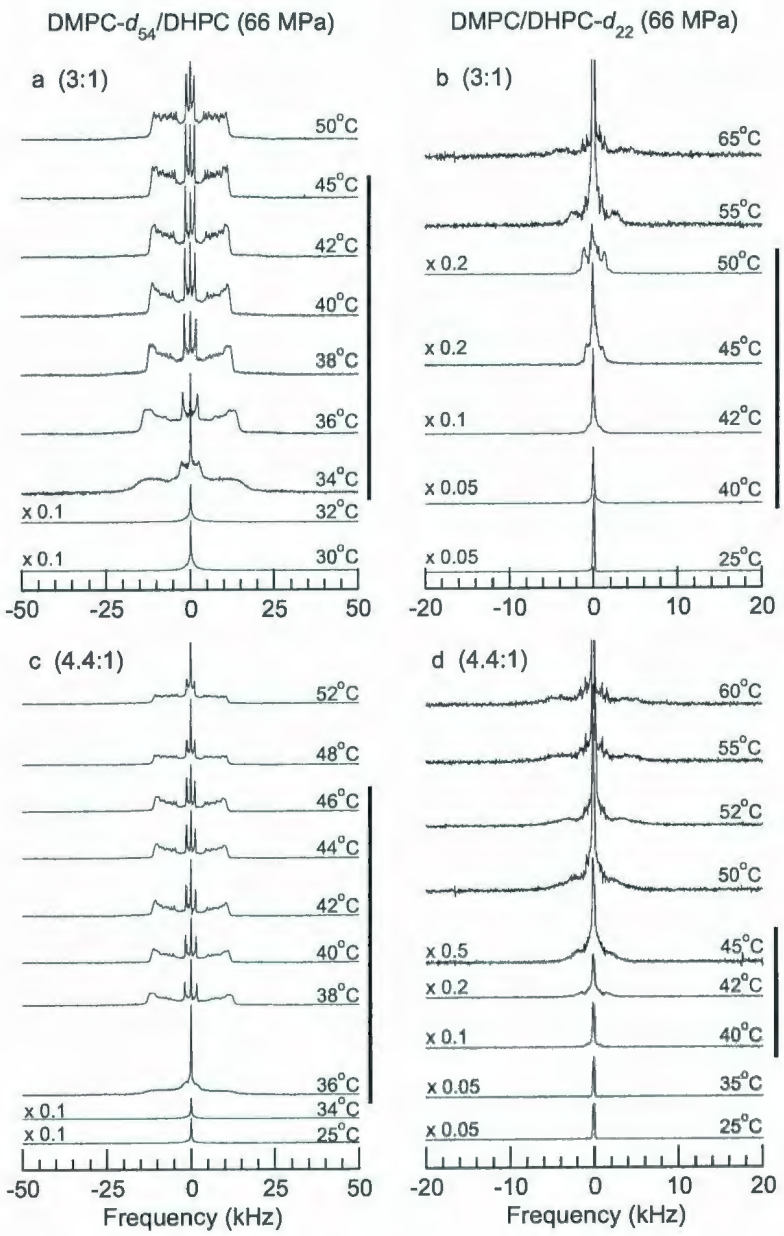


Figure 5.2: $^2$H-NMR spectra at 66 MPa and selected temperatures for dispersions of (a) DMPC-$d_{54}$/DHPC (3:1), (b) DMPC/DHPC-$d_{22}$ (3:1), (c) DMPC-$d_{54}$/DHPC (4.4:1), and (d) DMPC/DHPC-$d_{22}$ (4.4:1) in 100 mM HEPES buffer (pH=7.0). Based on DMPC-$d_{54}$/DHPC spectra, vertical bars next to each spectra indicate the approximate temperature range over which each sample is presumed to be in the nematic phase.

sition temperatures ($\frac{dT}{dP}$) are $\sim 0.16$°C/MPa and $\sim 0.19$°C/MPa for DMPC/DHPC molar ratios of 3:1 and 4.4:1 respectively. These rates are comparable with the rate of $\sim 0.19$°C/MPa that can be inferred from the pressure-temperature phase diagram reported from small-angle X-ray scattering (SAXS) observations of DMPC/DHPC (3.2:1) [33]. The main gel-to-liquid crystalline phase transition for DMPC bilayers has been reported to rise by $\sim 0.19$°C/MPa on the basis of deuterium NMR observations [36] and by $\sim 0.23$°C/MPa on the basis of neutron diffraction [34].

Spectra for DMPC-$d_{54}$/DHPC (3:1) at 66 MPa, 102 MPa and 135 MPa are shown in Figs. 5.2(a), 5.3(a), and 5.4(a) respectively. Application of pressure reduces the extent to which DMPC-$d_{54}$ in this sample is oriented but the upper limit of the temperature range over which the spectrum is characteristic of partial orientation still rises at $\sim 0.14$°C/MPa, which is comparable to the pressure sensitivity of the isotropic-nematic transition temperature.

For DMPC-$d_{54}$/DHPC (3:1), the spectra at ambient pressure and 23°C, at 66 MPa and 34°C, and at 102 MPa and 40°C, are the first spectra observed above the isotropic-to-nematic transition and are all gel-like spectra consistent with almost all of the DMPC-$d_{54}$ undergoing anisotropic, non-axially-symmetric reorientation on the timescale of the quadruple echo experiment. The ambient pressure spectrum for DMPC-$d_{54}$/DHPC (4.4:1) at 23°C is similar in shape to these spectra. At 135 MPa, the 44°C and 46°C spectra for DMPC-$d_{54}$/DHPC (3:1) still show non-axially-symmetric anisotropic reorientation of most of the DMPC-$d_{54}$ but with a much larger fraction reorienting isotropically. For DMPC-$d_{54}$/DHPC (4.4:1), similar spectra are seen just above the isotropic-to-nematic transition at 36°C for 66 MPa, at 42°C for 102 MPa and at 48°C for 135 MPa. These temperatures for the isotropic to nematic transition at elevated pressure are consistent with a tentative P-T phase diagram based on SAXS observations of DMPC/DHPC (3.2:1) that shows the isotropic-to-

nematic transition occurring roughly at 38°C for 66 MPa and 44°C for 102 MPa [33].

Figs. 5.2(c), 5.3(c), and 5.4(c) show spectra for DMPC-$d_{54}$/DHPC (4.4:1) at 66 MPa, 102 MPa and 135 MPa respectively. In this sample, clear evidence for magnetic orientation of DMPC-$d_{54}$ is seen at all pressures in the nematic temperature range. The apparent rate at which the oriented to lamellar transition temperature changes with pressure in DMPC-$d_{54}$/DHPC (4.4:1) is $\sim 0.16$°C/MPa. The observation that the pressure dependence of the nematic-to-lamellar transition temperature in this sample is slightly weaker than the pressure dependence of the isotropic-nematic transition is again consistent with the difference that can be inferred from the nematic-lamellar transition shown on the previously-reported pressure-temperature phase diagram referred by Winter *et al.* [33].

The observation that DMPC-$d_{54}$/DHPC (3:1) and DMPC-$d_{54}$/DHPC (4.4:1) display slightly different responses to pressure was confirmed by repeating these observations on independent samples of these two lipid mixtures. It is noted that DHPC accounts for $\sim 25\%$ of the lipid content in the DMPC/DHPC (3:1) samples and $\sim 19\%$ of the lipid content in the DMPC/DHPC (4.4:1). While this difference has only a small effect on the pressure dependence of the isotropic-to-nematic and nematic-to-lamellar transitions, it does appear to the affect propensity for the nematic phase to magnetically orient at high pressures. The spectra for DMPC/DHPC-$d_{22}$ (3:1) and DMPC/DHPC-$d_{22}$ (4.4:1) at a given pressure also show small differences in the distribution of the short chain lipid between isotropic and more ordered environments.

It should be noted that in DMPC-$d_{54}$/DHPC, where the deuterated component accounts for either $\sim 75\%$ or $\sim 81\%$ of the lipid content, deuteration is expected to depress transition temperatures of the mixtures by 2-3 °C relative to an undeuterated

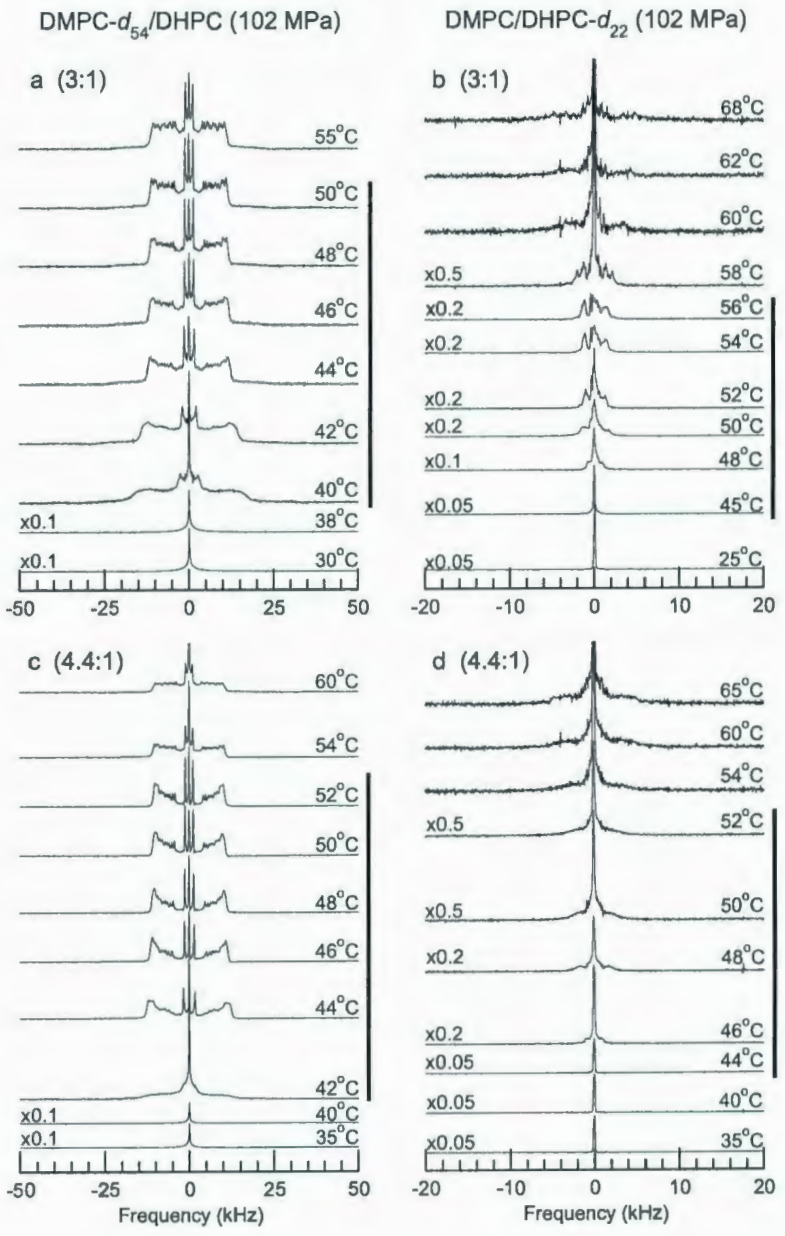


Figure 5.3: $^2$H-NMR spectra at 102 MPa and selected temperatures for dispersions of (a) DMPC-$d_{54}$/DHPC (3:1), (b) DMPC/DHPC-$d_{22}$ (3:1), (c) DMPC-$d_{54}$/DHPC (4.4:1), and (d) DMPC/DHPC-$d_{22}$ (4.4:1) in 100 mM HEPES buffer (pH=7.0). Based on DMPC-$d_{54}$/DHPC spectra, vertical bars next to each spectra indicate the approximate temperature range over which each sample is presumed to be in the nematic phase.

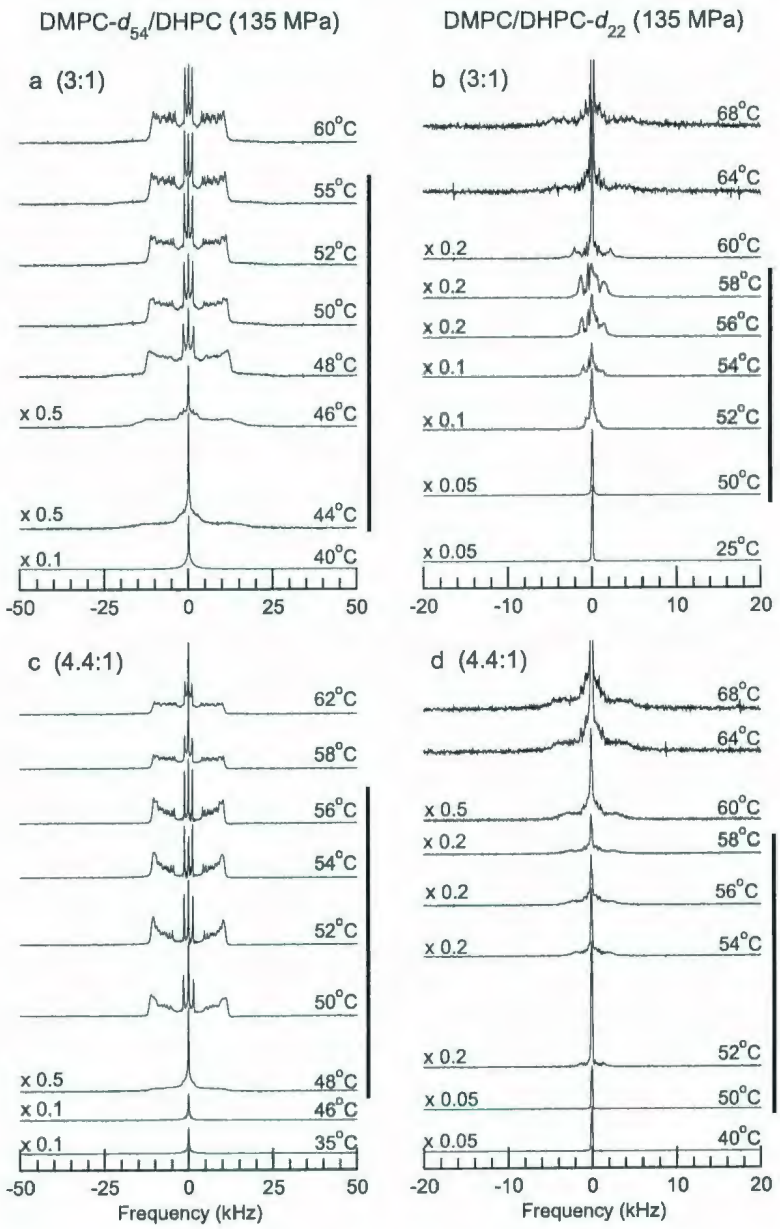


Figure 5.4: $^2$H-NMR spectra at 135 MPa and selected temperatures for dispersions of (a) DMPC-$d_{54}$/DHPC (3:1), (b) DMPC/DHPC-$d_{22}$ (3:1), (c) DMPC-$d_{54}$/DHPC (4.4:1), and (d) DMPC/DHPC-$d_{22}$ (4.4:1) in 100 mM HEPES buffer (pH=7.0). Based on DMPC-$d_{54}$/DHPC spectra, vertical bars next to each spectra indicate the approximate temperature range over which each sample is presumed to be in the nematic phase.

mixture. For the DMPC/DHPC-$d_{22}$ samples, where the deuterated component carries fewer deuterons and accounts for proportionally less of the lipid content, deuteration is expected to depress transitions by a few tenths of a degree at most [12].

The spectral sequences for DMPC/DHPC-$d_{22}$ (3:1) at 66 MPa, 102 MPa and 135 MPa are shown in Figs. 5.2(b), 5.3(b) and 5.4(b) respectively. In this sample, spectra for all pressures show decreasing amounts of isotropically-reorienting DHPC-$d_{22}$ as temperature is increased through the nematic range. For each pressure, the fraction of DHPC-$d_{22}$ undergoing isotropic reorientation is a minimum just below the nematic-to-lamellar transition. This fraction increases sharply as the sample is warmed through the transition into the lamellar phase. This change, at the nematic-to-lamellar transition, in the fraction of DHPC-$d_{22}$ undergoing isotropic reorientation, seen here in DMPC/DHPC-$d_{22}$ (3:1) at elevated pressure, is similar to the previous observations of DMPC/DHPC-$d_{22}$ (4.5:1) at ambient pressure [12].

Spectra for DMPC/DHPC-$d_{22}$ (4.4:1) at ambient pressure, 66 MPa, 102 MPa and 135 MPa are shown in Figs. 5.1(d), 5.2(d), 5.3(d), and 5.4(d) respectively. For this sample, the isotropic-to-nematic transition is easily identified and the transition temperature rises with pressure by $\sim 0.17$°C/MPa. As temperature is increased from the isotropic-to-nematic transition, splitting of the anisotropically-reorienting DHPC-$d_{22}$ spectral component increases. In contrast to the observations for DMPC/DHPC-$d_{22}$ (3:1), the fraction of isotropically-reorienting DHPC-$d_{22}$ in the nematic phase of DMPC/DHPC-$d_{22}$ (4.4:1) appears to be lower at ambient pressure than at elevated pressure. It should be noted that the DMPC/DHPC-$d_{22}$ (4.5:1) spectra displayed by Sternin *et al.* also indicate a very small fraction of isotropically-reorienting DHPC-$d_{22}$ in the ambient pressure nematic phase [12].

Comparison of the ambient pressure and high pressure spectra at corresponding temperatures above the transition yields some additional information. With increas-

ing pressure, the fraction of isotropically reorienting DHPC-$d_{22}$ in the nematic temperature range increases for DMPC/DHPC-$d_{22}$ (4.4:1) but decreases for DMPC/DHPC-$d_{22}$ (3:1). To understand this puzzling behavior, it is important to note that an isotropic spectral component can reflect rapid tumbling of small particles or rapid diffusion of lipid molecules within a highly curved region of a larger structure. The isotropic DHPC-$d_{22}$ spectral component may reflect rapid tumbling of small particles at low temperatures where some bicelle organization may persist but the situation at high temperature is less clear.

Another interesting behavior of DHPC-$d_{22}$ in DMPC/DHPC-$d_{22}$ is that spectra at ambient pressure for the mixture with molar ratio 4.4:1 are qualitatively similar to spectra for the mixture with molar ratio 3:1 at higher pressures. Within the nematic temperature range DHPC-$d_{22}$ is slightly more ordered in DMPC/DHPC-$d_{22}$ (4.4:1) at ambient pressure than in DMPC/DHPC-$d_{22}$ (3:1) at 135 MPa. In trying to account for these differences between the behaviors of the 3:1 and 4.4:1 samples, it may be useful to consider the effect of particle size in the samples with different molar ratio. For bicelles or wormlike micelles with edges enriched in DHPC, increasing the fraction of DHPC in a sample might be expected to increase the perimeter to area ratio and hence decrease the particle size. Thus particles size should be smaller in the sample with molar ratio 3:1 than in the 4.4:1 sample. The possible effects of such a difference are considered below.

Another point to be noted is that the temperatures for onset and disappearance of the nematic phase rise almost linearly with applied hydrostatic pressure. Allowing for the pressure-induced shift in transition temperatures, chain orientational order at corresponding points within each sequence of DMPC-$d_{54}$/DHPC spectra is only slightly affected by pressure. This is an interesting difference from the response of DHPC-$d_{22}$ to pressure at the two lipid ratios.

One noticeable difference between the two lipid mixtures is the effect of pressure on the extent to which the nematic phases orient at high pressure. The formation of a nematic phase in the 3:1 sample at 135 MPa is demonstrated by the DMPC/DHPC-$d_{22}$ (3:1) spectra shown in Fig. 5.4(b) but there is almost no evidence of orientation in the DMPC-$d_{54}$/DHPC (3:1) spectra at that pressure. This is in contrast to the clear evidence for orientation in the DMPC-$d_{54}$/DHPC (4.4:1) spectra at 135 MPa. As noted above, wormlike micelles for the 3:1 sample are expected to be narrower than for the 4.4:1 sample because of the expected difference in edge to area ratio. As discussed below, the weak orientation of the 3:1 sample in the nematic phase at high pressure may be related to the micelle dimensions for that sample and the higher temperatures at which the nematic phase forms at high pressure.

### 5.1.3 Phase Diagrams

A number of temperature-composition phase diagrams for bicellar mixtures have been previously reported [12, 28, 49, 60]. A tentative pressure-temperature phase diagram for bicellar mixtures was constructed by Winter *et al.* [33] using SAXS with 3.2:1 molar ratio and 15 %wt lipid in water reported over a range of temperatures (10-70°C) with pressures up to 250 MPa. They observed the nematic phase at ambient pressure in the temperature range 25-49°C.

Fig. 5.5 shows pressure-temperature phase diagrams derived from inspection of the spectra obtained from DMPC-$d_{54}$/DHPC samples with molar ratios 3:1 and 4.4:1. Open symbols denote spectra most characteristic of the nematic phase. Within the nematic phase, circles and squares denote spectra in which DMPC-$d_{54}$ reorientation was observed to be axially symmetric or not, respectively, on the timescale of the $^2$H-NMR experiment. A small number of spectra which could not be assigned to a single

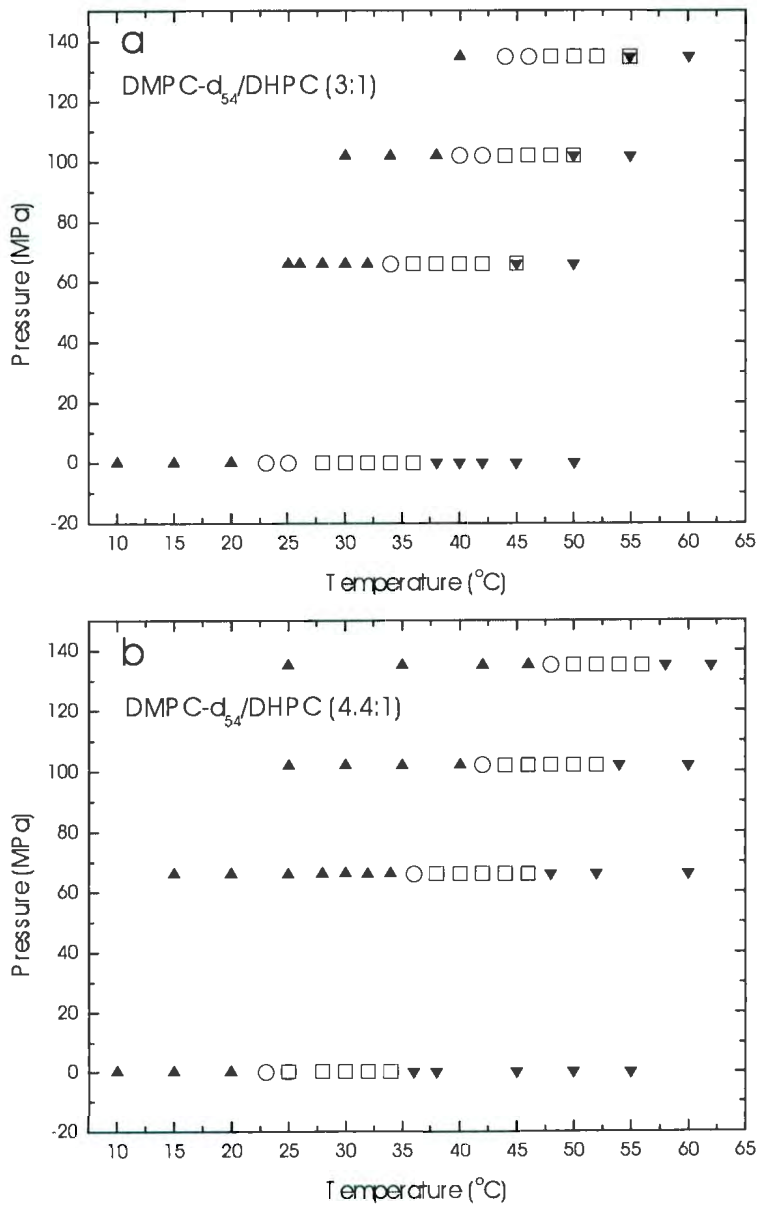


Figure 5.5: Pressure-temperature phase diagrams obtained from spectra for (a) DMPC-$d_{54}$/ DHPC (3:1) and (b) DMPC-$d_{54}$/ DHPC (4.4:1). Phases distinguished are isotropic (▲), nematic (◯ for non-axially symmetric spectra and □ for axially symmetric spectra), and lamellar (▼). Superimposed symbols denote spectra which could not be unambiguously identified with a single phase.

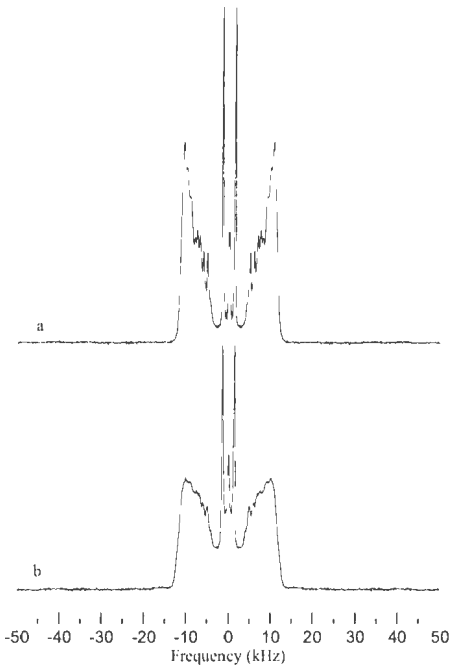


Figure 5.6: $DMPC_{54}$/DHPC spectra at ambient pressure for the sample (4.4:1) at 30°C a) after cooling and b) before cooling.

phase are denoted by overlapping symbols. For each sample, the upper and lower boundaries of the nematic phase differ only slightly in their pressure dependence. As noted earlier, the nematic phase boundary temperatures for DMPC-$d_{54}$/DHPC (4.4:1) are slightly more sensitive to pressure than those of DMPC-$d_{54}$/DHPC (3:1). The phase diagrams are qualitatively similar to those reported by Winter *et al.* [33].

It should be noted that orientation of the lipid molecules in bicellar mixtures (molar ratio 4.4:1) depends on the thermal history. Fig. 5.6 displays an example where Fig. 5.6(a) is the spectrum at 30°C after cooling the sample down to 10°C and Fig. 5.6(b) is the spectrum at 30°C before cooling and immediately after the

preparation of the sample at ambient pressure. It is also noted that $^2$H spectral shape of bicellar mixtures (molar ratio 3:1 and constant temperature 40°C) changes with time [79]. In this work, each $^2$H NMR experiment was done starting from low temperature after cooling the sample as required to avoid these problems.

## 5.2 Differential Scanning Calorimetry

Differential scanning calorimetry (DSC) endotherms exhibited by samples of DMPC/ DHPC (3:1), DMPC/DHPC (4.4:1), DMPC-$d_{54}$/DHPC (4.4:1) and DMPC/ DHPC-$d_{22}$ (4.4:1) are shown in Figs. 5.7(a), 5.7(b), 5.7(d) and 5.7(c) respectively. The DMPC/DHPC samples with molar ratios 3:1 and 4.4:1 were prepared specifically for DSC, and small amounts of the DMPC-$d_{54}$/DHPC (4.4:1) and DMPC/DHPC-$d_{22}$ (4.4:1) samples were extracted during preparation of those mixtures for deuterium NMR. Superimposed traces shown in Fig. 5.7 are the results of consecutive scans of individual sample. Heat capacity curves have been normalized to show excess heat capacity per mole of DMPC in each sample. The traces have been shifted vertically by unit amounts to aid visibility. Taking into account the effects of chain perdeuteration, the temperature ranges over which these samples exhibit excess heat capacity correspond to that of the nematic phase based on inspection of the DMPC-$d_{54}$/DHPC spectral series.

In the DSC measurements, the lipid mixtures exhibit broadened transition characteristic of a fairly uncooperative phase change relative to that of a pure lipid. The broadened peak at the nematic temperature range is also evident from recent observations reported by Takajo *et al.* [41]. It is noted that in pure DMPC, DSC traces display two distinct transitions. The main transition for pure DMPC bilayers occurs at 23.9°C with a transition enthalpy 5.4 kcal/mole for DMPC [80]. The thermody-

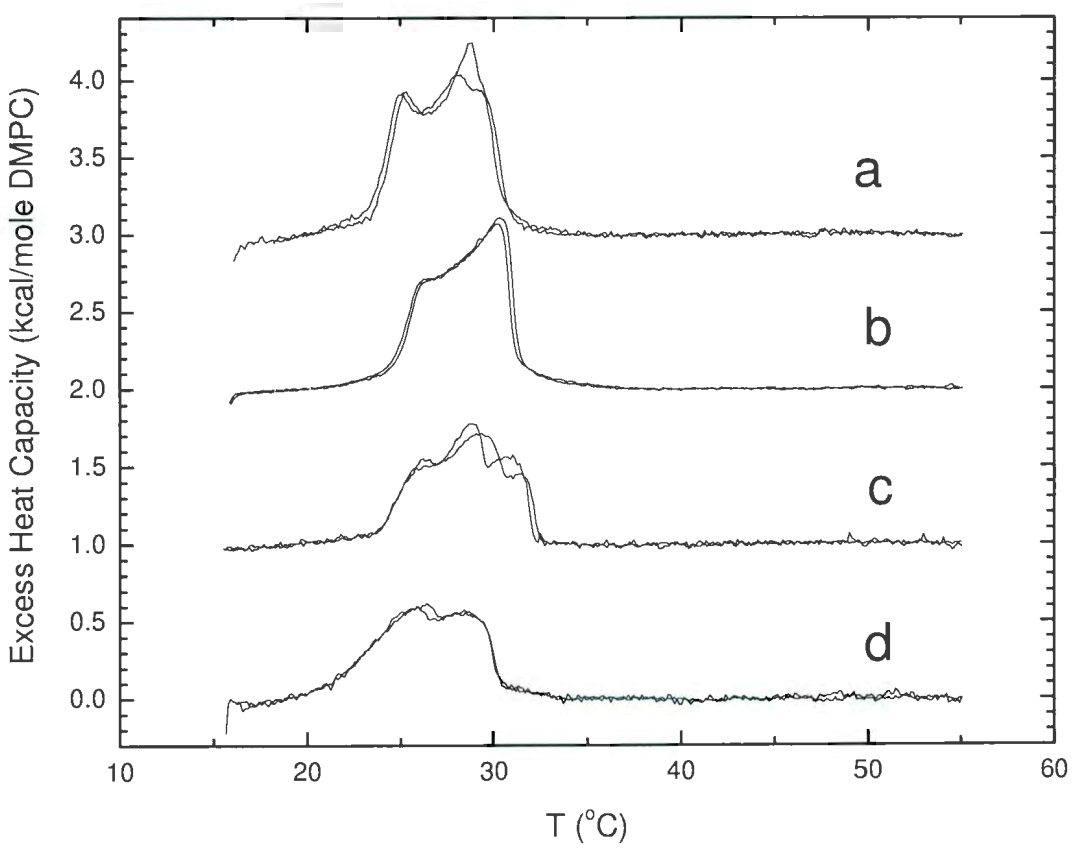


Figure 5.7: Differential scanning calorimetry (DSC) traces for dispersions of (a) DMPC/ DHPC (3:1), (b) DMPC/DHPC (4.4:1), (c) DMPC/DHPC-$d_{22}$ (4.4:1), and (d) DMPC-$d_{54}$/DHPC (4.4:1). Scans have been normalized to show excess heat capacity per mole of DMPC in each sample. For each sample, scans from two consecutive DSC runs are superimposed.

Table 5.1: Transition enthalpy from DSC measurements.

| Lipid mixtures | Concentration (mg/ml) | Volume (ml) | DMPC-normalized enthalpy ($\Delta H_{DMPC}$) (kcal/mole DMPC) | Average enthalpy ($\Delta H_{tot-lip}$) (kcal/mole lipids) |
|---|---|---|---|---|
| DMPC/DHPC (4.4:1) | 4.3 | 1.1 | 5.5 | 4.5 |
| | 4.3 | 1.1 | 5.5 | 4.4 |
| DMPC/DHPC-$d_{22}$ (4.4:1) | 2.0 | 1.1 | 4.3 | 3.5 |
| | 2.0 | 1.1 | 4.2 | 3.4 |
| DMPC-$d_{54}$/DHPC (4.4:1) | 2.4 | 1.1 | 4.0 | 3.3 |
| | 2.4 | 1.1 | 4.1 | 3.4 |
| DMPC/DHPC (3:1) | 2.0 | 1.1 | 5.9 | 4.4 |
| | 2.0 | 1.1 | 6.0 | 4.5 |

namical parameters obtained from the DMPC/DHPC mixtures studied here are listed in Table 5.1. In caption of table state that uncertainty due to uncertainies in sample composition, sample volume, and area determination are estimated to be $\sim 15\%$.

The average enthalpy associated with the excess heat capacity features shown in Figs. 5.7(a) and 5.7(b), measured relative to the total lipid content of each sample, was 4.5 kcal/mole for the DMPC/DHPC (3:1) and 3.5 kcal/mole for the DMPC/DHPC (4.4:1) samples respectively. For the DMPC-$d_{54}$/DHPC (4.4:1) and DMPC/DHPC-$d_{22}$ (4.4:1) samples extracted from the NMR mixtures (Figs. 5.7(c) and 5.7(d)), the average enthalpy was 3.3 kcal/mole and 3.5 kcal/mole respectively. For comparison, the transition enthalpies were also normalized to the DMPC content of each sample. The results were 5.9 kcal/mole DMPC and 5.5 kcal/mole DMPC for the DMPC/DHPC (3:1) sample (Fig. 5.7(a)) and DMPC/DHPC (4.4:1) sam-

ple (Fig. 5.7(b)) respectively. For the samples extracted from the NMR mixtures, the DMPC-$d_{54}$-normalized enthalpies were 4.3 kcal/mole DMPC-$d_{54}$ for the DMPC-$d_{54}$/DHPC (4.4:1) sample (Fig. 5.7(c)) and 4.1 kcal/mole DMPC for the DMPC/ DHPC-$d_{22}$ (4.4:1) sample (Fig. 5.7(d)). Within the estimated uncertainty, the DMPC-normalized transition enthalipes for the undeuterated samples are thus comparable to the main gel-to-liquid crystalline phase transition enthalpy for bilayers of DMPC alone.

Some important points regarding the DSC results are noted below. The pressure dependence of a transition depends on the transition enthalpy and the change in molar volume of the material through the Clausius-Clapeyron equation ($\frac{\Delta P}{\Delta T} = \frac{\Delta H}{T\Delta V}$). The DMPC in these bicellar mixtures goes from gel-like to liquid-crystal-like through the isotropic-nematic-lamellar transition so it is not too surprising that the transition enthalpy is similar to DMPC. The correspondences of the mixture transition enthalpies and transition temperature dependence with those of a DMPC bilayer suggests a coupling between the DMPC main transition and the changes in morphology of DMPC/DHPC bicellar mixtures as has been suggested by Harroun *et al.* [29]. In fact, it is possible that the onset of the isotropic-to-nematic transition reflects an instability of the bicelle morphology as the DMPC chains which are likely ordered in the bicelle phase begin to melt. When they start to melt, the area per lipid will tend to increase but the area of the bicelle is constrained by the ring of disordered DHPC at the bicelle edge. The only way the DMPC can then expand laterally is if the bicelles fuse into non-disk structures, presumably the worm-like micelles.

One interesting observation is that as the temperature is raised, part of the DHPC population becomes more ordered. This cannot reflect the behavior of DHPC lipids that are entirely dissolved in DMPC bilayers because the DMPC is becoming less ordered as temperature increases. The increase in DHPC order must therefore reflect

DHPC molecules that are diffusing between a less ordered and a more ordered environment (i.e. the DMPC) such that the fraction of time a DMPC molecule spends, on average, in the more ordered environment increases as the temperature goes up.

Based on these considerations, the widths of the excess enthalpy peaks observed by DSC raise interesting questions. For most of the nematic temperature range, based on the $^2$H NMR spectra as described earlier, the orientational order of the DMPC-$d_{54}$ does not decrease very much and the orientational order of DHPC-$d_{22}$ actually increases. This suggests that some of the heat input recorded by DSC does not go into disordering the DMPC chains. If the heat is not going into disordering the chains, perhaps it is going into changing the hydration of the DHPC headgroups. In the bicelle phase, the DHPC molecules are in a very highly curved environment which probably increases their interaction with water. As they move into a less curved environment in the nematic phase and ultimately lamellar phases, the headgroups may become less accessible to water. That would raise their energy and would require heat. It may be this process of progressive DHPC headgroup dehydration that accounts for the absorption of heat well into the nematic phase temperature range. Future studies using headgroup deuterated DHPC could be a useful way to test this suggestion.

# Chapter 6

# Summary and Concluding Remarks

In order to understand the phase behavior of 'bicellar mixtures', experiments were performed by using $^2$H NMR spectroscopy and differential scanning calorimetry (DSC). $^2$H NMR spectra provide some information about the behavior of the long-chain and short-chain lipid components at ambient and high pressure. High pressure behavior was studied by comparing DMPC-$d_{54}$/DHPC (3:1) to DMPC-$d_{54}$/DHPC (4.4:1) and DMPC/DHPC-$d_{22}$ (3:1) to DMPC/DHPC-$d_{22}$ (4.4:1) bicellar mixtures at appropriate temperatures and pressures up to 135 MPa. The DSC observations and the pressure-dependence of the observed transitions provide more insights into the nature of the transitions observed in the DMPC/DHPC bicellar system.

For both mixtures, $^2$H NMR spectra shown in Figs. 5.1-5.4 and explained in section 5.1, indicate that the isotropic-nematic and the nematic-lamellar transition temperatures increase with pressure at roughly the same rate as the DMPC gel-liquid crystal transition. From DSC measurements, described in chapter 5 (Fig. 5.7 and Table 5.1), it is seen that the total transition enthalpy per mole of DMPC is similar to that of pure DMPC. Taken together, the above two observations suggest that the isotropic-nematic-lamellar change in the DMPC/DHPC mixture is strongly coupled

to the melting of ordered DMPC in the bicelles as suggested by Harroun *et al.* [29].

$^2$H NMR spectra of the DMPC-$d_{54}$/DHPC mixtures shown in Figs. 5.1-5.4 in chapter 5, indicate that the orientational order of DMPC does not change much over the nematic temperature range but DSC traces (shown in Fig. 5.7 in the previous chapter) indicate that the samples absorb heat over a temperature range of about 10°C, corresponding to the observed range of the nematic phase. This implies that the melting of DMPC chains is not the only process driving the isotropic-nematic-lamellar phase behavior. It is noted that DHPC chains are already disordered in the nematic phase and they become slightly more ordered as temperature increases so that disordering of DHPC chains are unlikely to account for the observed absorption of heat. One of the possibilities is that heat may be absorbed as DHPC headgroups become less hydrated during migration of DHPC from highly curved edge environments to the more planar DMPC-rich environment.

DMPC-$d_{54}$ chain order through the nematic temperature range is similar for the different pressures studied. This indicates that DMPC-$d_{54}$ chain order within the nematic phase for a given pressure is insensitive to the specific value of that pressure even though transitions are shifted with increasing pressure. Within the nematic phase temperature range for a given pressure, DMPC-$d_{54}$ chain order is roughly constant.

Observations of independent samples do seem to confirm that pressure reduces the magnetic orientability of the 3:1 mixture compared to the 4.4:1 mixture in the 'nematic phase' temperature range. In the nematic phase, chain order of DMPC-$d_{54}$ is not much different for the two mixtures at high temperature. This suggests that the bilayer thickness in the wormlike micelles or ribbons is not too different in the two mixtures and that the DMPC environment is not too different in the two mixtures for a given pressure in the nematic phase. Thus the extent to which the bilayer region

is perturbed by dissolved DHPC is also not very different for the two molar ratios. One way in which molar ratio might affect properties that could affect orientation is through particle size. Particles should be larger in the 4.4:1 sample than in the 3:1 sample because there is less 'edge' material per unit area in the 4.4:1 sample. The weaker degree of orientation of the 3:1 ribbons may simply be because it is harder to orient narrower ribbons at the high temperatures for which the samples are in the nematic phase at high pressure.

As temperature increases through the nematic and lamellar phase, spectra shown in Figs. 5.1 (b,d), 5.2 (b,d), 5.3 (b,d) and 5.4 (b,d) in chapter 5, the anisotropically reorienting DHPC-$d_{22}$ fraction becomes more ordered. The extent to which DHPC-$d_{22}$ chains are ordered must reflect fast exchange between highly curved 'edge' environments and more planar DMPC-rich environments. The observed temperature dependence suggests that the probability of finding a given DHPC molecule in the more ordered environment increases with increasing temperature. Exchange of DHPC between the edge and planar environments may destabilize the micellar organization and drive the nematic-lamellar transition as suggested by Katsaras and co-workers [13].

Without additional repetition, we cannot preclude the possibility that differences between the behaviors of DHPC-$d_{22}$ in the two molar ratio samples are due to sensitivity to the way in which temperature and pressure are cycled. Nevertheless, some comments on possible sources of the observed differences are as follow. In the nematic phase, two general behaviors of DHPC-$d_{22}$ are observed: (i) All of the DHPC-$d_{22}$ reorienting anisotropically with no isotropic reorientation and (ii) A superposition of spectral components characteristic of anisotropic reorientation and isotropic reorientation. In the lamellar phase, all DHPC-$d_{22}$ spectra are superpositions of spectral components characteristic of anisotropic reorientation and isotropic reorientation. The DHPC-$d_{22}$

lamellar phase spectra may thus be a clue to understanding differences between the DHPC-$d_{22}$ spectra in the nematic phase. In lamellar phase, there are suggestions that the organization is planar with DHPC lined pores [30, 54]. Diffusion around a small pore would give a nearly isotropic spectral component while exchange into the planar DMPC-rich region would give doublet spectra characteristic of anisotropic reorientation. Absence of an isotropic DHPC-$d_{22}$ component in the nematic phase may indicate that all of the DHPC-$d_{22}$ in the nematic phase is exchanging between edge and DMPC-rich planar environments. Presence of an isotropic DHPC-$d_{22}$ component in the nematic phase may indicate that a fraction of the DHPC-$d_{22}$ is diffusing around pore edges while another fraction of the DHPC-$d_{22}$ may be exchanging between edge and DMPC-rich planar environments.

At ambient pressure in the nematic phase temperature range, all of the DHPC-$d_{22}$ in the 4.4:1 sample (spectra are shown in Fig. 5.1d) is exchanging with the DMPC-rich region and thus showing anisotropic reorientation whereas a fraction of the DHPC-$d_{22}$ in the 3:1 sample is reorienting isotropically. This may reflect the larger fraction of DHPC-$d_{22}$ in the 3:1 sample (spectra are shown in Fig. 5.1b). The larger fraction of DHPC-$d_{22}$ in the 3:1 sample might be accommodated by making smaller particles (i.e., increasing the amount of edge environment), as suggested above, or by forming pores, or by a combination. In the 4.4:1 sample at ambient pressure, all of the DHPC-$d_{22}$ in the nematic phase may be exchanging between edge and DMPC-rich planar environments.

At higher pressure, the fraction of DHPC-$d_{22}$ exchanging with the DMPC-rich environment is large in the 3:1 sample and the fraction of DHPC-$d_{22}$ undergoing isotropic reorientation is small. In contract, the fraction of isotropically-reorienting DHPC-$d_{22}$ in the 4.4:1 sample increases as pressure is raised. The observation of nematic phase DHPC-$d_{22}$ spectra with and without a significant contribution from

isotropically-reorienting DHPC-$d_{22}$ from the same sample as pressure is varied suggests that whether or not the isotropic DHPC fraction is present in the nematic phase may be very sensitive to the way in which pressure and temperature are cycled. Further experiments would be needed to determine if the isotropic fraction in the nematic phase is metastable.

The nematic phase DHPC-$d_{22}$ spectra for the 3:1 and 4.4:1 samples change in opposite ways as pressure is increased. Nematic phase isotropic fraction decreases in the 3:1 sample but increases in the 4.4:1 sample with increasing pressure. These observations indicate that for a given sample there can be different environments for DHPC-$d_{22}$ in the nematic phase depending on sample conditions and possibly thermal history. Further experiments needed to determine if observed effects of pressure and composition are systematic or if they reflect metastable behavior.

DMPC-$d_{54}$ chain order in the nematic phase is not very sensitive to pressure or DMPC/DHPC molar ratio. Presence or absence of isotropic a DHPC-$d_{22}$ fraction in nematic phase is not correlated with differences in DMPC-$d_{54}$ behavior. This implies that observed differences in DHPC behavior with pressure and DMPC/DHPC molar ratio are likely not due to changes in the ability of the DMPC-rich region to accommodate dissolved DHPC molecules or due to significant changes in the organization of the DMPC-rich planar regions. Further NMR studies of 'bicellar mixture' containing headgroup-deuterated DHPC might provide some insight into its environment.

# Bibliography


[1] Bruce Alberts, *Molecular biology of the cell,* **5th ed** (2008).

[2] Philip L Yeagle, *The structure of biological membranes,* CRC Press **2nd edition,** 54 (2005).

[3] Thomas Heimburg, *Thermal Biophysics of Membrane,* Wiley-VCH Verlag GmbH and Co. 16 (2007).

[4] Arora A., and Tamm L. K., Biophysical approaches to membrane protein structure determination, *Current option in structural biology,* **11** Issue 5 540-547 (2001).

[5] Luzzati V., *Biological membrane,* **V. 1,** ed. by D.Chapman, Academic press, London (1968).

[6] Hauser H., Short-chain phospholipids as detergents, *Biochim. Biophys. Acta,* **1508** 164-181 (2000).

[7] Kleinschmidt JH, Tamm LK, Structural Transitions in Short-Chain Lipid Assemblies Studied by $^{31}$P-NMR Spectroscopy, *Biophysical Journal,* **83 (2)**, 994-1003 (Aug 2002).

[8] Sanders C. R., Schwonek J. P., Characterization of Magnetically Orientable Bilayers in Mixtures of Dihexanoylphosphatidylcholine and Dimyristoylphosphatidylcholine by Solid-state NMR, *Biochemistry,*, **31** 8898-8905 (1992).

[9] Struppe J., Vold R. R., Dilute Bicellar Solutions for Structural NMR Work, *J. Magn. Reson.,* **135** 541-546 (1998).

[10] Sanders C.R., Prosser R.S., Bicelles: a model membrane system for all seasons?, *Structure* **6** 1227-1234 (1998).

[11] Prosser R.S., Hwang J.S., Vold R.R., Magnetically aligned phospholipid bilayers with positive ordering: a new model membrane system, *Biophysical Journal,* **74** 2405-2418 (1998).

[12] Sternin E., Nizza D., Gawrisch K., Temperature Dependence of DMPC/DHPC Mixing in a Bicellar Solution and Its Structural Implications, *Langmuir,* **17** 2610-2616 (2001).

[13] Soong R., Nieh M.P., Nicholson E., Katsaras J., Macdonald P. M., Bicellar Mixtures Containing Pluronic F68: Morphology and Lateral Diffusion from Combined SANS and PFG NMR Studies, *Langmuir,* **26(4)** 26302638 (2010).

[14] Ram P., Prestegard J. H., Magnetic field induced ordering of bile salt/phospholipid micelles: new media for NMR structural investigations, *Biochim Biophys Acta,* **940** 289-294 (1988).

[15] Marcotte I., Auger M., Bicelles as Model Membranes for Solidand Solution-State NMR Studies of Membrane Peptides and Proteins, *Concepts Magn. Reson.,* Part A, **24A** 17-37 (2005).

[16] Braganza L. F., and Worcester D. L., Structural Changes in Lipid Bilayers and Biological Membranes Caused by Hydrostatic Pressure, *Biochemistry,* **25** 7484-7488 (1986).

[17] Czeslik C., Reis O., Winter R., Rapp G., Effect of high pressure on the structure of dipalmitoylphosphatidylcholine bilayer membranes: a synchrotron x-ray diffraction and FTIR spectroscopy study using the diamond anvil technique, *Chem. Phys. Lipids,* **91** 135-144 (1998).

[18] Wong P. T. T., Siminovitch D. J., Mantsch H. H., Structure and properties of model membranes - new knowledge from high pressure vibrational spectroscopy, *Biochim. Biophys. Acta,* **947** 139-171 (1988).

[19] Choma C. T. and Wong P. T. T., The structure of anhydrous and hydrated dimyristoylphosphatidyl glycerol: a pressure tuning infrared spectroscopic study, *Chemistry and Physics of Lipids,* **61** 131137 (1992).

[20] Ahn T. and Yun C. H., Phase properties of liquid-crystalline phosphatidylcholine/phosphatidyl-ethanolamine bilayers revealed by fluorescent probes, *Archives of Biochemistry and Biophysics*, **369(2)** 288294 (1999).

[21] Winter R., Pilgrim W. C., A SANS study of high pressure phase transitions in model biomembranes, *Ber. Bunsenges. Phys. Chem.,* **93** 708-717 (1989).

[22] Driscoll D. A., Jonas J., Jonas A., High pressure $^2$H nuclear magnetic resonance study of the gel phases of dipalmitoylphosphatidylcholine, *Chem. Phys. Lipids,* **58** 97-104 (1991).

[23] Kaneshina S., Tamura K., Kawakami H., Matsuki H., Effects of pressure and ethanol on the phase behavior of dipalmitoylphosphatidylcholine multilamellar vesicles, *Chem. Lett.,* **Issue 10** 1963-1966 (1992).

[24] Maruyama S., Hata T., Matsuki H., Kaneshina S., Effects of pressure and local anesthetic tetracaine on dipalmitoylphosphatidylcholine bilayers, *Biochim. Biophys. Acta,* **1325** Issue 2 272-280 (1997).

[25] Bottner M., Ceh D., Jacobs U., Winter R. Z., High pressure volumetric measurements on phospholipid bilayers, *Phys. Chem.,* **184** 205-218 (1994).

[26] Aussenac F., Laguerre M., Schmitter J. M., Dufourc E. J., Detailed Structure and Dynamics of Bicelle Phospholipids Using Selectively Deuterated and Perdeuterated Labels. $^2$H NMR and Molecular Mechanics Study, *Langmuir*, **19** 10468-10479 (2003).

[27] Nieh M. P., Raghunathan V.A., Glinka C.J., Harroun T.A., Pabst G., Katsaras J., Magnetically alignable phase of phospholipid 'bicelle' mixtures is a chiral nematic made up of wormlike micelles, *Langmuir*, **20** 7893-7897 (2004).

[28] Katsaras J., Harroun T. A., Pencer J., Nieh M. P., 'Bicellar' lipid mixtures as used in biochemical and biophysical studies, *Naturwissenschaften*, **92** 355-366 (2005).

[29] Harroun T. A., Koslowsky M., Nieh M. P., de Lannoy C.F., Raghunathan V.A., Katsaras J., Comprehensive examination of mesophases formed by DMPC and DHPC mixtures, *Langmuir* **21** 5356-5361 (2005).

[30] Nieh M. P., Glinka C.J., Krueger S., Prosser R.S., Katsaras J., SANS study of the structural phases of magnetically alignable lanthanide-doped phospholipid mixtures, *Langmuir,* **17** 2629-2638 (2001).

[31] Dam L. van, Karlsson G., Edwards K., Direct observation and characterization of DMPC/DHPC aggregates under conditions relevant for biological solution NMR, *Biochimica et Biophysica Acta,* **1664** 241 256 (2004).

[32] Ronald Soong and Peter M. Macdonald, Water Diffusion in Bicelles and the Mixed Bicelle Model, *Langmuir,* **25** 380-390 (2009).

[33] Winter R., Jeworrek C., Effect of pressure on membranes, *Soft Matter,* **5** 3157-3173 (2009).

[34] Braganza L. F., Worcester D. L., Hydrostatic pressure induces hydrocarbon chain interdigitation in single-component phospholipid bilayers, Biochemistry, **25** 2591-2595 (1986).

[35] Singh H., Emberley J., Morrow M. R., Pressure induces interdigitation differently in DPPC and DPPG, *Eur. Biophys. J.,* **37** 783-792 (2008).

[36] Bonev B. B., Morrow M. R., Effect of pressure on the dimyristoylphosphatidylcholine bilayer main transition, *Phys. Rev. E,* **55** 5825-5833 (1997).

[37] Brown A., Skanes I., Morrow M. R., Pressure-induced ordering in mixed-lipid bilayers, *Phys. Rev. E,* **69** 011913 (2004).

[38] Brunner E., Arnold M. R., Kremer W., Kalbitzer H. R., Pressure-stability of phospholipid bicelles: Measurement of residual dipolar couplings under extreme conditions, *J. Biomol. NMR,* **21** 173-176 (2001).

[39] Gutberlet T., Hoell A., Kammel M., Frank J., Katsaras J., Neutron scattering from magnetically aligned biomimetic substrates, *Appl. Phys. A,* **74 (Suppl.)** S1260-S1261 (2002).

[40] Kozak M., Kempka M., Szpotkowski K., Jurga S., NMR in soft materials: A study of DMPC/DHPC bicellar system, *Journal of Non-Crystalline Solids,* **353** 42464251 (2007).

[41] Takajoa, Y., Matsukib H., Matsubaraa H., Tsuchiyac K., Aratonoa M. and Yamanakaa M., Structural and morphological transition of long-chain phospholipid vesicles induced by mixing with short-chain phospholipid, *Colloids and Surfaces B: Biointerfaces,* **76** 571576 (2010).

[42] Cevc G., *phospholipids Handbook,* Marcel Dekker, Inc., New York (1993).

[43] Rawicz W., Olbrich K. C., McIntosh T., Needham D., Evans E., Effect of chain length and unsaturation on elasticity of lipid bilayers, *Biophysical Journal,* **V 79 (1)** 328-39 (July 2000).

[44] Maibaum L., Dinner A. R., and Chandler D., Micelle Formation and the Hydrophobic Effect, *J. Phys. Chem. B,* **108** 6778-6781 (2004).

[45] Sanders C.R., Landis G.C., Reconstitution of membrane proteins into lipid-rich bilayered mixed micelles for NMR studies, *Biochemistry,* **34** 4030-4040 (1995).

[46] Diller A., Loudet C., Aussenac F., Raffard G., Fournier S., Laguerre M, Grelard A., Opella S. J., Marassi F. M., Dufourc E. J., Bicelles: A natural 'molecular goniometer' for structural, dynamical and topological studies of molecules in membranes, *Biochimie,* **91** 744751 (2009).

[47] Sanders C. R., Development and Application of Bicelles for Use in Biological NMR and Other Biophysical Studies, *Modern Magnetic Resonance,* **Part I** Graham A. Webb (ed.), Springer Netherlands 233239 (2008).

[48] Lynn W. Jelinski, Solid State Deuterium NMR Studies of Polymer Chain Dynamics, *Ann. Rev. Mater. Sci.,* ***15,*** 359-377 (1985)

[49] Raffard G., Steinbruckner S., Arnold A., Davis J.H., Dufourc E.J., Temperature composition diagram of dimyristoylphosphatidylcholine dicaproylphosphatidylcholine 'bicelles' self-orienting in the magnetic field. A solid state $^{2}H$ and $^{31}P$ NMR study, *Langmuir,* **16** 7655-7662 (2000).

[50] Arnold A., Labrot T., Oda R., Dufourc E.J., Cation modulation of bicelle size and magnetic alignment as revealed by solid-state NMR and electron microscopy, *Biophysical Journal,* **83** 2667-2680 (2002).

[51] Vold R. R., AND Prosser R. S., Magnetically Oriented Phospholipid Bilayered Micelles for Structural Studies of Polypeptides. Does the Ideal Bicelle Exist? *Journal of Magnetic Resonance,* Series B **113** 267271 (1996).

[52] Andersson A., *The application of isotropic bicelles as model membrane,* PhD thesis, Stockholm University (2005)

[53] Loudet C., Manet S., Gineste S., Oda R., Achard M.F., Dufourc E.J., Biphenyl bicelle disks align perpendicular to magnetic fields on large temperature scales: a study combining synthesis, solid-state NMR, TEM, and SAXS; *Biophysical Journal,* **92** 3949-3959 (2007).

[54] Nieh M. P., Raghunathan V. A., Wang H., and Katsaras J., Highly Aligned Lamellar Lipid Domains Induced by Macroscopic Confinement, *Langmuir,* **19** 6936-6941 (2003).

[55] Gaemers S. and Bax A., Morphology of three lyotropic liquid crystalline biological NMR media studied by translational diffusion anisotropy, *Journal of the American Chemical Society,* **123** 1234312352 (2001).

[56] Soong R., and Macdonald P.M., Lateral diffusion of PEG-lipid in magnetically aligned bicelles measured using stimulated echo pulsed field gradient H-1 NMR, *Biophysical Journal,* **88** 255268 (2005).

[57] Triba M. N., Warschawski D. E., and Devaux P. F., Reinvestigation by Phosphorus NMR of Lipid Distribution in Bicelles, *Biophysical Journal, V 88* 18871901 (March 2005).

[58] Katsaras J., Donaberger R. L., Swainson I. P., Tennant D. C., Tun Z., Vold R. R., and Prosser R. S., Rarely Observed Phase Transitions in a Novel Lyotropic Liquid Crystal System, *Physical Review Letters,*5 **78** 899-902 (1997).

[59] Prosser R.S., Hunt S.A., DiNatale J.A., Vold R.R., Magnetically aligned membrane model systems with positive order parameter: switching the sign of $S_{zz}$ with paramagnetic ions, *Journal of the American Chemical Society,* **118** 269-270 (1996).

[60] Nieh M. P., Glinka C. J., Krueger S., Prosser R. S., Katsaras J., SANS Study on the Effect of Lanthanide Ions and Charged Lipids on the Morphology of Phospholipid Mixtures, *Biophys. J.,* **82** 2487-2498 (2002).

[61] J. H. Davis, Deuterium Nuclear Magnetic Resonance Spectroscopy in Partially Ordered Systems, *Isotopes in the Physical and Biomedical Sciences,* ***Volume 2,*** Elsevier Science Publishers B. V., 99-157 (1991).

[62] J. H. Davis, The description of membrane lipid conformation, order and dynamics by $^2$H-NMR. *Biochim. Biophys. Acta,* ***737,*** 117-171, (1983).

[63] J. C. Huschilt, R. S. Hodges, and J. H. Davis, Phase equilibria in an amphiphilic peptide-phospholipid model membrane by deuterium nuclear magnetic resonance difference spectroscopy. *Biochemistry,* ***24,*** 1377-1386 (1985).

[64] J. Seelig, Deuterium magnetic resonance: theory and application to lipid membranes. *Quarterly Reviews of Biophysics,* ***10(3),*** 353-418 (1977).

[65] Valentina Domenici, Marco Geppi, Carlo Alberto Veracini, NMR in chiral and achiral smectic phases: Structure, orientational order and dynamics, *Progress in Nuclear Magnetic Resonance Spectroscopy,* ***50,*** 150 (2007).

[66] C. P. Slichter, *Principles of magnetic Resonance,* Springer-Verlag, 1 (1978).

[67] C. A. de Lange and E. E. Burnell. Basics of NMR of Molecules in Uniaxial Anisotropic environments, *NMR of Ordered Liquids,* ***chapter 1,*** Kluwer Academic Publishers 6 (2003).

[68] Oleg Jardetzky and G. C. K. Roberts. *NMR in Molecular Biology,* Academic Press, (1981).

[69] J. H. Davis, K. R. Jeffrey, M. Bloom, M. I. Valic, and T. P. Higgs. Quadrupole echo deuteron magnetic resonance spectroscopy in ordered hydrocarbon chains, *Chemical Physics Letters,* **42**, 390394, (1976).

[70] M. Bloom, C. Morrison, E. Sternin, and J. L. Thewalt, *In Pulsed Magnetic Resonance: NMR, ESR, and Optics*, Clarendon Press, Oxford, 274316, (1992).

[71] J. H. Davis, The influence of membrane proteins on lipid dynamics, *Chemistry and Physics of Lipids,* **40**, 223258, (1986).

[72] Michael R. Morrow, Transverse nuclear spin relaxation in phosphatidylcholine bilayers containing gramicidin, *Biochimica et Biophysica Acta.,* **1023** 197205, 1990.

[73] Bonev B. B., and Morrow M. R., Simple probe for variable pressure deuterium nuclear magnetic resonance studies of soft matreials, *Review of Scientific Instruments,* **68** 18271830, (1997).

[74] Prosser R. S., Davis J. H., Dahlquist F. W., and Lindorfer M. A., $^2$H nuclear magnetic resonance of the gramicidin a backbone in a phospholipid bilayer, *Biochemistry,* **30** 4687 4696, (1991).

[75] Mabrey, S., and J. Sturtevant, High sensitive differential scanning calorimetry in the study of biomembranes and related model systems, *In Methods of Membrane Biology,* E. D. Korn, editor. Plenum Publishing Corp., New York. 237-274 (1978).

[76] Mcelhaney R., The use of differential scanning calorimetry and differential thermal-analysis in studies of model and biological membranes, *Chemistry and Physics of Lipids,*, **V 30** Issue 2-3 229-259 (1982).

[77] Menczel J. D., Prime R. B., *Thermal Analysis of Polymers: Fundamentals and Applications,* John Wiley and Sons, Inc., **Chapter 2**, (2009).

[78] Cooper, A., Johnson, C. M., Differential scanning calorimetry, *Methods Mol. Biol.,* **22**, Microscopy, Optical Spectroscopy, and Macroscopic Techniques, Ed. C.Jones, B.Mulloy and A.H.Thomas, Humana Press, Totowa, N.J., Chapter 10, 125-136 (1994).

[79] Struppe J., Whiles J. A., and Vold R. R., Acidic Phospholipid Bicelles: A Versatile Model Membrane System, *Biophysical Journal,* **V. 78** 281289 (2000).

[80] Mabrey, S., and J. Sturtevant, Investigation of phase transitions of lipids mixtures by high sensitivity differential scanning calorimetry, *Pros. Natl. Acad. Sci. USA,* **V 73** No. 11 3862-3866 (1976).

# Appendix A

# Full $^2$H-NMR Spectra

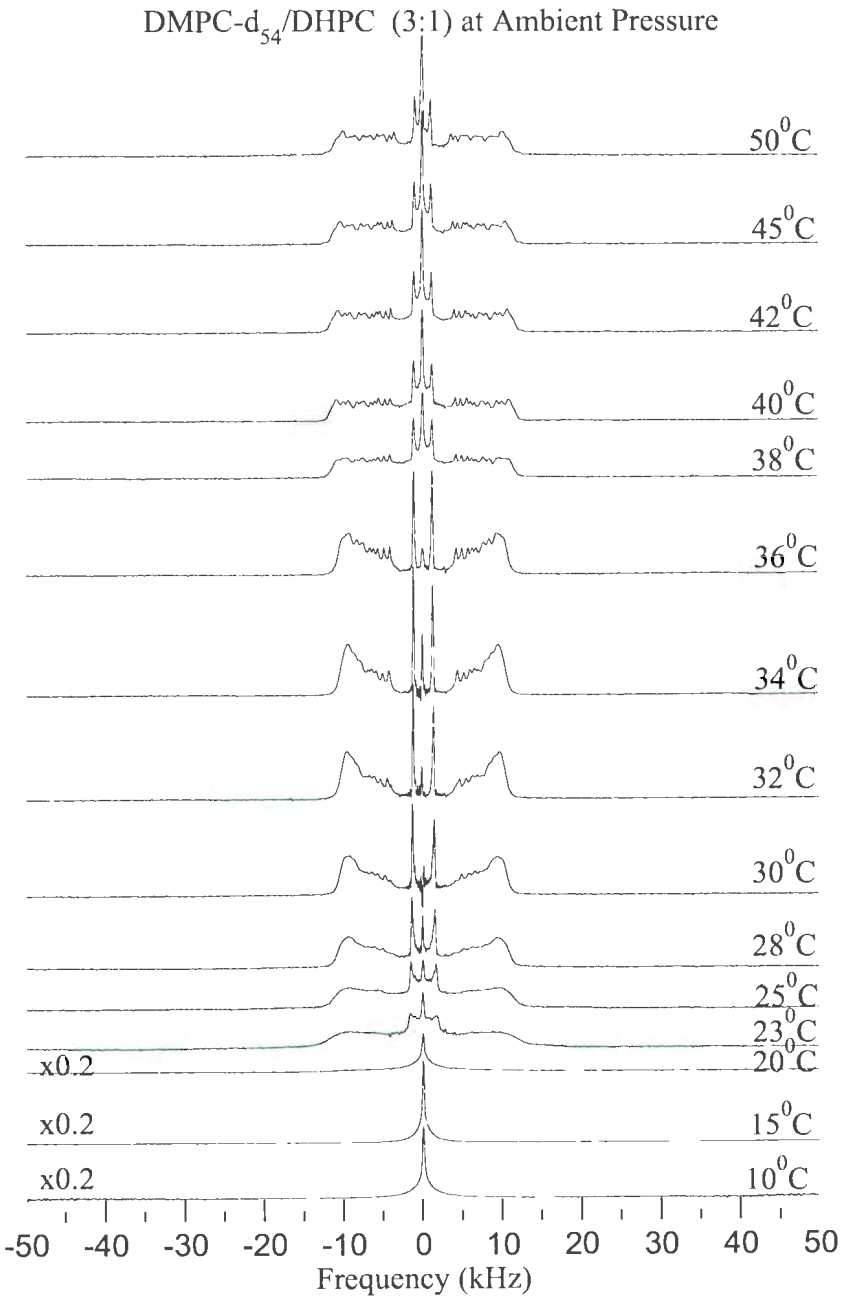


Figure A.1: A1: Full $^2$H-NMR spectra at ambient pressure and 10°C to 50°C for dispersions of DMPC-$d_{54}$/DHPC (3:1) in 100 mM HEPES buffer (pH=7.0).

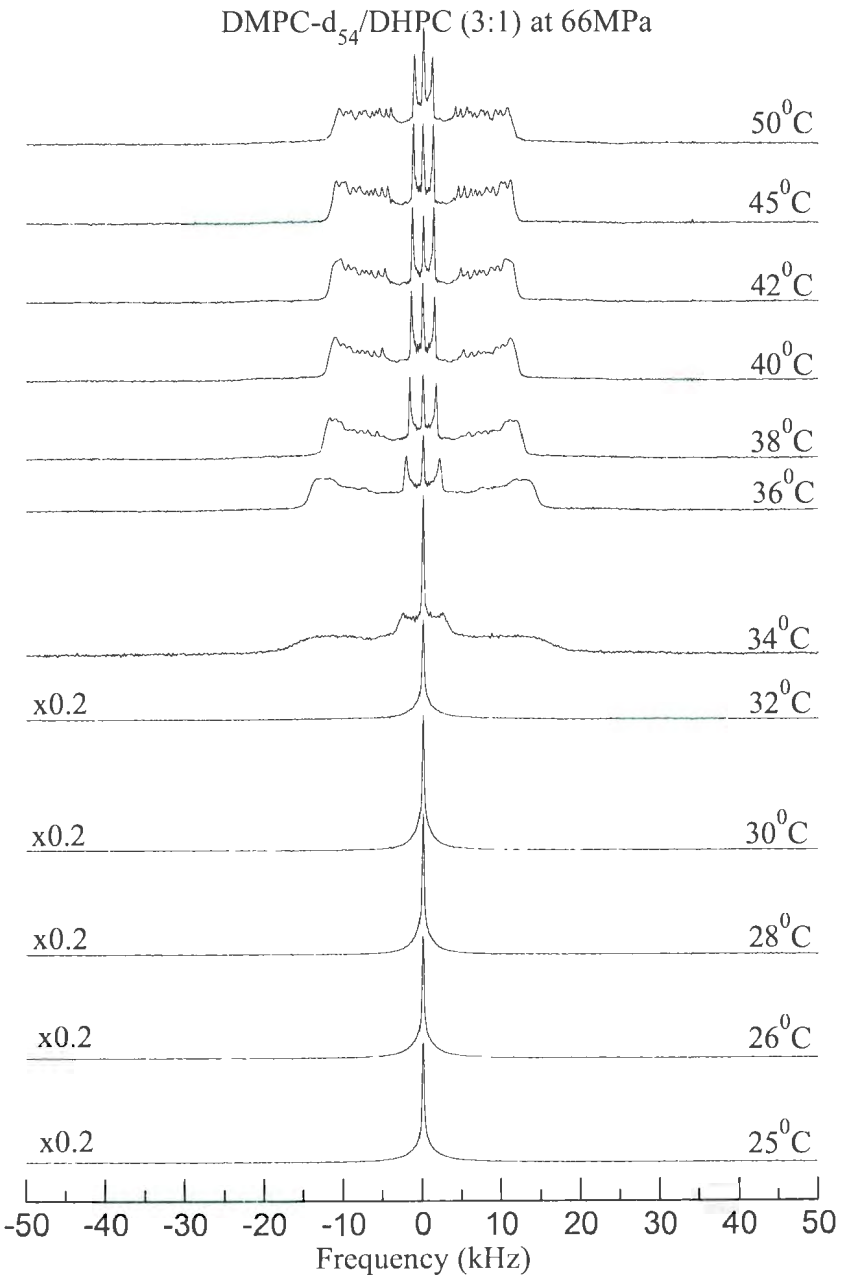


Figure A.2: A2: Full $^2$H-NMR spectra at 66 MPa and 25°C to 50°C for dispersions of DMPC-$d_{54}$/DHPC (3:1) in 100 mM HEPES buffer (pH=7.0).

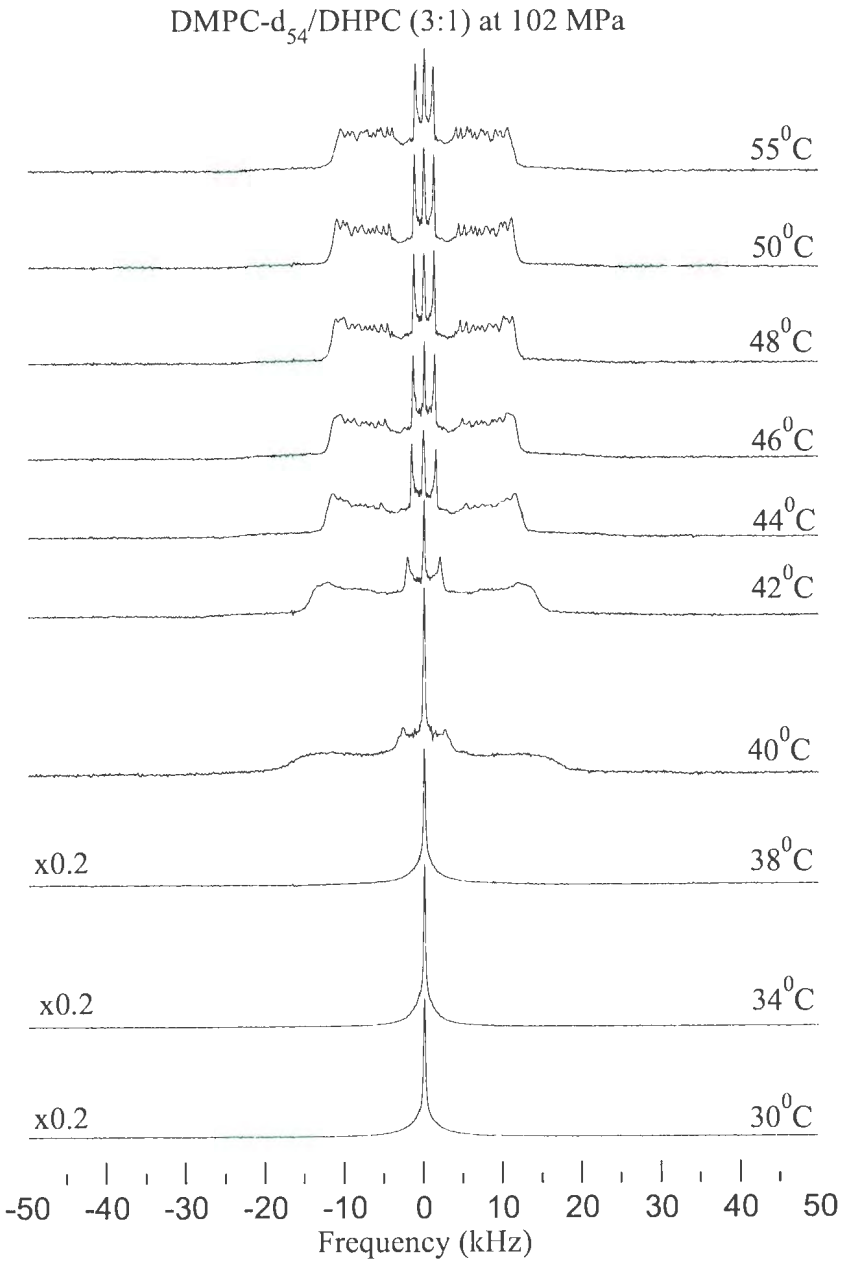


Figure A.3: A3: Full $^2$H-NMR spectra at 102 MPa and 30°C to 55°C for dispersions of DMPC-$d_{54}$/DHPC (3:1) in 100 mM HEPES buffer (pH=7.0).

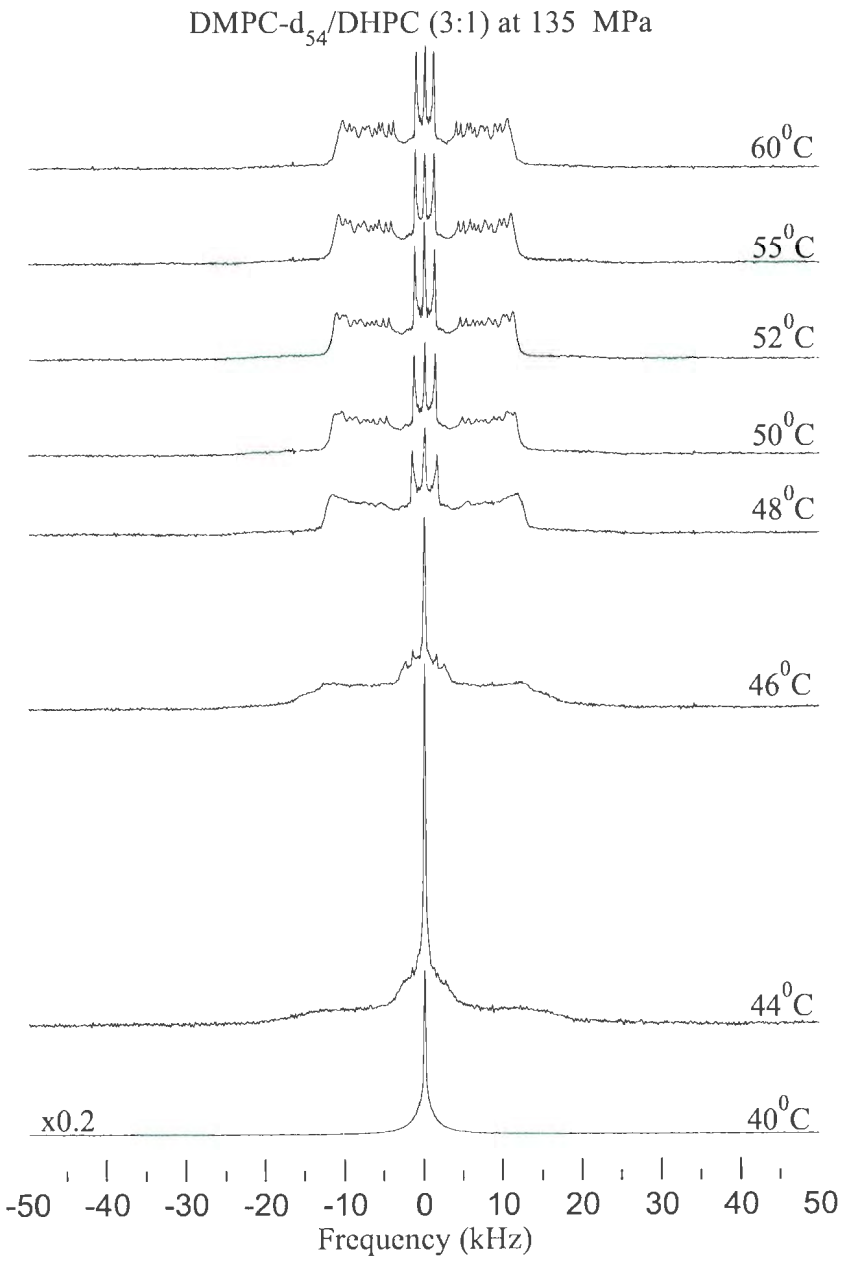


Figure A.4: A4: Full $^2$H-NMR spectra at 135 MPa and 40°C to 60°C for dispersions of DMPC-$d_{54}$/DHPC (3:1) in 100 mM HEPES buffer (pH=7.0).

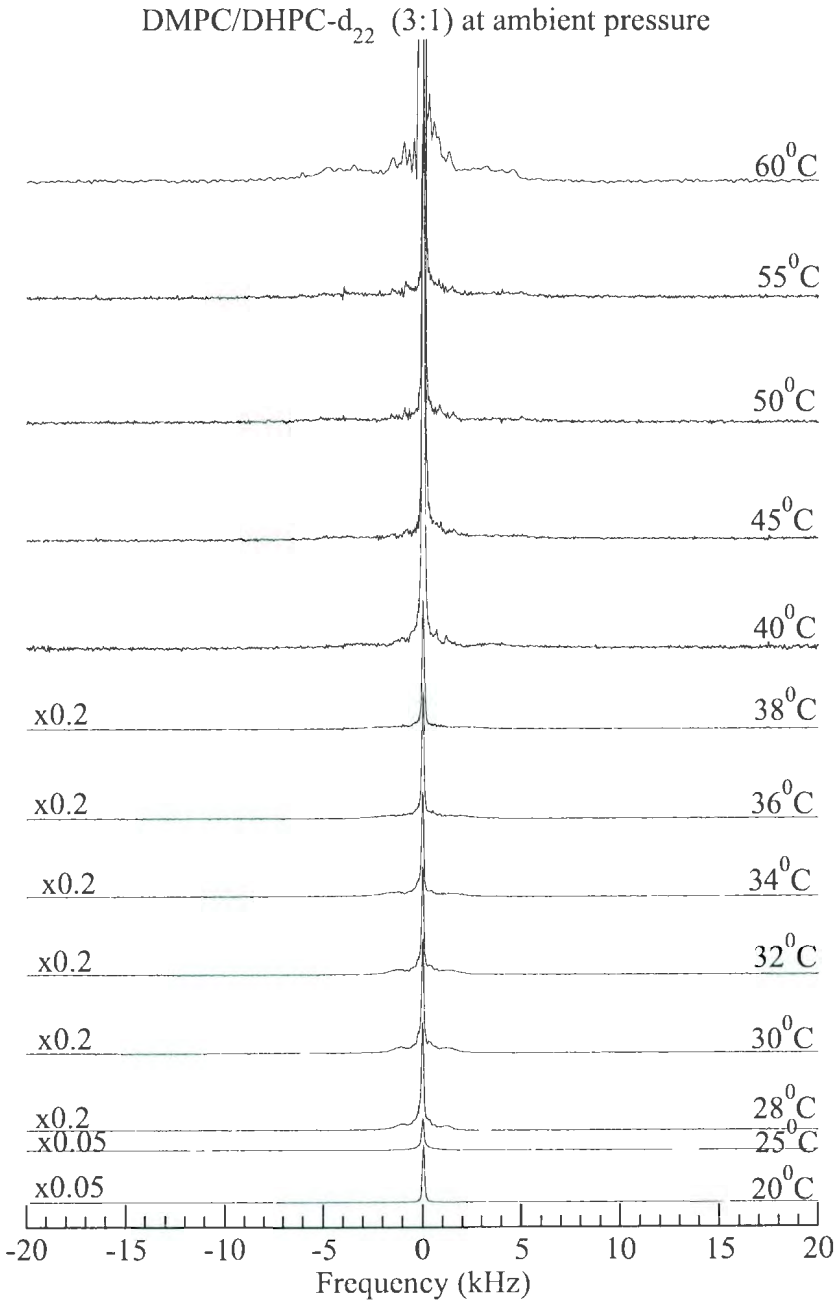


Figure A.5: B1: Full $^2$H-NMR spectra at ambient pressure and 20°C to 60°C for dispersions of DMPC/DHPC-$d_{22}$ (3:1) in 100 mM HEPES buffer (pH=7.0).

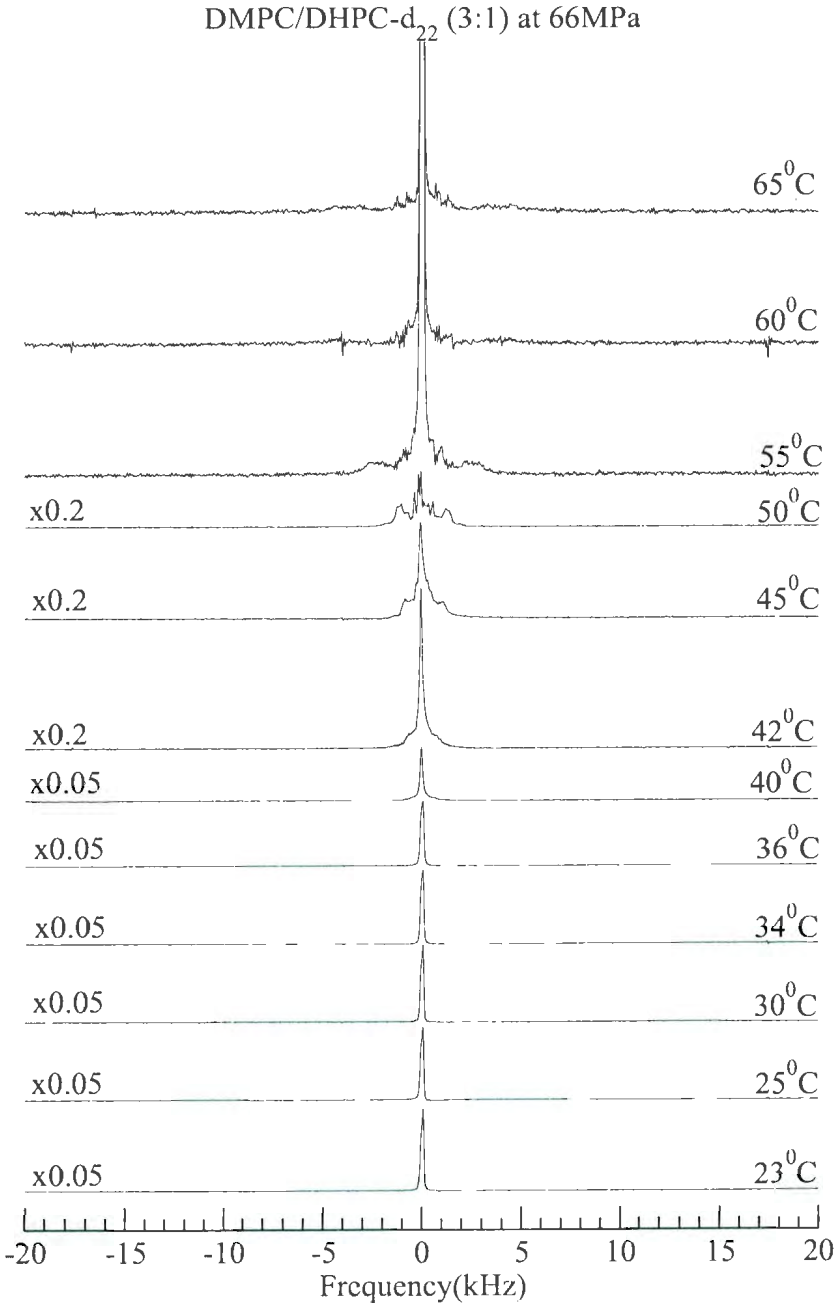


Figure A.6: B2: Full $^2$H-NMR spectra at 66 MPa and 23°C to 65°C for dispersions of DMPC/DHPC-$d_{22}$ (3:1) in 100 mM HEPES buffer (pH=7.0).

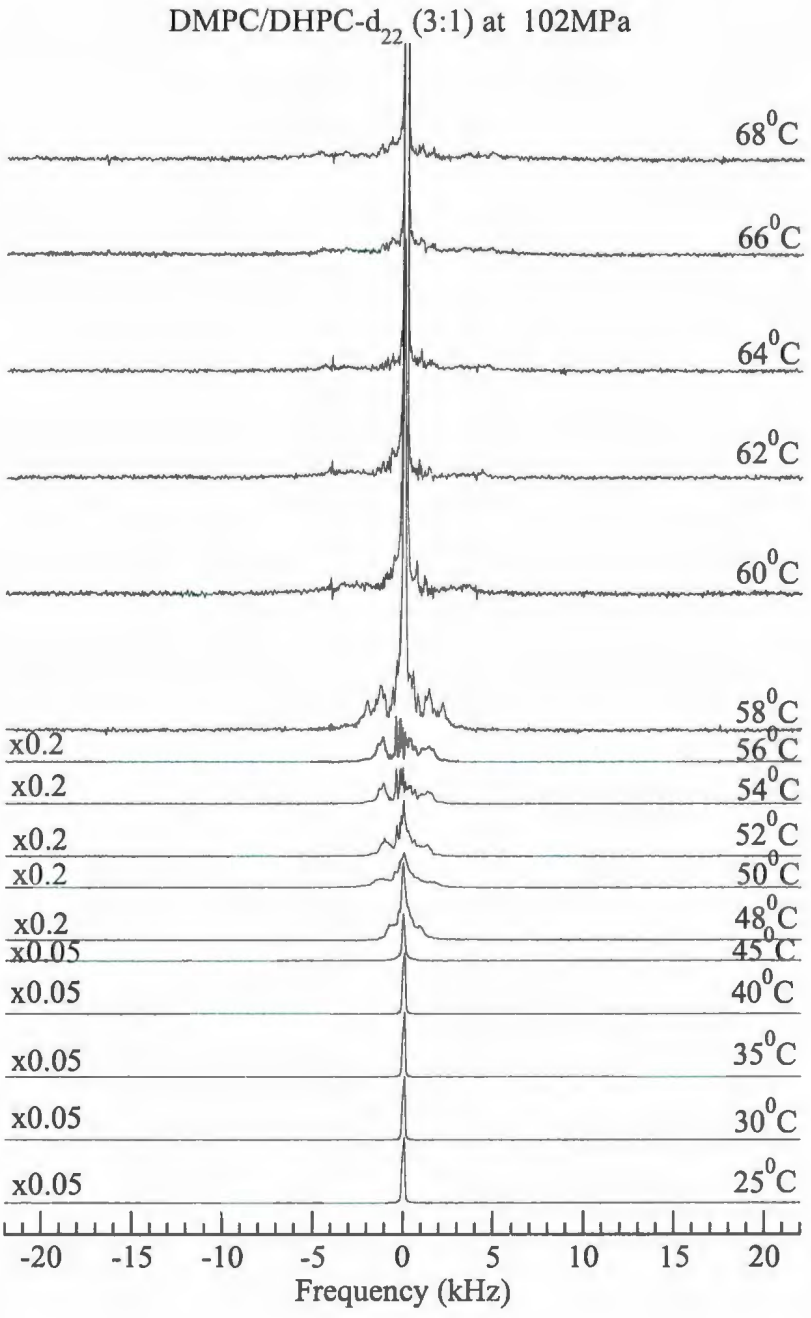


Figure A.7: B3: Full $^2$H-NMR spectra at 102 MPa and 25°C to 68°C for dispersions of DMPC/DHPC-$d_{22}$ (3:1) in 100 mM HEPES buffer (pH=7.0).

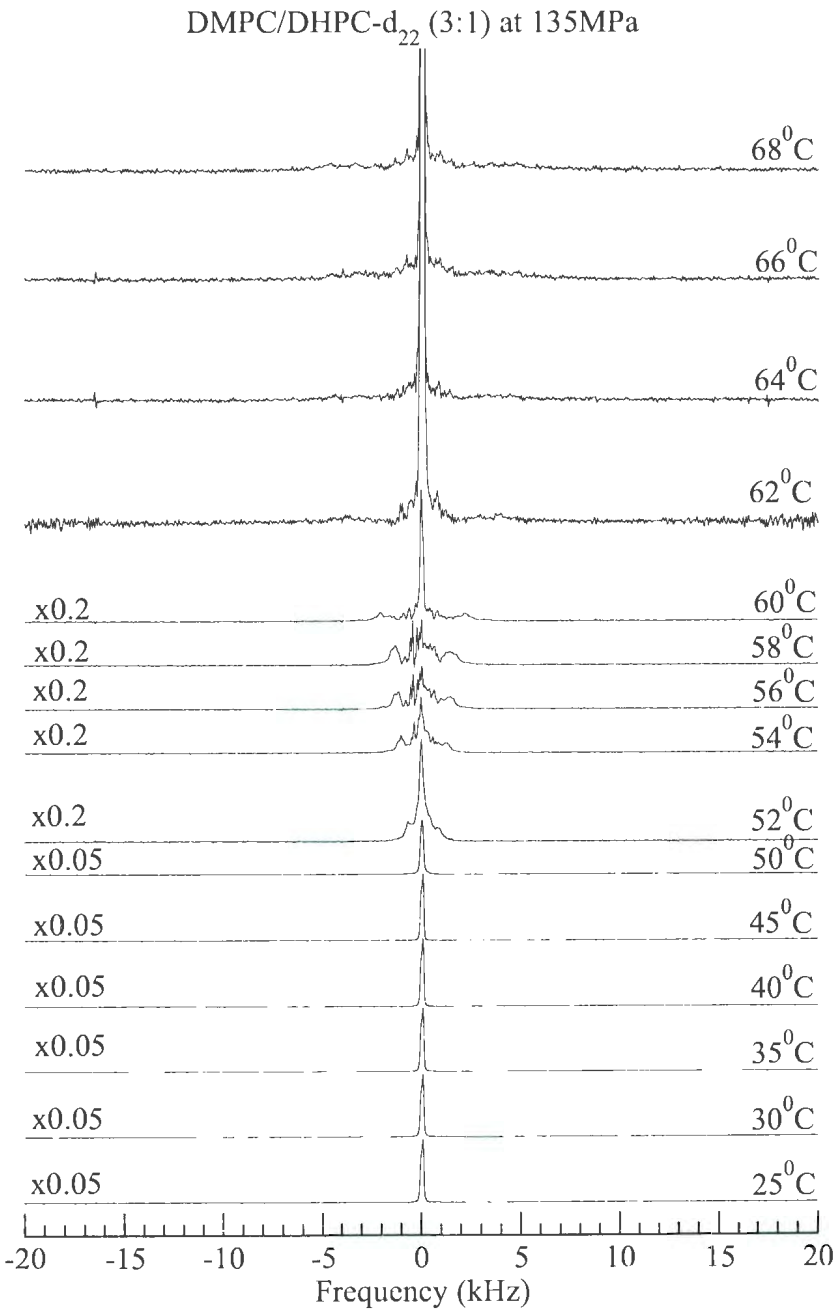


Figure A.8: B4: Full $^2$H-NMR spectra at 135 MPa and 25°C to 68°C for dispersions of DMPC/DHPC-$d_{22}$ (3:1) in 100 mM HEPES buffer (pH=7.0).

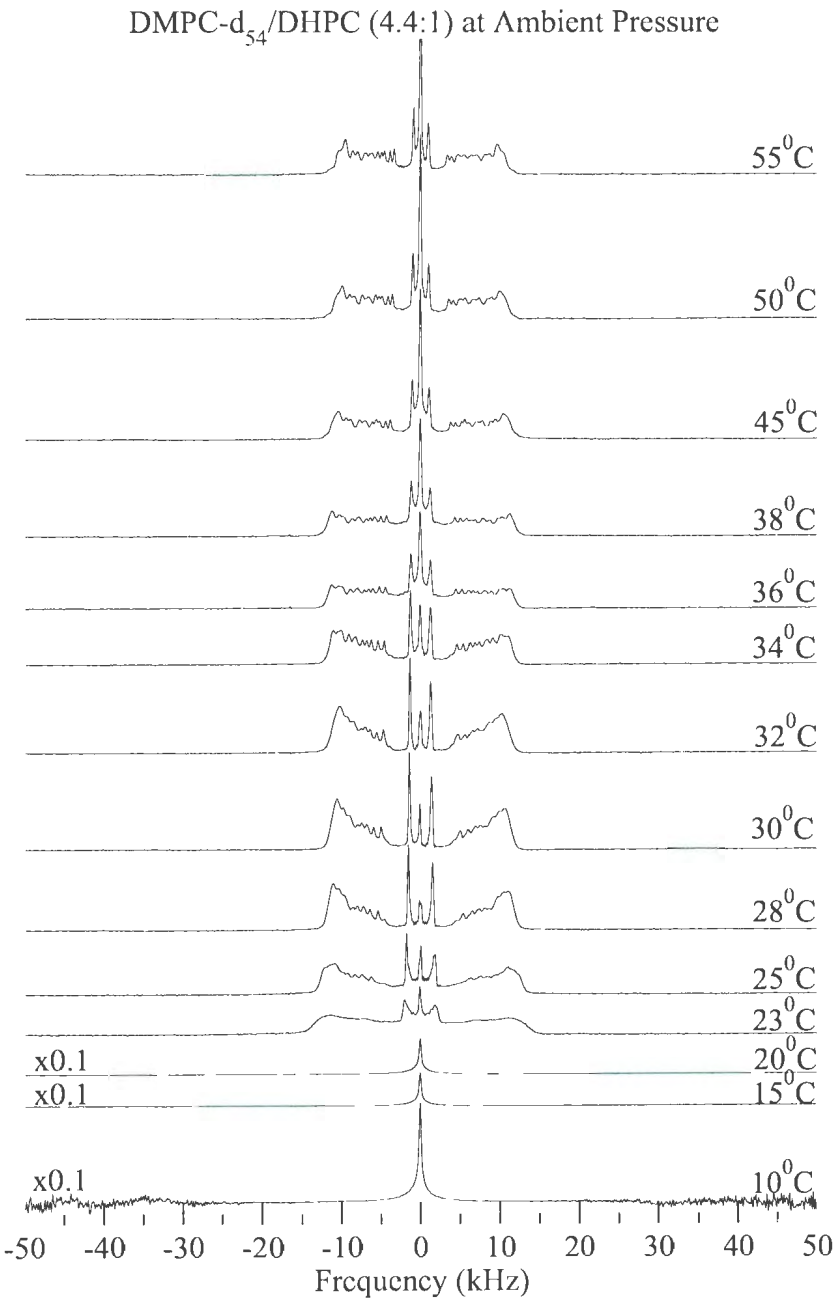


Figure A.9: C1: Full $^2$H-NMR spectra at ambient pressure and 10°C to 55°C for dispersions of DMPC-$d_{54}$/DHPC (4.4:1) in 100 mM HEPES buffer (pH=7.0).

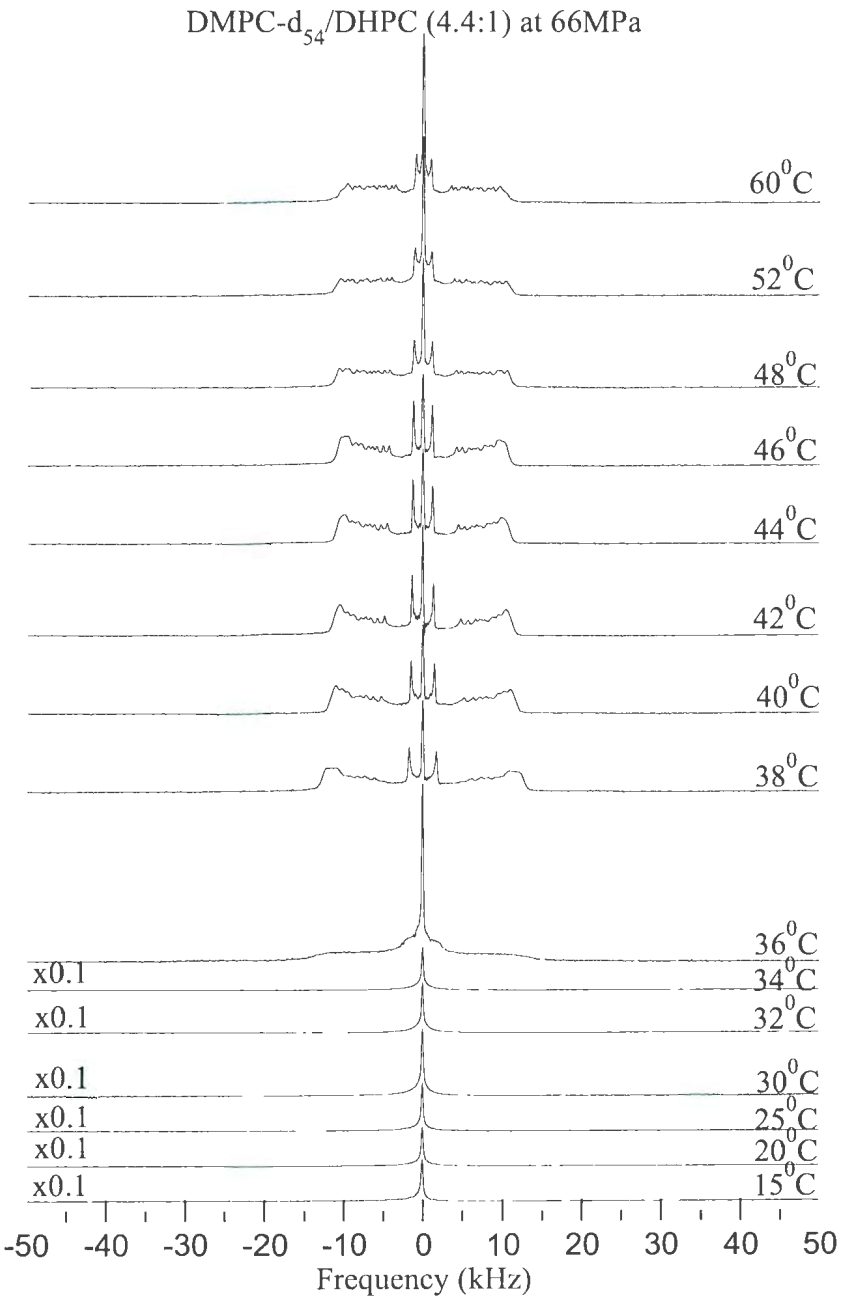


Figure A.10: C2: Full $^2$H-NMR spectra at 66 MPa and 15°C to 60°C for dispersions of DMPC-$d_{54}$/DHPC (4.4:1) in 100 mM HEPES buffer (pH=7.0).

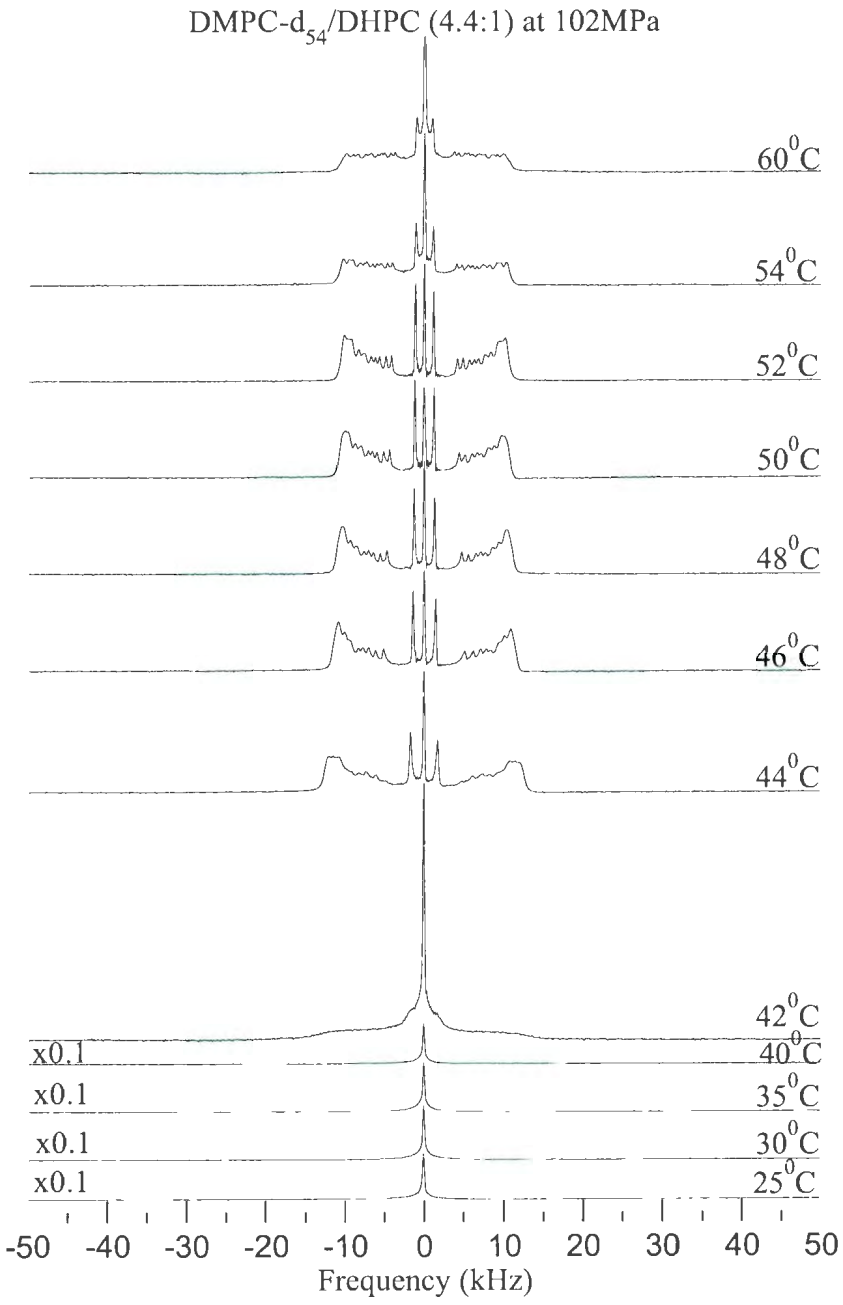


Figure A.11: C3: Full $^2$H-NMR spectra at 102 MPa and 25°C to 60°C for dispersions of DMPC-$d_{54}$/DHPC (4.4:1) in 100 mM HEPES buffer (pH=7.0).

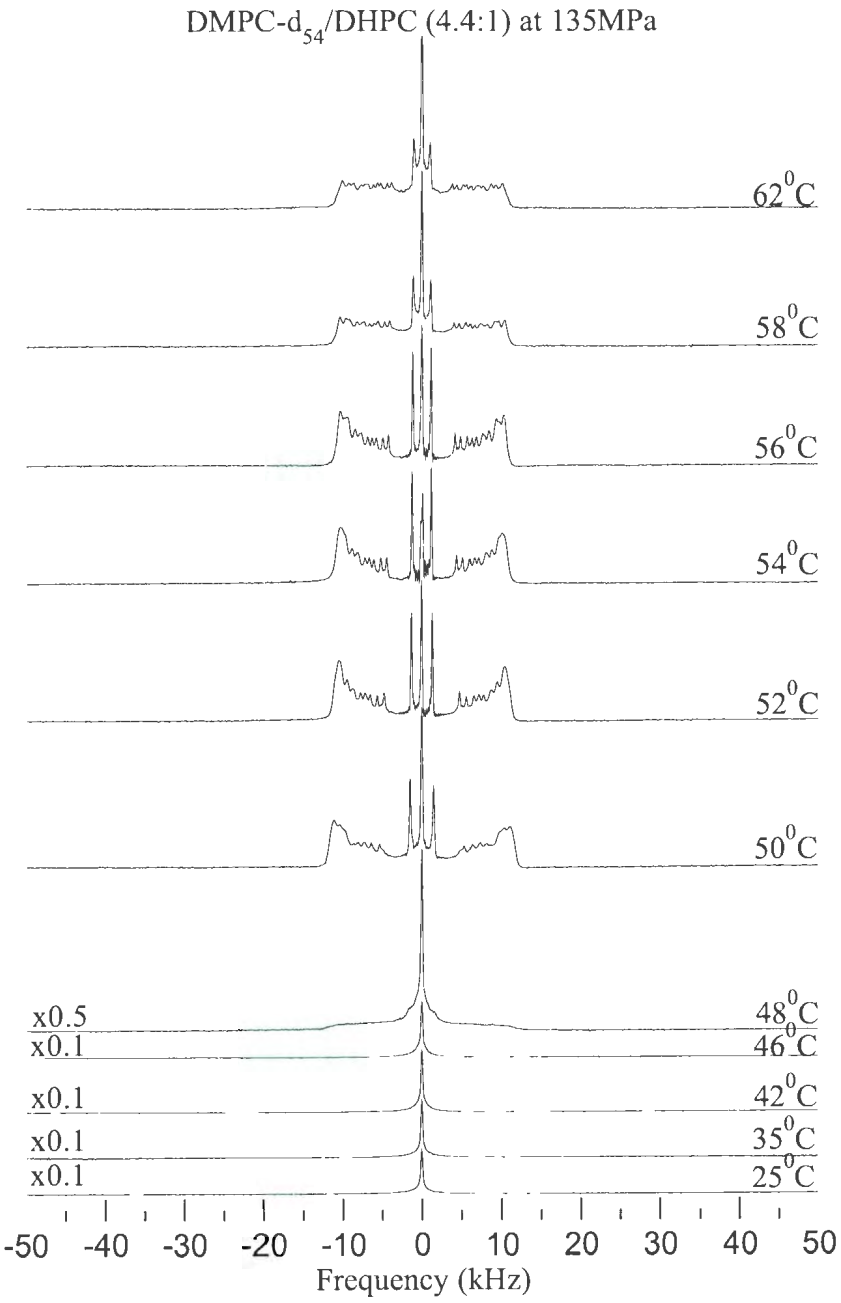


Figure A.12: C4: Full $^2$H-NMR spectra at 135 MPa and 25°C to 62°C for dispersions of DMPC-$d_{54}$/DHPC (4.4:1) in 100 mM HEPES buffer (pH=7.0).

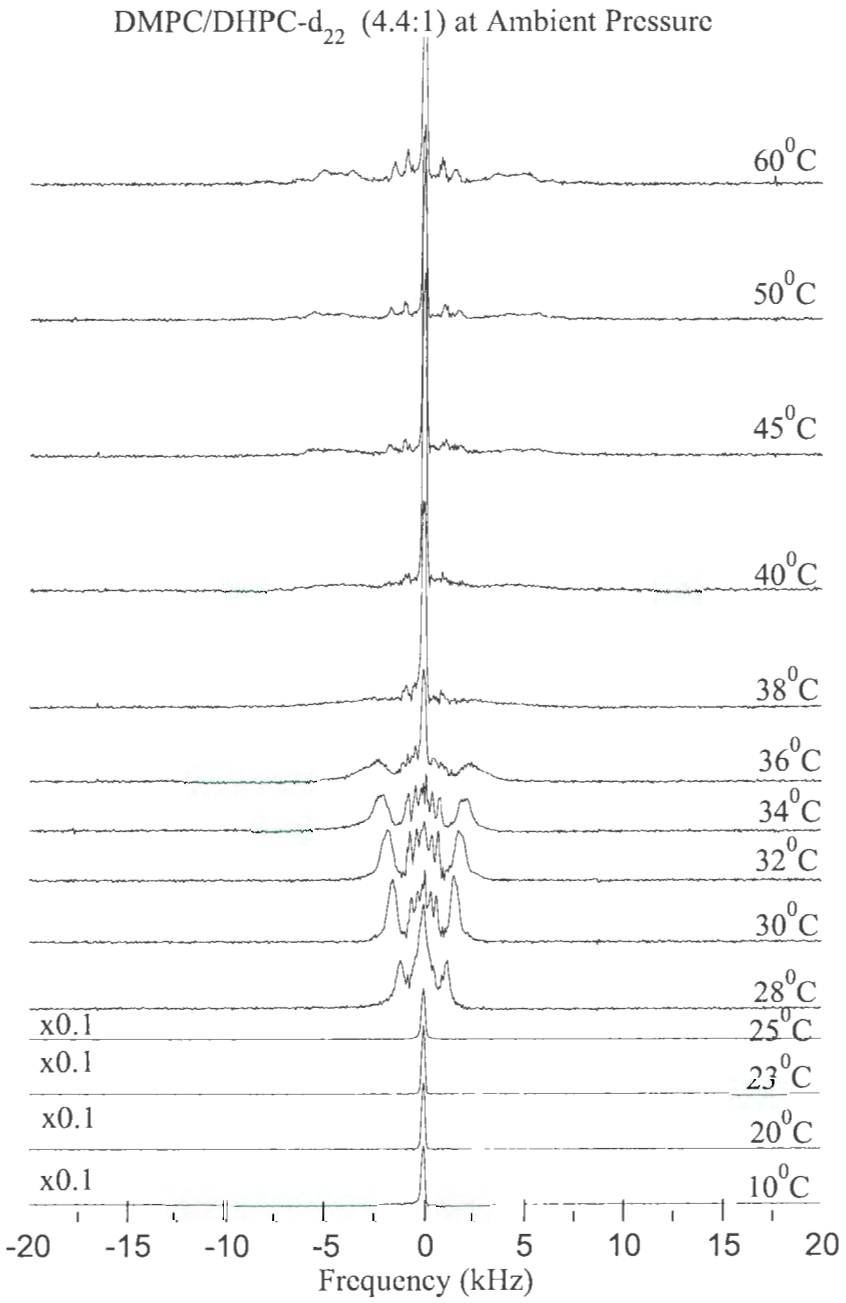


Figure A.13: D1: Full $^2$H-NMR spectra at ambient pressure and 10°C to 60°C for dispersions of DMPC/DHPC-$d_{22}$ (4.4:1) in 100 mM HEPES buffer (pH=7.0).

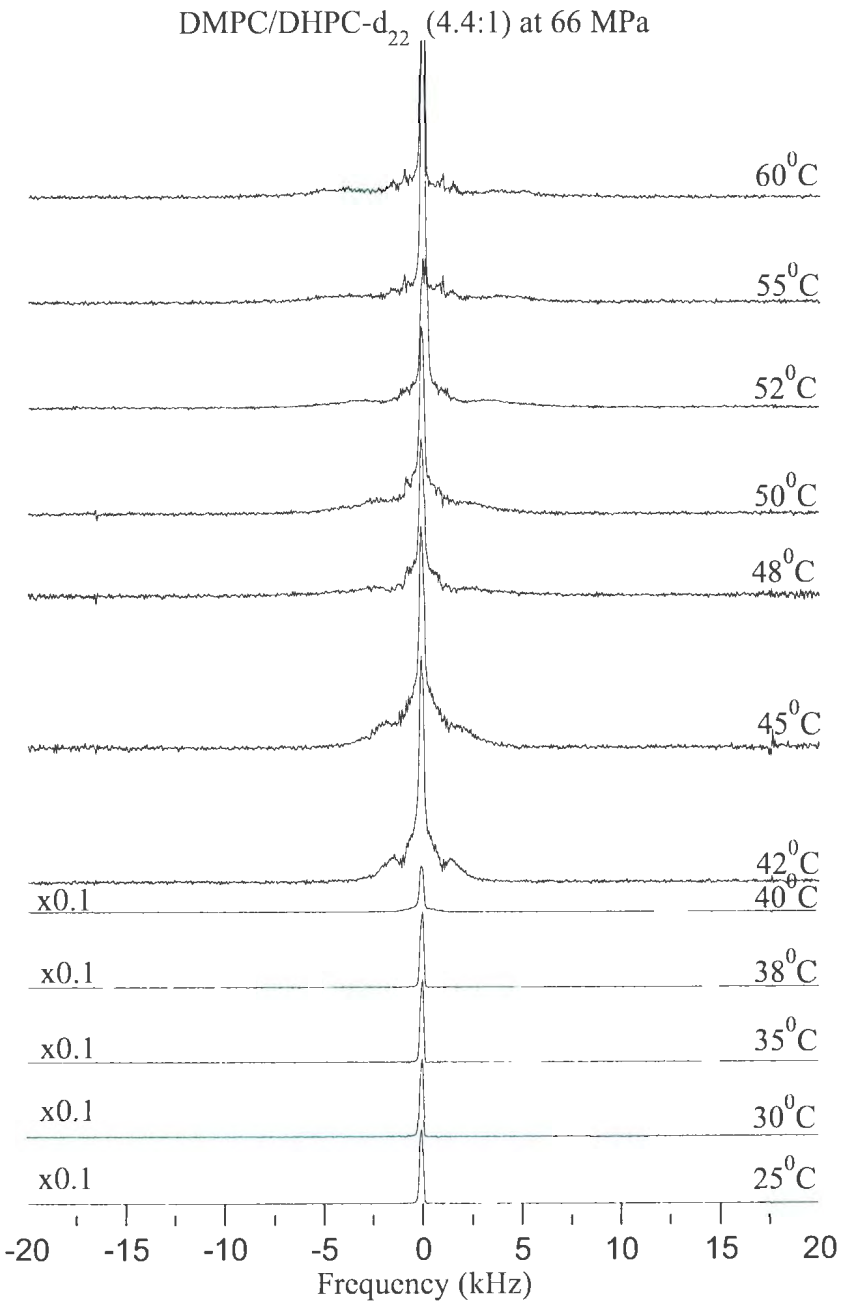


Figure A.14: D2: Full $^2$H-NMR spectra at 66 MPa and 25°C to 60°C for dispersions of DMPC/DHPC-$d_{22}$ (4.4:1) in 100 mM HEPES buffer (pH=7.0).

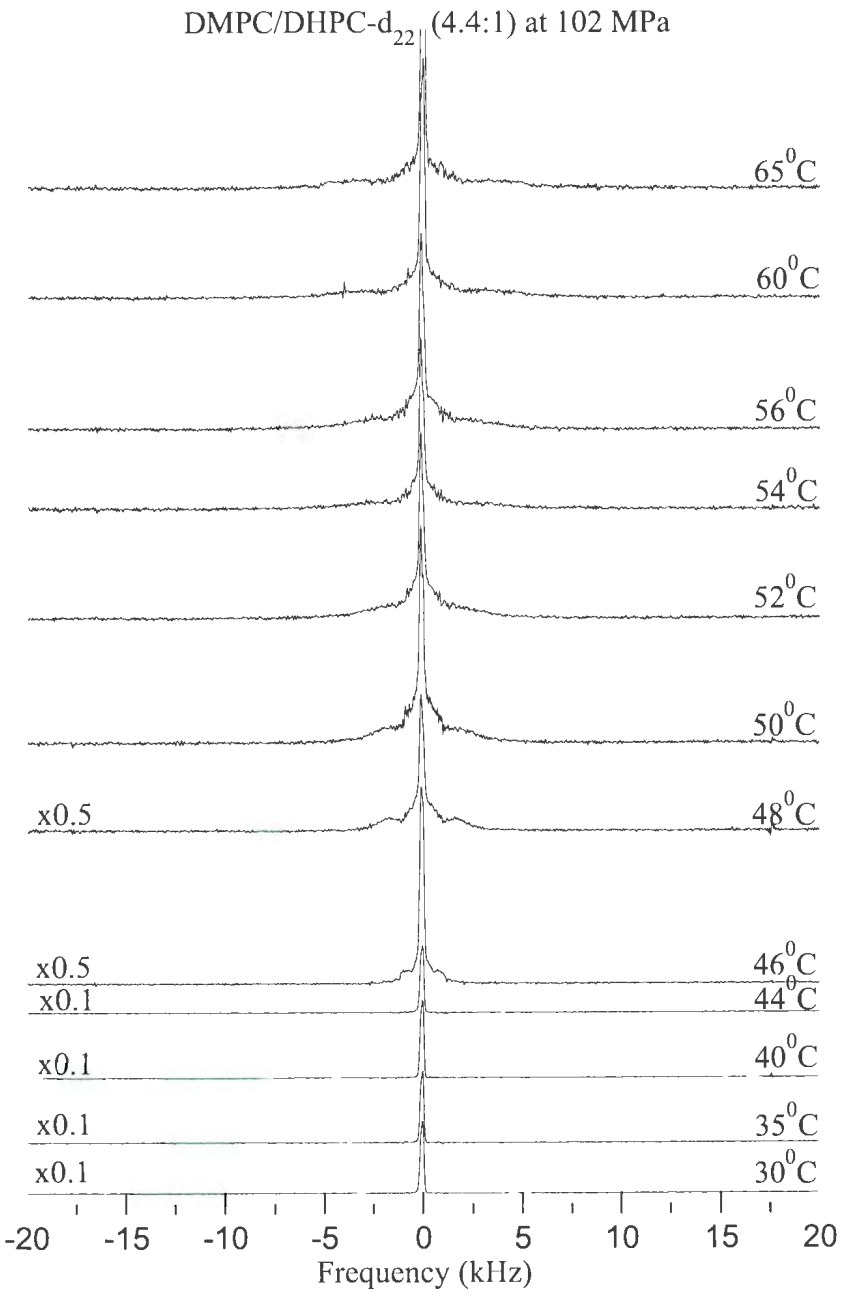


Figure A.15: D3: Full $^2$H-NMR spectra at 102 MPa and 30°C to 65°C for dispersions of DMPC/DHPC-$d_{22}$ (4.4:1) in 100 mM HEPES buffer (pH=7.0).

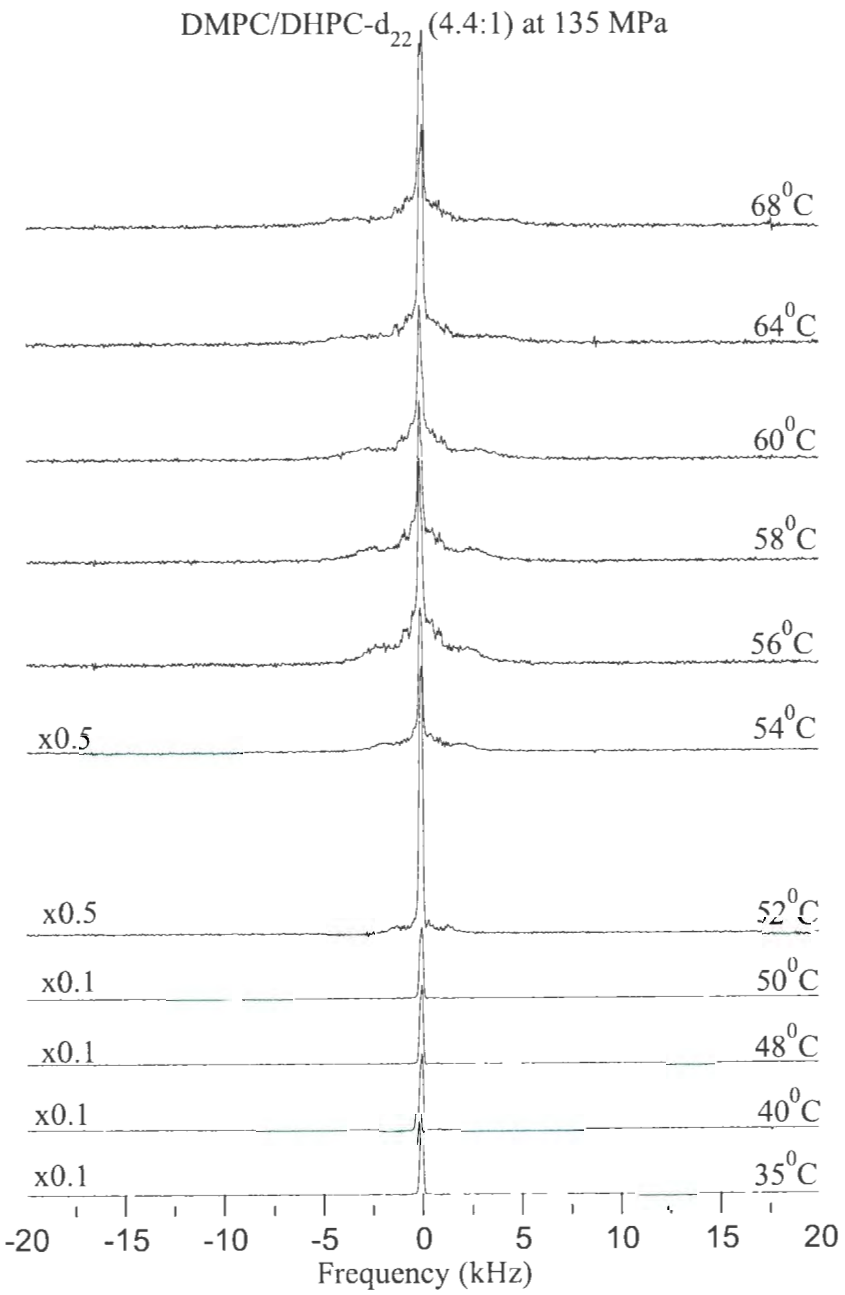


Figure A.16: D4: Full $^2$H-NMR spectra at 135 MPa and 35°C to 68°C for dispersions of DMPC/DHPC-$d_{22}$ (4.4:1) in 100 mM HEPES buffer (pH=7.0).